Nuclear Magnetic Resonance and Molecular Orbital Studies of Conformational Properties and Spin-Spin Coupling Transmission for Phenylallene and 2-Formylstyrene

by

Scott Christopher Kroeker

A Thesis

Submitted to the Faculty of Graduate Studies

in Partial Fulfilment of the Requirements

for the Degree of

MASTER OF SCIENCE

Department of Chemistry

University of Manitoba

Winnipeg, Manitoba

ISBN 0-612-13268-4

Canada

Name _____

Dissertation Abstracts International is arranged by broad, general subject categories. Please select the one subject which most nearly describes the content of your dissertation. Enter the corresponding four-digit code in the spaces provided.

Physical Chemistry
SUBJECT TERM

0494
SUBJECT CODE

U·M·I

Subject Categories

THE HUMANITIES AND SOCIAL SCIENCES

COMMUNICATIONS AND THE ARTS
Architecture 0729
Art History 0377
Cinema 0900
Dance 0378
Fine Arts 0357
Information Science 0723
Journalism 0391
Library Science 0399
Mass Communications 0708
Music 0413
Speech Communication 0459
Theater 0465

EDUCATION
General 0515
Administration 0514
Adult and Continuing 0516
Agricultural 0517
Art 0273
Bilingual and Multicultural 0282
Business 0688
Community College 0275
Curriculum and Instruction 0727
Early Childhood 0518
Elementary 0524
Finance 0277
Guidance and Counseling 0519
Health 0680
Higher 0745
History of 0520
Home Economics 0278
Industrial 0521
Language and Literature 0279
Mathematics 0280
Music 0522
Philosophy of 0998
Physical 0523
Psychology 0525
Reading 0535
Religious 0527
Sciences 0714
Secondary 0533
Social Sciences 0534
Sociology of 0340
Special 0529
Teacher Training 0530
Technology 0710
Tests and Measurements 0288
Vocational 0747

LANGUAGE, LITERATURE AND LINGUISTICS
Language
- General 0679
- Ancient 0289
- Linguistics 0290
- Modern 0291

Literature
- General 0401
- Classical 0294
- Comparative 0295
- Medieval 0297
- Modern 0298
- African 0316
- American 0591
- Asian 0305
- Canadian (English) 0352
- Canadian (French) 0355
- English 0593
- Germanic 0311
- Latin American 0312
- Middle Eastern 0315
- Romance 0313
- Slavic and East European 0314

PHILOSOPHY, RELIGION AND THEOLOGY
Philosophy 0422
Religion
- General 0318
- Biblical Studies 0321
- Clergy 0319
- History of 0320
- Philosophy of 0322

Theology 0469

SOCIAL SCIENCES
American Studies 0323
Anthropology
- Archaeology 0324
- Cultural 0326
- Physical 0327

Business Administration
- General 0310
- Accounting 0272
- Banking 0770
- Management 0454
- Marketing 0338

Canadian Studies 0385
Economics
- General 0501
- Agricultural 0503
- Commerce-Business 0505
- Finance 0508
- History 0509
- Labor 0510
- Theory 0511

Folklore 0358
Geography 0366
Gerontology 0351
History
- General 0578
- Ancient 0579
- Medieval 0581
- Modern 0582
- Black 0328
- African 0331
- Asia, Australia and Oceania 0332
- Canadian 0334
- European 0335
- Latin American 0336
- Middle Eastern 0333
- United States 0337

History of Science 0585
Law 0398
Political Science
- General 0615
- International Law and Relations 0616
- Public Administration 0617

Recreation 0814
Social Work 0452
Sociology
- General 0626
- Criminology and Penology 0627
- Demography 0938
- Ethnic and Racial Studies 0631
- Individual and Family Studies 0628
- Industrial and Labor Relations 0629
- Public and Social Welfare 0630
- Social Structure and Development 0700
- Theory and Methods 0344

Transportation 0709
Urban and Regional Planning 0999
Women's Studies 0453

THE SCIENCES AND ENGINEERING

BIOLOGICAL SCIENCES
Agriculture
- General 0473
- Agronomy 0285
- Animal Culture and Nutrition 0475
- Animal Pathology 0476
- Food Science and Technology 0359
- Forestry and Wildlife 0478
- Plant Culture 0479
- Plant Pathology 0480
- Plant Physiology 0817
- Range Management 0777
- Wood Technology 0746

Biology
- General 0306
- Anatomy 0287
- Biostatistics 0308
- Botany 0309
- Cell 0379
- Ecology 0329
- Entomology 0353
- Genetics 0369
- Limnology 0793
- Microbiology 0410
- Molecular 0307
- Neuroscience 0317
- Oceanography 0416
- Physiology 0433
- Radiation 0821
- Veterinary Science 0778
- Zoology 0472

Biophysics
- General 0786
- Medical 0760

EARTH SCIENCES
Biogeochemistry 0425
Geochemistry 0996
Geodesy 0370
Geology 0372
Geophysics 0373
Hydrology 0388
Mineralogy 0411
Paleobotany 0345
Paleoecology 0426
Paleontology 0418
Paleozoology 0985
Palynology 0427
Physical Geography 0368
Physical Oceanography 0415

HEALTH AND ENVIRONMENTAL SCIENCES
Environmental Sciences 0768
Health Sciences
- General 0566
- Audiology 0300
- Chemotherapy 0992
- Dentistry 0567
- Education 0350
- Hospital Management 0769
- Human Development 0758
- Immunology 0982
- Medicine and Surgery 0564
- Mental Health 0347
- Nursing 0569
- Nutrition 0570
- Obstetrics and Gynecology 0380
- Occupational Health and Therapy 0354
- Ophthalmology 0381
- Pathology 0571
- Pharmacology 0419
- Pharmacy 0572
- Physical Therapy 0382
- Public Health 0573
- Radiology 0574
- Recreation 0575
- Speech Pathology 0460
- Toxicology 0383

Home Economics 0386

PHYSICAL SCIENCES
Pure Sciences
Chemistry
- General 0485
- Agricultural 0749
- Analytical 0486
- Biochemistry 0487
- Inorganic 0488
- Nuclear 0738
- Organic 0490
- Pharmaceutical 0491
- Physical 0494
- Polymer 0495
- Radiation 0754

Mathematics 0405
Physics
- General 0605
- Acoustics 0986
- Astronomy and Astrophysics 0606
- Atmospheric Science 0608
- Atomic 0748
- Electronics and Electricity 0607
- Elementary Particles and High Energy 0798
- Fluid and Plasma 0759
- Molecular 0609
- Nuclear 0610
- Optics 0752
- Radiation 0756
- Solid State 0611

Statistics 0463

Applied Sciences
Applied Mechanics 0346
Computer Science 0984
Engineering
- General 0537
- Aerospace 0538
- Agricultural 0539
- Automotive 0540
- Biomedical 0541
- Chemical 0542
- Civil 0543
- Electronics and Electrical 0544
- Heat and Thermodynamics 0348
- Hydraulic 0545
- Industrial 0546
- Marine 0547
- Materials Science 0794
- Mechanical 0548
- Metallurgy 0743
- Mining 0551
- Nuclear 0552
- Packaging 0549
- Petroleum 0765
- Sanitary and Municipal 0554
- System Science 0790

Geotechnology 0428
Operations Research 0796
Plastics Technology 0795
Textile Technology 0994

PSYCHOLOGY
General 0621
Behavioral 0384
Clinical 0622
Developmental 0620
Experimental 0623
Industrial 0624
Personality 0625
Physiological 0989
Psychobiology 0349
Psychometrics 0632
Social 0451

NUCLEAR MAGNETIC RESONANCE AND MOLECULAR ORBITAL STUDIES OF CONFORMATIONAL PROPERTIES AND SPIN-SPIN COUPLING TRANSMISSION FOR PHENYLALLENE AND 2-FORMYLSTYRENE

BY

SCOTT CHRISTOPHER KROEKER

A Thesis submitted to the Faculty of Graduate Studies of the University of Manitoba in partial fulfillment of the requirements of the degree of

MASTER OF SCIENCE

To Donna

Abstract

An investigation of some conformational properties of styrene is carried out indirectly, using two related compounds, phenylallene and 2-formylstyrene. Long range intergroup coupling constants (lrJs) from very high-resolution ^{1}H NMR spectra of phenylallene solutions in acetone-d_6 and benzene-d_6 are discussed in terms of angle-dependent σ and π electron spin-spin coupling mechanisms. Molecular orbital (MO) computations at the MP2/6-31G* level of correlation-gradient theory predict the height of the internal rotational potential as 16 kJ/mol, suggesting a 4 kJ/mol steric repulsion energy for styrene. Absolute signs of lrJs to the methylene protons are inferred from a positive dipolar coupling between these protons. Some coupling constants between protons and the sidechain ^{13}C nuclei are discussed in terms of spin coupling mechanisms. Anomalous perturbations of $^1J(^1H,^{13}C)$ within the sidechain are also noted. A similar NMR study of acetone-d_6 and CS_2/C_6D_{12} solutions of 2-formylstyrene yields lrJs indicating a 55% population of the O-*trans* conformer. MO calculations at the HF/6-31G* level imply a similar comformational distribution, with a low energy minimum at a vinyl torsion angle, θ, of 38° for the O-*cis* conformer, and two distinct minima for the O-*trans* conformer at $\theta = 45$ and 130°. This latter conformer appears to be consonant with an hypothesis used to explain the photochemistry of this molecule. The observed lrJs demonstrate no significant solvent dependence and are consistent with the computed conformational properties of the free molecule. A through-space coupling constant of -0.16 Hz is observed between the formyl and the vinyl methine protons. Preliminary MO and NMR results from 2,6-difluorostyrene and 2-hydroxynaphthaldehyde are mentioned with regard to through-space interactions.

Acknowledgements

I wish to thank the Natural Sciences and Engineering Research Council of Canada for supporting this research in a variety of ways — notably through a Post Graduate Scholarship.

Kirk Marat has been invaluable in his excellent maintenance of the spectrometer, and his willingness to share his wisdom on everything from shimming techniques to LaTeX tricks.

Dr. David MacKinnon is acknowledged for synthesizing the title compounds in high purity.

I thank Dr. Frank Hruska for providing me with a quiet place to work, and for interrupting that silence with engaging conversation.

My colleagues have participated in this research through interesting questions and discussions. In particular, I thank Rob Schurko, Guy Bernard and Paul Hazendonk for introducing me to the techniques of this laboratory, and guiding me through the frustrations of the sometimes confusing spectrometer and computer idiosyncracies. Mark Soliven and Younes Bekkali are acknowledged for their experimental contributions to this work and its continuation.

My heartfelt appreciation goes to Professor Ted Schaefer, who, in addition to providing me with a first-rate education in the physical sciences, has been an affirming presence and mentor during my tenure as his student.

Finally, it is with great joy that I thank the strong network of family and friends with whom I am blessed. Their unfaltering support of me as I pursue this path, and apparent interest in my work, plays a crucial role in my enthusiasm and energy.

Thank You!

Contents

List of Figures

List of Tables

1 Introduction

Conflicting reports have been published concerning the barrier to internal rotation in styrene. Many experimental and theoretical techniques have been employed, and nearly as many internal rotational potential functions have been suggested. The earliest barrier was derived in the gas phase from thermodynamic measurements in 1946 [1].

Molecular spectroscopists have attempted to evaluate the internal rotational potential using Raman [2], single vibronic level (SVL) fluorescence [3, 4] and microwave [5] spectroscopy. The form of the potential to which experimental data are fit is

$$V(\theta) = \frac{1}{2}\sum_i V_i(1 - \cos i\theta) = \sum_i V_i \sin^2\left(\frac{i\theta}{2}\right). \quad (1)$$

The symmetry characteristic of this rotation in styrene demands that only evenfold terms contribute.

An early experiment using low-frequency, gas-phase Raman spectroscopy [2] reported the potential function

$$V(kJ\,mol^{-1}) = 7.45(8)\sin^2\theta + 0.32(4)\sin^2 2\theta. \quad (2)$$

Subsequently, SVL fluorescence spectroscopic measurements [3] provided evidence which allowed a reinterpretation of the Raman data, yielding

$$V(kJ\,mol^{-1}) = 13.7(1)\sin^2\theta - 3.32(6)\sin^2 2\theta. \quad (3)$$

The salient feature of this revised potential is the substantial negative fourfold component. This crucial difference modifies the shape of the potential well, as illustrated in Figure 2.

Physically, the effect of this term is to flatten the potential curve near planarity, allowing for larger amplitude torsional vibrations than with a strictly twofold potential. Based on vibrational level populations, Hollas *et al.* [3] suggest that at room temperature, gas phase styrene exists in high probability with a dihedral angle ranging between $\pm 45°$.

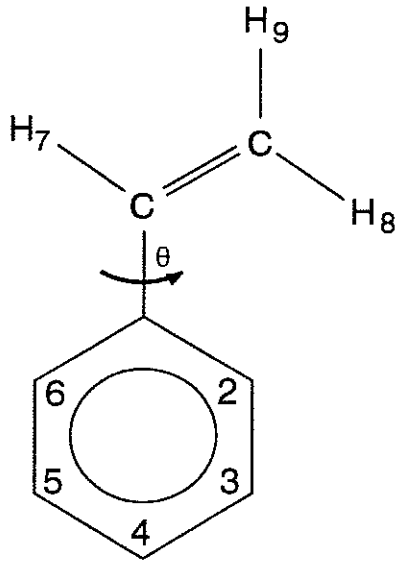

Figure 1: Molecular structure of styrene and atomic numbering scheme.

Combining newly available geometric information, the electronic absorption spectrum, Raman data and SVL fluorescence measurements on styrene-β-d_2 with the existing data on styrene, Hollas *et al.* [4] were able to improve on their previously determined potential, arriving at what is now widely taken to be the definitive experimental potential for styrene:

$$V(kJ\,mol^{-1}) = 12.8(1)\sin^2\theta - 3.29(1)\sin^2 2\theta + 0.084(6)\sin^2 3\theta. \qquad (4)$$

A few years later, this potential was further investigated using the rotational spectrum of styrene observed by microwave fourier transform (MWFT) spectroscopy [5]. Accounting, this time, for structural relaxation on large amplitude vibrations and incorporating MWFT data from ground and excited states, the *original* potential [3] obtained by Hollas' group was supported. No attempt was made, however, to reconcile this potential with the preferred potential from the more recent and more comprehensive investigation by Hollas *et al.* [4] and, indeed, it was not mentioned. In addition, measurements of the moments of inertia were interpreted to provide "conclusive evidence of molecular planarity" [5].

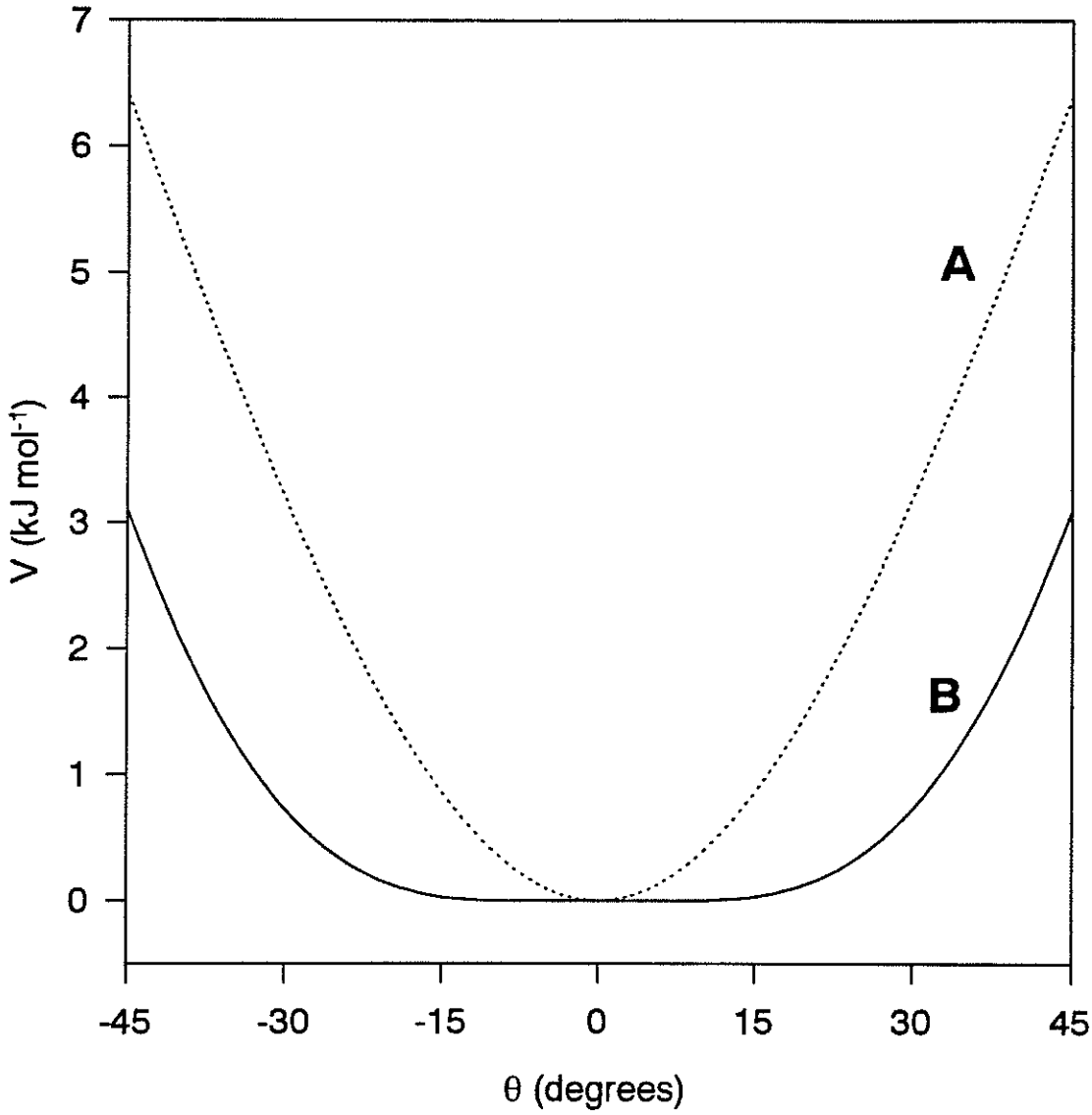

Figure 2: Potential function from equation 4 around the minimum for styrene: A) only V_2, B) only V_2 and V_4.

Theoretical computations of styrene, however, tell a somewhat different story. Early investigations using semi-empirical methods [6, 7] or *ab initio* molecular orbital (MO) calculations [8] with standard (fixed) geometries poorly described the rotational barriers, but signalled the possibility of a small barrier to planarity. Two 1985 reports explored this possibility using *ab initio* MO computations with geometry optimization[1] [9, 10]. Of the four basis sets used, STO-3G, 4-21G, 4-31G [9] and 6-31G [10], the three highest agree that there is a substantial fourfold component, negative in sign, which competes with the positive twofold component to produce a deviation from planarity in the minimum energy conformation. 6-31G, for example, yields the flattest potential, with a V_2 of 13.19(15) $kJ\,mol^{-1}$ and a V_4 of -3.18(15) $kJ\ mol^{-1}$. The condition for planarity in the presence of a negative V_4 is that the magnitude of V_2 exceed four times the magnitude of V_4. Examining the two experimental potentials in equations 3 and 4 demonstrates the conflict between them with respect to this question. The potential derived from SVL fluorescence data indicates a double minimum, whereas MWFT data demand planarity. This ambiguity is not resolved by the theoretical potential at the 6-31G level, for which the uncertainty in the numbers permits either conclusion.

The point in question arises from the relation of conjugational energy favouring planarity and steric destablization between ortho and vinyl protons. Given recent interest in the importance of electron correlation effects on the evaluation of conjugational energy, this barrier has been examined theoretically using Møller-Plesset perturbation theory [11]. Full geometry optimization at the Hartree-Fock (HF) level using the 6-31G* basis set (denoted HF/6-31G*), yields a small barrier to planarity of 170 $J\,mol^{-1}$ and a minimum energy torsion angle of 15°. The twofold barrier height is 12.05 $kJ\,mol^{-1}$, in reasonable accord with that determined by SVL fluorescence and Raman spectroscopy. Remarkably, jumping to the MP2/6-31G*//HF/6-31G*

[1]The computational methods varied slightly: Schaefer and Penner maintained the benzene ring as a planar hexagon, calculating seven energies from 0 to 90° in 15° increments; Bock *et al.* assumed a planar ring and vinyl group, obtaining energies at 0, 15, 30, 60 and 90°.

treatment causes a 1.1 $kJ\,mol^{-1}$ decrease in V_2, even further from the most reliable experimental values[2]. Fourth-order perturbation theory in the form of MP4(SDQ)/6-31G*//HF/6-31G* brings the barrier down to 10.25 $kJ\,mol^{-1}$.

This work is, of course, predicated on the assumption that the HF geometry is little-changed by correlation-gradient geometry calculations. Supporting this assumption are calculations which suggest negligible geometry effects for butadiene [14]. This same study, however, concluded that correlation effects are very small for the barrier in butadiene, contrasting sharply with the situation for styrene. Our own calculations demonstrate significant geometry modifications arising from correlation-gradient MP2/6-31G* treatment. For example, bonds between carbon and hydrogen are extended by 0.01 Å or more, whereas the ring-vinyl carbon-carbon bond is shortened by as much. Furthermore, the $C_{ipso}C_\alpha C_\beta$ angle is decreased in the planar form by 0.7°. These changes may contribute to increased steric destablisation for planar styrene. The energy difference between planar and perpendicular conformers in these calculations is 10.42 $kJ\,mol^{-1}$. Single-point electron correlation computations described above cite this difference as 10.33 $kJ\,mol^{-1}$ [11].

A more recent theoretical attempt [15] uses an approach which purports to correct for the systematic nature of HF errors, applying scale factors to styrene bond lengths based on known errors in benzene and butadiene computations. Again, theory predicts a small barrier to planarity and an energy minimum when the torsion angle is about 15-20°.

In sum, the discussion surrounding the internal rotational potential of styrene is commonly seen as one between experimentalists favouring a planar structure with a twofold barrier around 13 $kJ\,mol^{-1}$ and theoreticians claiming a small barrier to planarity and V_2 values ranging from 11 to 12 $kJ\,mol^{-1}$. When each contribution is carefully examined, however, the categories are not as straightforward, there being

[2]For differing views about the basis set dependence of computed barriers in benzene derivatives, and the reliability of various approaches to accounting for electron correlation, see references [12, 13].

disagreement among both experimentalists and theoreticians. Common to all treatments is the recognition that any barrier to planarity is well below the zero-point level, yielding a molecule which can be treated as planar with a very flat minimum for most practical purposes.

A variety of NMR experiments has also been used to evaluate the barriers in styrene and its derivatives. Deuterium NMR spectra of deuterated styrenes at high field strengths display measurable quadrupolar splittings due to partial molecular alignment which can be analyzed to reveal information about geometry and internal motional averaging. By this method, Bothner-By *et al.* [16] have determined an average value for $\sin^2\theta$ from which they obtain a purely twofold barrier of 16.7 $kJ\,mol^{-1}$. No attempt was made to introduce a fourfold term into the potential, limiting the utility of this expression. Another application of NMR to address this question indirectly, entails adding electron-releasing substituents in the para and *trans-* β positions, thereby increasing the conjugational energy and boosting the barrier into the region accessible to dynamic NMR methods. Anderson observed the temperature-dependent NMR spectra of p-dimethylaminocinnamaldehyde and p-methoxycinnamaldehyde to obtain twofold rotational barriers of 30.5 and 25.9 $kJ\,mol^{-1}$, respectively [17]. Discussion of these results, however, assumes *a priori* that styrene itself is planar.

One NMR approach which has met with reasonable success involves correlating long-range indirect spin-spin coupling constants (lrJs) between vinyl protons and ring protons with conformational preferences. In general, it is well established that spin state information can be transmitted over many bonds according to known mechanisms which vary predictably with the dihedral angle describing sidechain torsion. This procedure requires that such relationships be developed for a particular system using derivatives containing substituents which influence conformation in a predictable way. By measuring lrJs in many similar compounds, it is possible to evaluate the validity of the model, eventuating in a consistent picture of the angle-dependence of intergroup J couplings.

For styrene, the seminal work using this approach appeared in 1971 [18]. Barfield *et al.* showed that lrJs in ring-substituted halostyrenes could be semi-quantitatively reproduced by molecular orbital (MO) and valence bond calculations on styrene. The semiempirical valence bond formalism [19] accounts only for contributions from π-electron delocalization, maximal for planarity, and σ-π interactions, maximized when the plane of the vinyl fragment is perpendicular to the benzene plane. In contrast, MO results are based on all valence electrons using the INDO [20, 21] wave functions and finite perturbation theory (FPT), thus also include contributions from the σ-framework and proximity effects.

Assuming that variations in lrJs are dominated by conformational rather than substituent effects[3], these derivatives with approximately known conformations provided a testing ground for styrene calculations. An exemplar in this regard is the utility of the six-bond coupling to the α-proton ($^6J_{4\alpha}$) for understanding vinyl torsion. In planar styrene, the calculated value agrees with that obtained experimentally for the planar derivative 3-bromostyrene, whereas the large increase in magnitude observed for the substantially non-planar 2,6-dichlorostyrene is consistent with the predicted dominance of a σ-π coupling mechanism. In addition, seven-bond couplings to the methylene protons were also found to agree with theoretical predictions, providing further conformational indicators. A third potentially useful coupling is the stereospecific six-bond couplings to the β-proton *trans* to the ring where the "all-*trans*" arrangement gives rise theoretically to a large, positive value transmitted via the σ-framework. Subsequent work on monofluorostyrenes has borne this out experimentally [23]. Similar relationships were found for the five-bond couplings to the α-proton.

The publication of this study preceeded the SVL and MWFT spectroscopic work described above, so that comparison of these conformational predictions with experimentally determined internal rotational potentials was not possible. With the advent

[3]This assumption was subsequently verified for halostyrenes by Reynolds *et al.* [22].

of better instrumentation and new experimental potentials, these relationships were re-examined by Schaefer *et al.* [24]. Accepting the gas phase potential in equation 4 as valid in solution and thereby evaluating an average $\sin^2\theta$ by the hindered rotor treatment, Barfield's INDO relationships were scaled to reproduce the experimental lrJs in styrene [25]. These revised equations were applied to high-resolution NMR data for methylstyrene derivatives to determine characteristic $\langle\sin^2\theta\rangle$ values. From comparison of these numbers to theoretical internal rotational potentials evaluated at the 6-31G level of MO theory there emerged a reasonably consistent picture for the majority of lrJs. In particular, six and seven-bond couplings from the sidechain protons to the para position are sufficiently sensitive to conformation to provide a reliable measure of conformational bias.

An alternate development of the angle-dependence of $^6J_{4\alpha}$ was constructed on the basis of an elaborate set of modified INDO-FPT calculations [26] suggesting the existence of a *spin-polarizability* coupling mechanism maximised in the planar conformer of styrene. Using molecular mechanics to predict the $\langle\sin^2\theta\rangle$ of β,β-dibromo-2,6-dichlorostyrene as greater than 0.9, $^6J_{4\alpha}$ was measured in this nearly perpendicular derivative to provide an estimate for the σ-π contribution. $^6J_{4\alpha}$ from planar 3,5-dichlorostyrene was taken to represent the spin-polarizability term [27]. The resulting expression differs substantially from those of Schaefer *et al.* [24] and Barfield *et al.* [18].

In a follow-up study [23], Schaefer and Sebastian subjected 2-, 3- and 4-fluorostyrenes to the same treatment with results suggestive of a slightly higher barrier for the fluoro derivatives than in styrene itself. This conclusion is supported by theoretical evidence. Also pertinent to this discussion is the utility of stereospecific five-bond couplings to the α-proton as indicators of conformational populations in asymmetrically substituted styrenes. Based on theoretical predictions that this predominantly σ coupling should be maximal in all-*trans* conformers and on their relative insensitivity to non-planarity, it is asserted that couplings from the meta proton situated

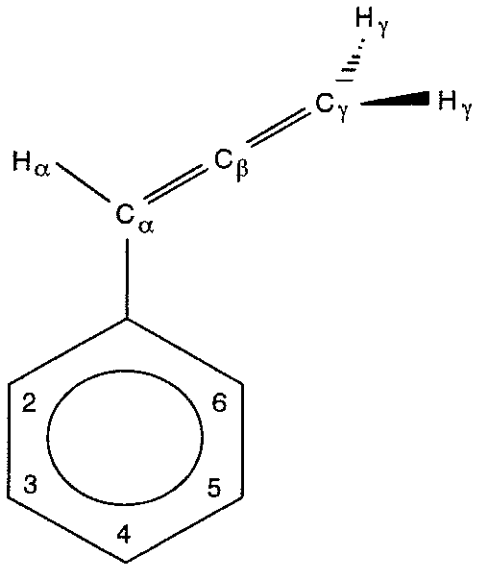

Figure 3: Molecular structure of phenylallene and atomic numbering scheme.

cis to the α-proton are negligible. In 3-fluorostyrene, for instance, the magnitude of $^5J_{5\alpha}$ relative to the sum of $^5J_{5\alpha}$ and $^5J_{3\alpha}$ in 4-fluorostyrene yields a *trans* population of 41%. This agrees with 6-31G computations and microwave data, for which values of 45% and 47% are obtained. A recent reinterpretation [28] of the supersonic jet SVL fluorescence spectrum succeeded in adjusting the conflicting *trans* population of 25% [29] published in 1989 to give a population of 42%. Furthermore, the populations deduced for 2- and 3-fluorostyrene as well as the related barriers for all three derivatives appear to be independent of solvent, lending support for the use of a gas phase potential in solution studies. Finally, long range couplings between ring fluorine and vinyl protons are discussed, demonstrating qualitative support for various mechanisms postulated on the precedent of analogous proton-proton lrJs.

Having developed what seems to be a reliable method for evaluating rotational barriers from lrJs in solution, a remaining problem is whether a barrier to planarity exists in styrene. Given the importance of steric factors in destablizing the planar conformer, it is of interest to examine a compound with similar conjugational energetics, but lacking the steric congestion between the beta and ortho nuclei. Phenylallene

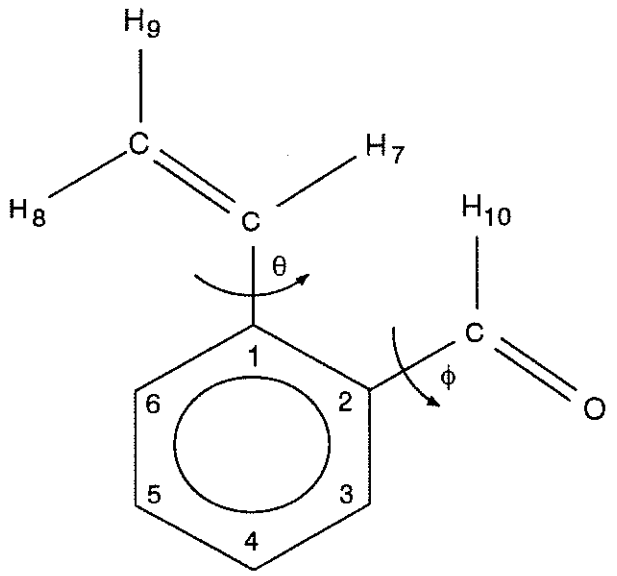

Figure 4: Molecular structure of 2-formylstyrene and atomic numbering scheme.

(Figure 3) appears to be a useful candidate for such a study. With its cumulenic carbon sidechain, there are expected to be no steric interactions in the region of interest, thus permitting an estimate of the steric destablization energy in styrene. In addition, the extended π system in the allenic group enables measurement of ${}^{n}\mathrm{J}(n = 6,7,8)$ for the methylene protons and an examination of their potential as conformational indicators.

An important test of these relationships for styrene emerges in 2-formylstyrene (Figure 4), where the close proximity and large rotational barrier of the formyl group force the vinyl group substantially out-of-plane, apparently without modifying the conjugational energy of the parent molecule[4]. Moreover, this molecule is of interest to photochemists because two chromophores are present in conjugation [30]. Apparently, irradiation of the O-*cis* conformer leads to the slow formation of a spiro

[4]MO computations on 4-formylstyrene indicate a negligible effect upon the barrier height in the styrene moiety (unpublished data). Specifically, in the 6-31G level computation, which is known to closely approximate experimental barrier determinations in styrene, no difference is observed for the barrier height in styrene and 4-formylstyrene. At the 6-31G* level, the difference is 160 J/mol.

triene, proceeding to further reaction, while the O-*trans* conformer undergoes a fast 1,5-hydrogen shift under irradiation to produce a methyl group at the β-carbon atom [30]. Clearly, the conformational information available from high-level computations and lrJs can illuminate the proposed photochemical mechanisms.

2 Experimental

2.1 Synthesis of compounds

2,6-Difluorostyrene, 2-hydroxynaphthaldehyde and all compounds required for the synthesis of phenylallene and 2-formylstyrene were obtained from Aldrich. Synthetic routes described below for phenylallene and 2-formylstyrene were performed by Dr. David M. MacKinnon.

Preparation of phenylallene followed the procedure published in the recent literature [31]. Bromoform was added dropwise to a solution of styrene and potassium hydroxide and stirred under nitrogen for 10 hours at room temperature. The mixture was extracted and dried over magnesium sulphate, yielding 1,1-dibromo-2-phenylcyclopropane by vacuum distillation. This compound was dissolved in ether and stirred vigourously with methyllithium for one minute before quenching the reaction with hydrochloric acid. After work-up, phenylallene was distilled as a colourless liquid. NMR samples were prepared immediately, due to instability of the monomer.

2-Formylstyrene was prepared from 3,4-dihydroisoquinoline by reaction with dimethyl sulfate in a solution of sodium hydroxide exactly as described in the literature [32]. The preparation of 3,4-dihydroisoquinoline involved treatment of *N*-2-phenethylformamide by heat and phosphoric acid. The desired product was distilled as a colourless oil and purified on a silica gel column.

2.2 Sample preparation

All compounds were prepared as dilute solutions (Table 1). For solvents lacking deuterium nuclei, a small amount of cyclohexane-d_{12} was added as an internal lock reference. Tetramethylsilane (TMS) was added to all solutions as an aid to shimming and chemical shift referencing in ^{1}H and ^{13}C NMR experiments. The 2,6-difluorostyrene solutions also included a few drops of hexafluorobenzene for shimming and shift referencing in the ^{19}F spectrum. All solutions were filtered into 5 *mm* od NMR tubes and degassed by six cycles of the freeze-pump-thaw procedure. The tubes were flame-sealed under vacuum such that reasonably symmetric tops were produced.

Table 1: Detailed composition of sample solutions

Compound	*Solvent*	*Conc.*	*Lock ref.*	*Shift ref.*
phenylallene	acetone-d_6	5.1 *mol*%	acetone-d_6	0.5 *mol*% TMS
	benzene-d_6	5.1 *mol*%	benzene-d_6	0.5 *mol*% TMS
2-formylstyrene	acetone-d_6	4.4 *mol*%	acetone-d_6	0.5 *mol*% TMS
	CS_2	5.6 *mol*%	10 *mol*% C_6D_{12}	0.5 *mol*% TMS
2,6-difluorostyrene	acetone-d_6	14.8 *mol*%	acetone-d_6	0.5 *mol*% TMS
				0.5 *mol*% C_6F_6
	CS_2	5.0 *mol*%	10 *mol*% C_6D_{12}	0.5 *mol*% TMS
				0.5 *mol*% C_6F_6
2-OH-naphthaldehyde	CCl_4	2.5 *mol*%	10 *mol*% C_6D_{12}	0.5 *mol*% TMS

2.3 Spectroscopy

All NMR spectra were acquired using a Bruker AM 300 spectrometer at a probe temperature of 300 K. Due to the importance of a stable and homogeneous external magnetic field in high-resolution NMR, the field homogeneity was typically monitored and refined every eight scans. This was done by shimming on the free induction decay (FID) of internal TMS to obtain an unenhanced linewidth less than 100 mHz and with a good Lorentzian lineshape. For high-resolution ^{1}H NMR spectra at 300.135 MHz, 32 FIDs were recorded using acquisition times of 20 to 40 seconds, depending on the sharpness of the resonances. The corresponding digital resolution is between 0.025 and 0.012 Hz/pt. After zero-filling to twice the original data table and multiplying by standard resolution enhancement functions (gaussian broadening, 0.6; lorentzian broadening, -0.1) fourier transformation produced frequency domain spectra with linewidths of 30 mHz or narrower. All chemical shifts are referenced to high frequency of the precisely-determined TMS resonance measured from the shimming procedure. For 2,6-difluorostyrene, ^{19}F NMR spectra at 282.38 MHz were acquired similarily, except that shimming procedures and chemical shift referencing utilized the C_6F_6 peak.

Carbon-13 NMR spectra of phenylallene were obtained at 75.48 MHz using acquisition times of 20 s, resulting in a digital resolution of 0.025 Hz/pt. Fully coupled high-resolution ^{13}C spectra were obtained for all three sidechain carbon nuclei in benzene-d_6 solution and for C_β in acetone-d_6 solution. These natural abundance samples required as many as 1800 scans to achieve a satisfactory signal-to-noise ratio. Carbon-hydrogen couplings within the sidechain were obtained by selectively decoupling the ring protons, which are separated from the allenyl protons by 280 Hz. Careful adjustment of the decoupling power ensured that intrachain couplings were not modified by residual irradiation. Chemical shifts for ^{13}C spectra were referenced to high frequency of the TMS resonance in survey spectra.

Numerous relative signs of long-range coupling constants were determined by par-

tial decoupling experiments [33]. Each sign determination is detailed in the text of section 3, and a more complete description is outlined with reference to phenylallene on page 37.

Spectra were analyzed using NUMMRIT, an extensively modified incarnation of NUMARIT [34], as embodied in the graphical user interface *Xsim* [35]. Proton and fluorine spectral analyses were carried out simultaneously, whereas carbon spectra were analysed separately for each carbon nucleus, owing to the vanishing probability of finding mutually coupled ^{13}C nuclei. For the sign determination of $^{5}J_{8,10}$ in 2-hydroxynaphthaldehyde, the spectrum was sufficiently complicated to preclude analysis by simple inspection. The program DOR [36], also available in the *Xsim* package, was used to disentangle the transitions and determine the relative sign.

While some difficulties were encountered in the analysis of the 2-hydroxynaphthaldehyde spectrum, many spectral parameters are certain. For this reason, a full discussion of this compound is not undertaken herein. Some points of interest, however, are mentioned in Section 4.

For 2,6-difluorostyrene, data from MO computations and NMR analyses appear to conflict. Further study is required to fully understand the nature of the internal rotational potential in this compound. A brief discussion of the available evidence is offered in Section 4.

2.4 Computations

Molecular orbital calculations of 2,6-difluorostyrene, 2-formylstyrene, phenylallene, 2-hydroxynaphthaldehyde, styrene and 2,6-dichlorostyrene were performed using the program *Gaussian 92* [37] installed on an IBM RS/6000 minicomputer. Hartree-Fock (HF) self consistent field (SCF) computations employed various basis sets available within this system as well as the semi-empirical AM1 algorithm [38]. Electron correlation was introduced using second-order Møller-Plesset perturbation theory with the 6-31G* basis. Computational details for each molecule are given within the text of section 3. In general, all geometric parameters were allowed to vary for a given value of the relevant torsion angle, θ, with the additional constraint that the benzene moiety remain planar. Total energies were evaluated for 15° increments of θ, spanning the appropriate range. At local minima, θ was allowed to relax, resulting in full geometry optimization.

These potentials were fit to equation 1 with NLIN, a non-linear regression subroutine within the SAS package. Plots of these functions were obtained using the SAS/Graph library's interpolation program and SigmaPlot version 1.02 from Jandel Scientific. Classical expectation values at 300 K were evaluated using the MAPLE V software package from the University of Waterloo.

Coupling constants were calculated using the INDO MO FPT approximation [20, 21] on the geometries obtained at HF/6-31G* in most cases. Conformational dependencies of these couplings were fit to various functions in $\cos^2\theta$, $\sin^2\theta$ and $\sin^2(\theta/2)$ using NLIN.

3 Results and Discussion

3.1 Phenylallene

3.1.1 Proton NMR

Proton NMR data from the phenylallene solutions described in Table 1 are detailed in Tables 2 and 3. Chemical shifts and coupling constants are given in units of *hertz (Hz)*. Numbers in parentheses are standard deviations in the last significant digit, as given by the NUMMRIT analysis. The spectra were treated as arising from an ABB′CC′XY$_2$ spin system. Representative examples[5] of spectral fits are displayed in Figures 5 to 19. The relative signs of long-range indirect spin-spin coupling constants (lrJs) from the methylene protons to the ring protons were determined by partial decoupling experiments [33]. A detailed description of this procedure is given in section 3.1.2 on page 37 with examples shown in Figures 20 to 23. The methylene spectral region could not be fit in the absence of a small, positive dipolar coupling between these protons (Figure 19).

The survey spectrum of phenylallene in acetone-d_6 was initially puzzling, the aromatic region containing only two multiplets, separated by less than 5 Hz, and a weak, broadly distributed signal 30 Hz to low frequency (Figure 5). Assuming the origin of this unique spectral pattern to be in strong second-order phenomena, a dilute solution of phenylallene in benzene-d_6 was prepared, and the resulting aromatic spectrum was sufficiently well-distributed to be analysable (Figure 13). On reapproaching the spectrum of the acetone-d_6 solution with spectral parameters obtained from the analysis of the benzene-d_6 solution, it was possible to reproduce the entire spectrum theoretically. The chemical shift difference between the ortho and meta protons in acetone-d$_6$ is 0.82 Hz (0.0027 ppm), giving rise to a spectrum dominated by two

[5]The computer program used to generate graphics in this document tends to introduce slight distortions into the spectra. Original experimental and theoretical spectral lineshapes are lorentzian or gaussian.

Table 2: ^{1}H NMR spectral parameters for phenylallene solutions in acetone-d_6 and benzene-d_6, excluding coupling constants between sidechain protons and ring nuclei.

Parameter	acetone-d_6	benzene-d_6
$\nu_2 = \nu_6$	2193.0697(9)	2164.4456(4)
$\nu_3 = \nu_5$	2192.251(1)	2133.8651(4)
ν_4	2158.7552(6)	2101.5166(5)
ν_α	1875.0779(9)	1813.4647(5)
ν_γ	1550.2593(8)	1458.0003(6)
$^4J_{\alpha,\gamma}$	- 6.8560(9)	- 6.8105(6)
$^3J_{23} = {}^3J_{56}$	7.779(1)	7.7768(6)
$^3J_{34} = {}^3J_{45}$	7.470(2)[a]	7.4419(5)
$^4J_{24} = {}^4J_{46}$	1.214(2)[a]	1.2434(5)
$^4J_{26}$	1.914(2)	1.9028(8)
$^4J_{35}$	1.427(2)	1.4327(8)
$^5J_{25} = {}^5J_{36}$	0.609(1)	0.6046(6)
$^2D_{\gamma,\gamma}$	+ 0.0124(5)	+ 0.0150(4)
Calculated trans.	826	826
Assigned trans.	622	617
Observed peaks	320	405
Largest difference	0.017	0.011
RMS deviation	0.008	0.005

a) These parameters are correlated by 0.875.

Table 3: ^{1}H NMR coupling constants between sidechain and ring protons for phenylallene solutions

Parameter	acetone-d_6	benzene-d_6
$^4J_{2,\alpha}$	$-0.376(1)^a$	$-0.3801(5)$
$^6J_{2,\gamma}$	$-0.583(1)^b$	$-0.5789(5)$
$^5J_{3,\alpha}$	$+0.282(1)^a$	$+0.2861(5)$
$^7J_{3,\gamma}$	$+0.207(1)^b$	$+0.2048(4)$
$^6J_{4,\alpha}$	$-0.213(1)$	$-0.2108(7)$
$^8J_{4,\gamma}$	$-0.6097(8)$	$-0.6038(6)$

a) These parameters are correlated by 0.563 b) These parameters correlated by 0.554.

prominent bands of peaks separated by 4.3 Hz, roughly the average value of para couplings to the ortho and meta protons (Table 2).

The presence of a small dipolar coupling between the methylene protons $D_{\gamma\gamma}$ arises from partial alignment of phenylallene in the external magnetic field. The spectral consequences of this incompletely averaged coupling are shown in Figure 19, where it can be seen that distinct splittings are observed in the high frequency portion of the methylene doublet. Introduction of a *negative* coupling of the same magnitude splits the peaks in the low frequency portion of the doublet.

The positive sign of $D_{\gamma\gamma}$ is consistent with the emerging conformational description of phenylallene. In particular, lrJs and MO computations, discussed below, suggest a predominantly planar molecule, with a $\langle \sin^2 \theta \rangle$ of about 0.1. For this conformation, the methylene interproton vector is perpendicular to the plane of the molecule. Given the sign of the diamagnetic anisotropy for aromatic molecules, a positive dipolar coupling is, indeed, anticipated [39, 40]. For the perpendicular conformer, therefore, this dipolar coupling would be negative. In view of this, if the anisotropy of the

diamagnetic susceptibility were known, along with the internuclear distance between the methylene protons in phenylallene, one could relate $D_{\gamma\gamma}$ to the torsional potential. Furthermore, if the calculated potential is, in fact, correct, and if the molecule orients in the same way as benzene, then the signs of the ring proton coupling constants to the gamma protons are absolute, and independent of the sign determinations described below.

The magnitude of $D_{\gamma\gamma}$ differs slightly for phenylallene solutions in acetone-d_6 and benzene-d_6, the values being 12.4(5) and 15.0(4) mHz, respectively. Initially, one may be tempted to conclude that this signifies a solvent-dependent change in the barrier. It is also necessary, however, to consider that the alignment factor may be higher in benzene-d_6 solution, thus increasing the observed dipolar coupling. A strategy for assessing alignment factors and the diamagnetic anisotropy uncomplicated by internal rotation would require deuteration at a ring proton, as described in references [39, 40]. Another approach might be to take advantage of the fact that D varies as the *square* of the applied magnetic field. At 500 MHz, then, $D_{\gamma\gamma}$ would be 34 and 42 mHz, for acetone-d_6 and benzene-d_6, still rather small. The available experimental data, therefore, do not permit adjudication between these two factors, or indeed any solid conclusion in this connection.

Observation of a finite dipolar coupling constant necessitates considering potential dipolar contributions to other, closely situated protons. Because, however, the magnitude of $D_{\gamma\gamma}$ decreases as the cube of internuclear distance, only intraring ortho couplings may be affected. The close approach of the alpha and ortho protons in the planar conformer may also qualify for consideration. Furthermore, for dipolar vectors parallel to the molecular plane, the geometric scaling factor is $-\frac{1}{2}$, in contrast to the $+1$ factor for perpendicular dipolar vectors. Accordingly, no improvement in spectral fits were realized on introduction of these small, negative dipolar couplings, but the corresponding Js may be assumed to have an uncertainty of about 3 mHz. More pertinent, perhaps, is the observed solvent-dependence of the proton-proton indirect

spin-spin coupling constants within the phenyl ring (Table 2). This dependence is larger than the expected dipolar coupling constants, as documented for a wide variety of benzene derivatives (see, for example, references [41] and [42].)

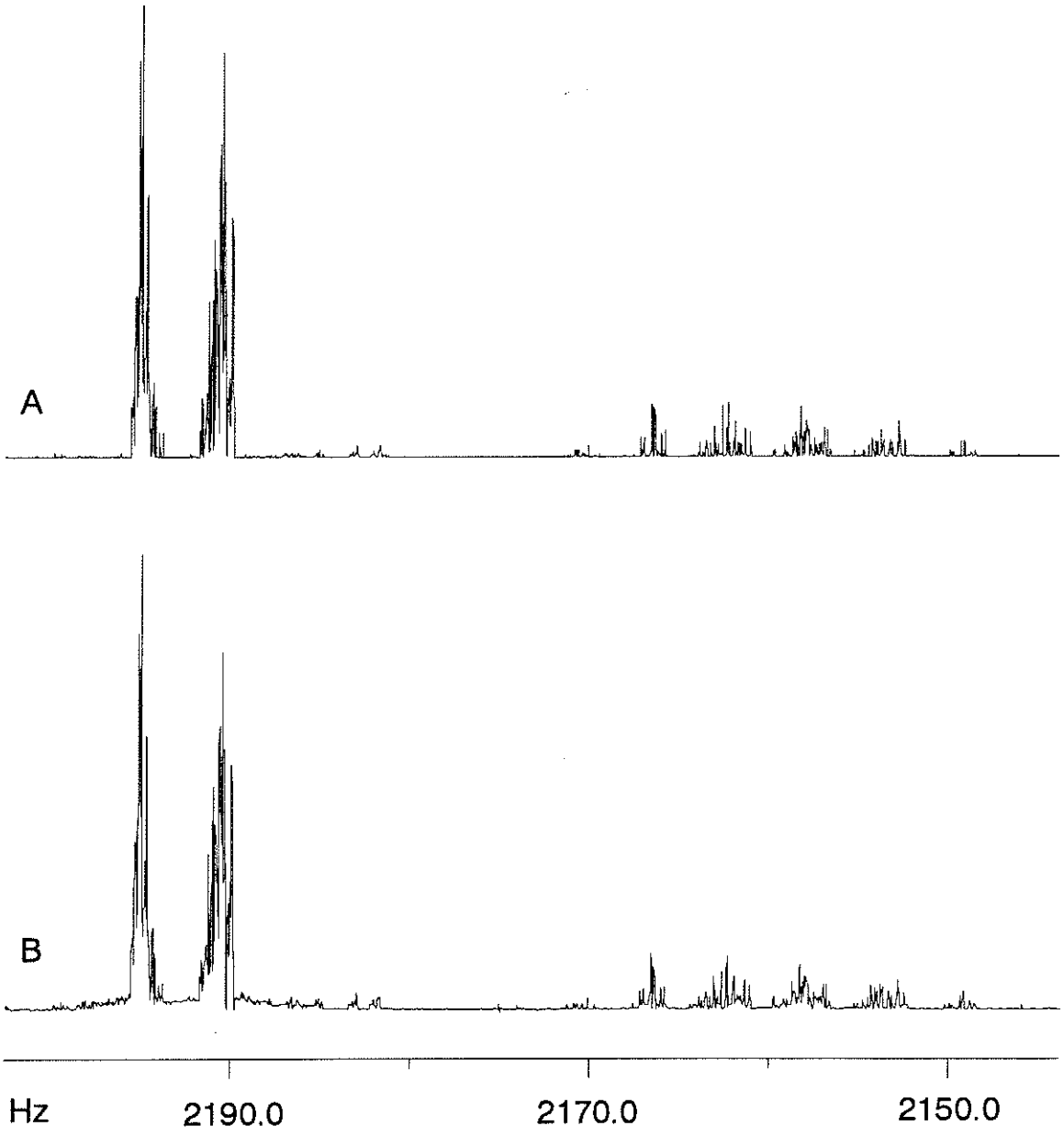

Figure 5: ^{1}H NMR spectrum of phenylallene aromatic region in acetone-d_6. A) Theoretical spectrum; B) Experimental spectrum.

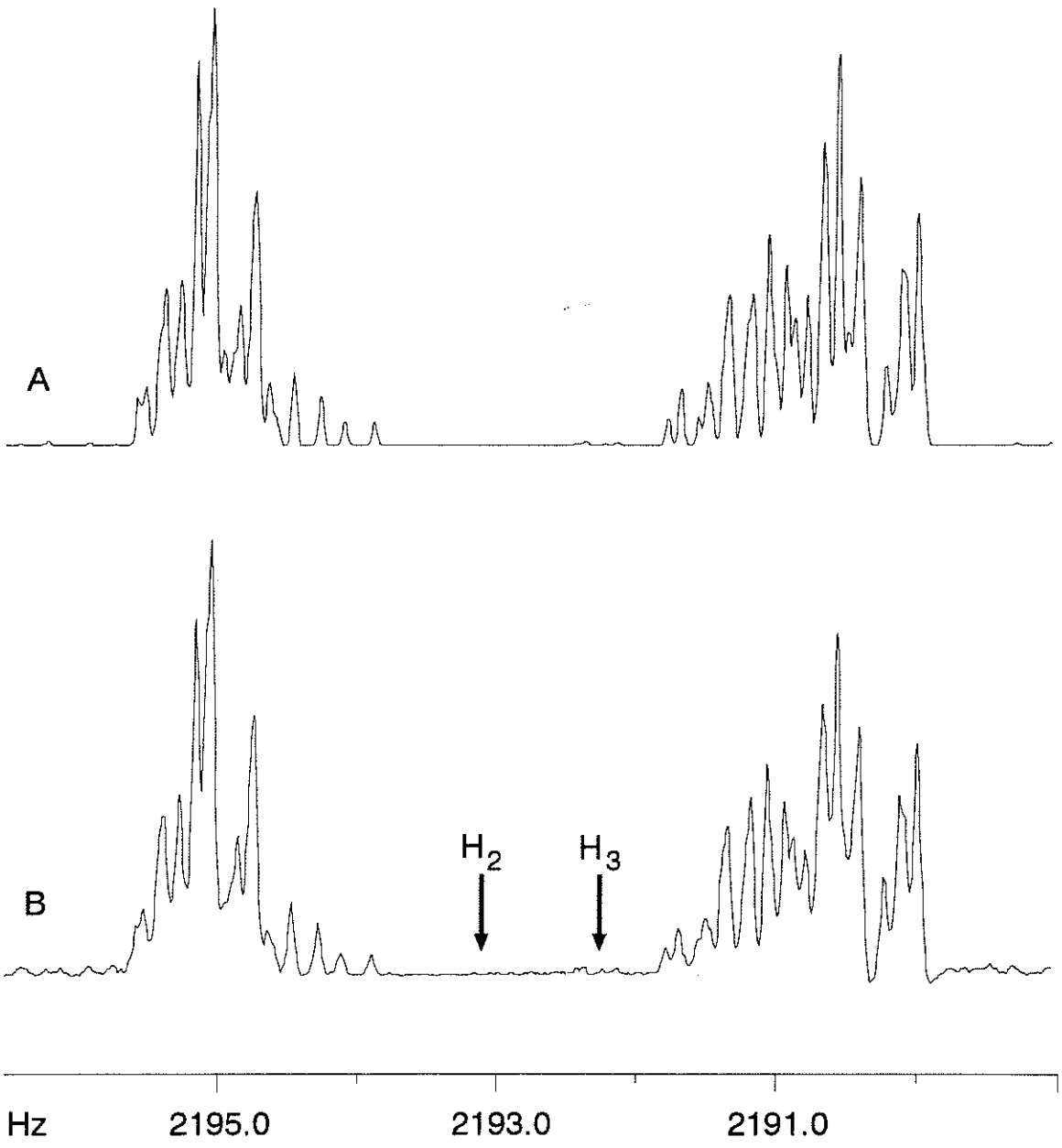

Figure 6: ^{1}H NMR spectrum of phenylallene ortho and meta protons in acetone-d_6. A) Theoretical spectrum with a linewidth of 0.05 Hz; B) Experimental spectrum.

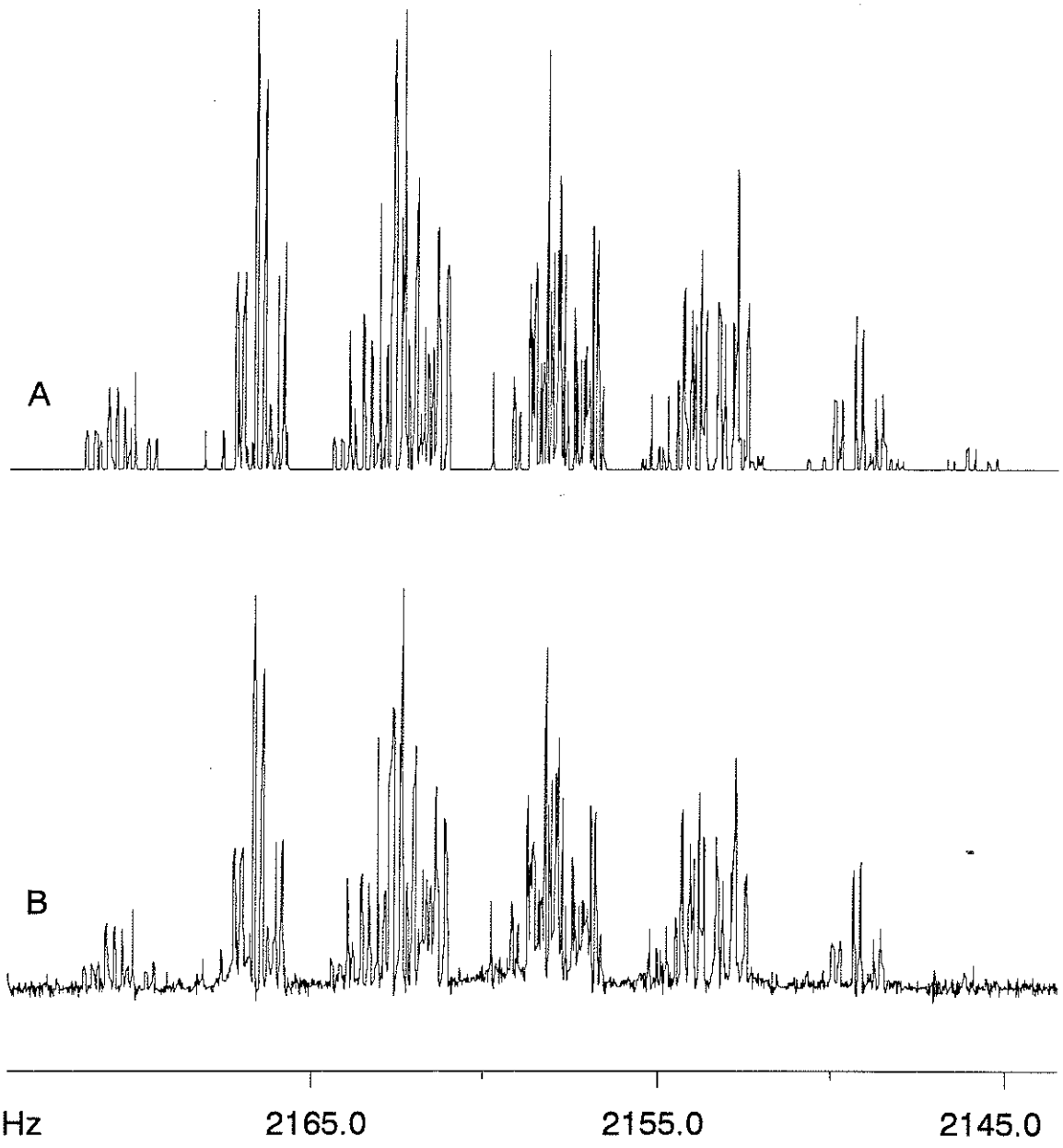

Figure 7: ^{1}H NMR spectrum of phenylallene para region in acetone-d_6. A) Theoretical spectrum with a linewidth of 0.05 Hz; B) Experimental spectrum.

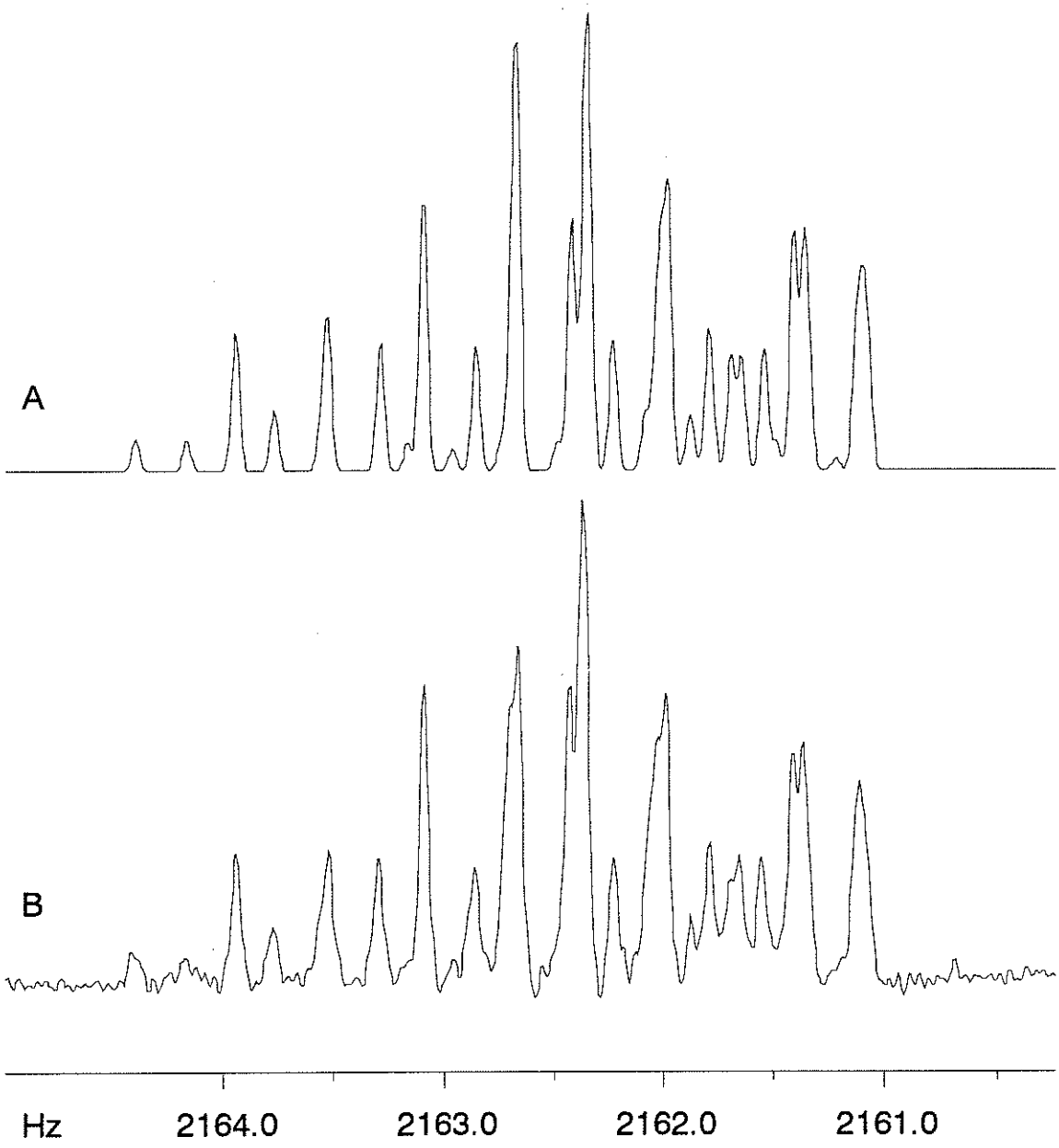

Figure 8: ^{1}H NMR spectral fragment of phenylallene para region in acetone-d_6. A) Theoretical spectrum with a linewidth of 0.04 Hz; B) Experimental spectrum.

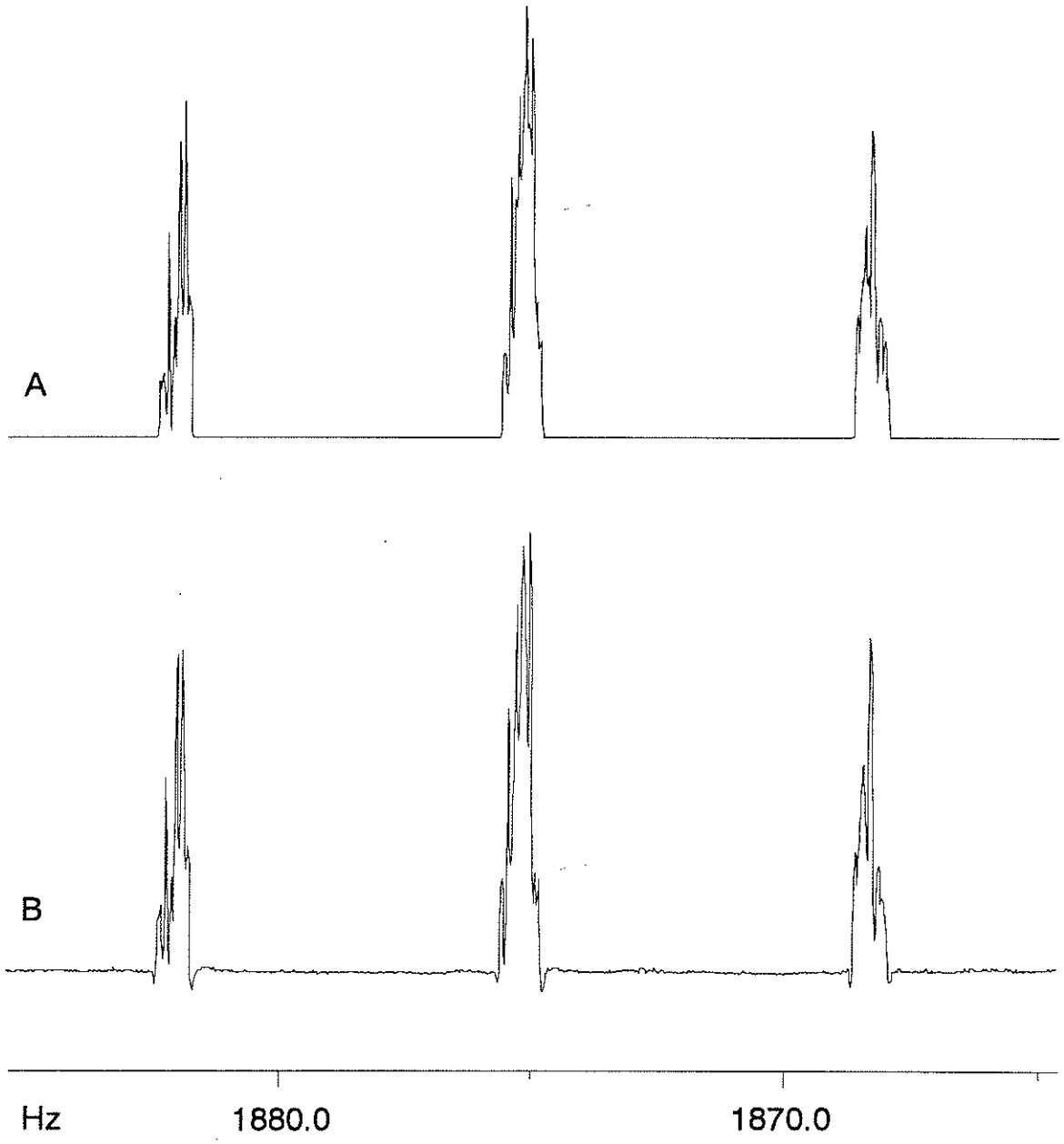

Figure 9: ^{1}H NMR spectrum of phenylallene alpha region in acetone-d_6. A) Theoretical spectrum; B) Experimental spectrum.

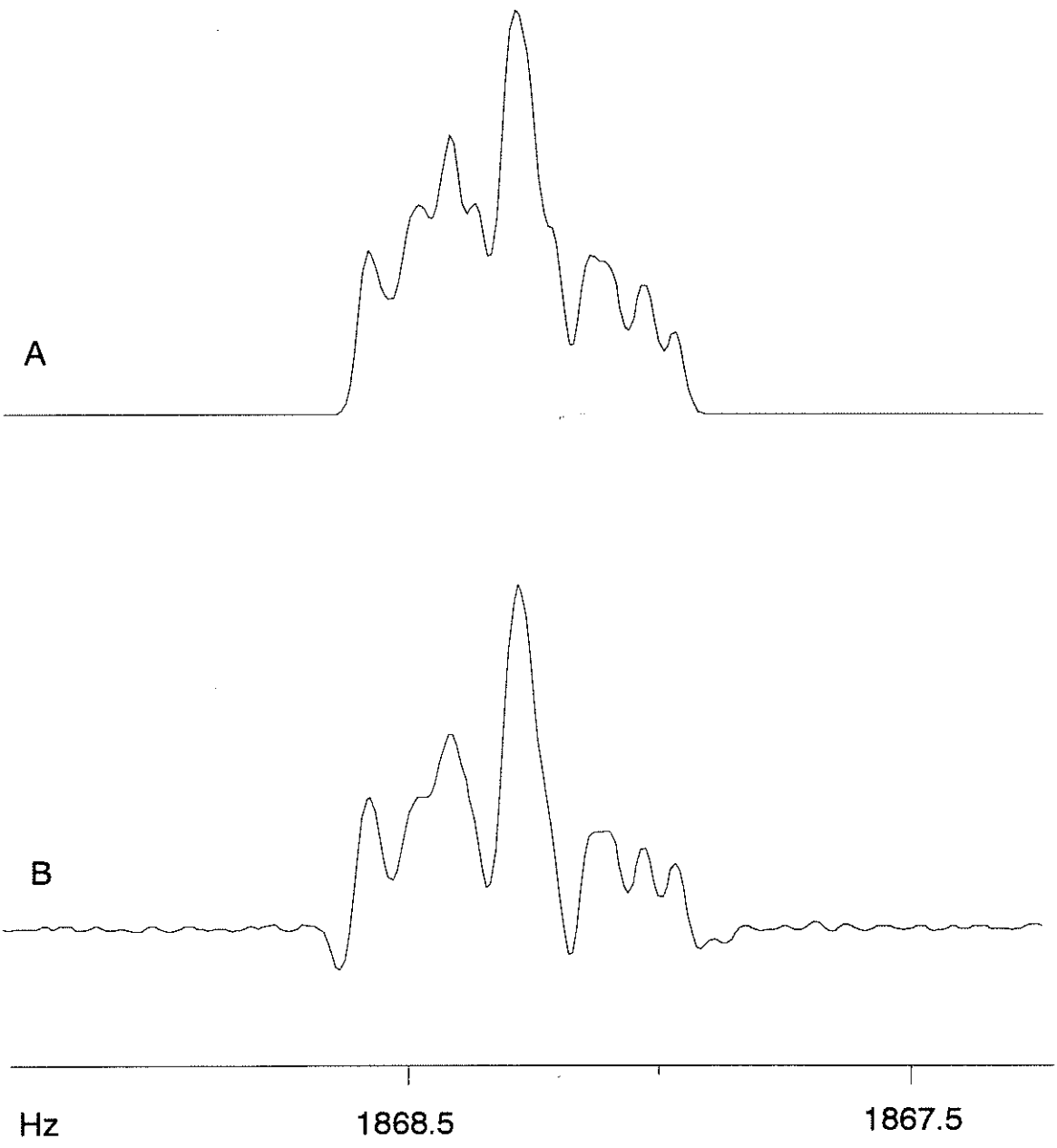

Figure 10: ^{1}H NMR spectrum of the low frequency portion of the phenylallene alpha region in acetone-d_6. A) Theoretical spectrum with a linewidth of 0.05 Hz; B) Experimental spectrum.

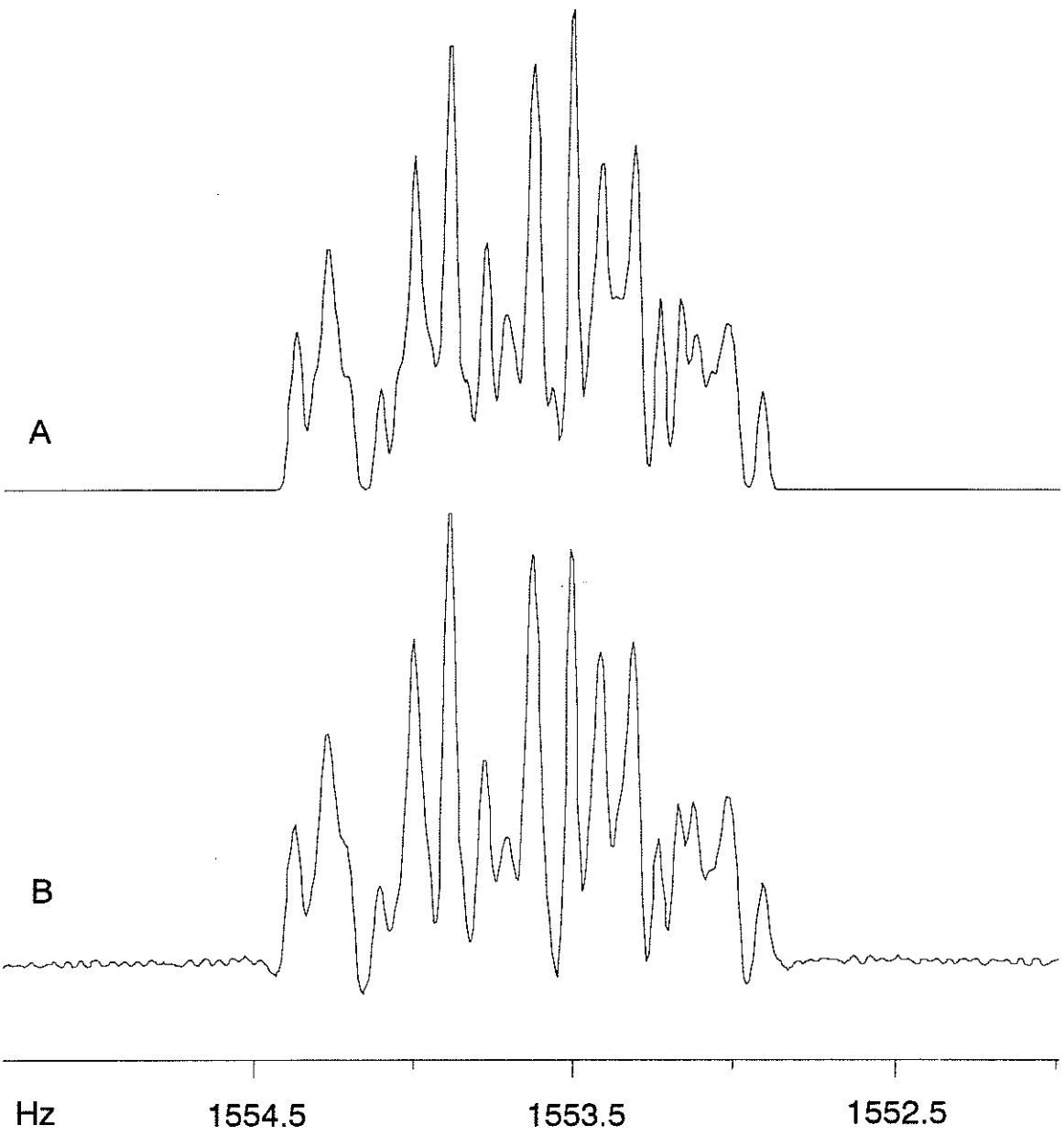

Figure 11: ^{1}H NMR spectrum of the high frequency portion of the phenylallene gamma 'doublet' in acetone-d_6. A) Theoretical spectrum with a linewidth of 0.04 Hz; B) Experimental spectrum.

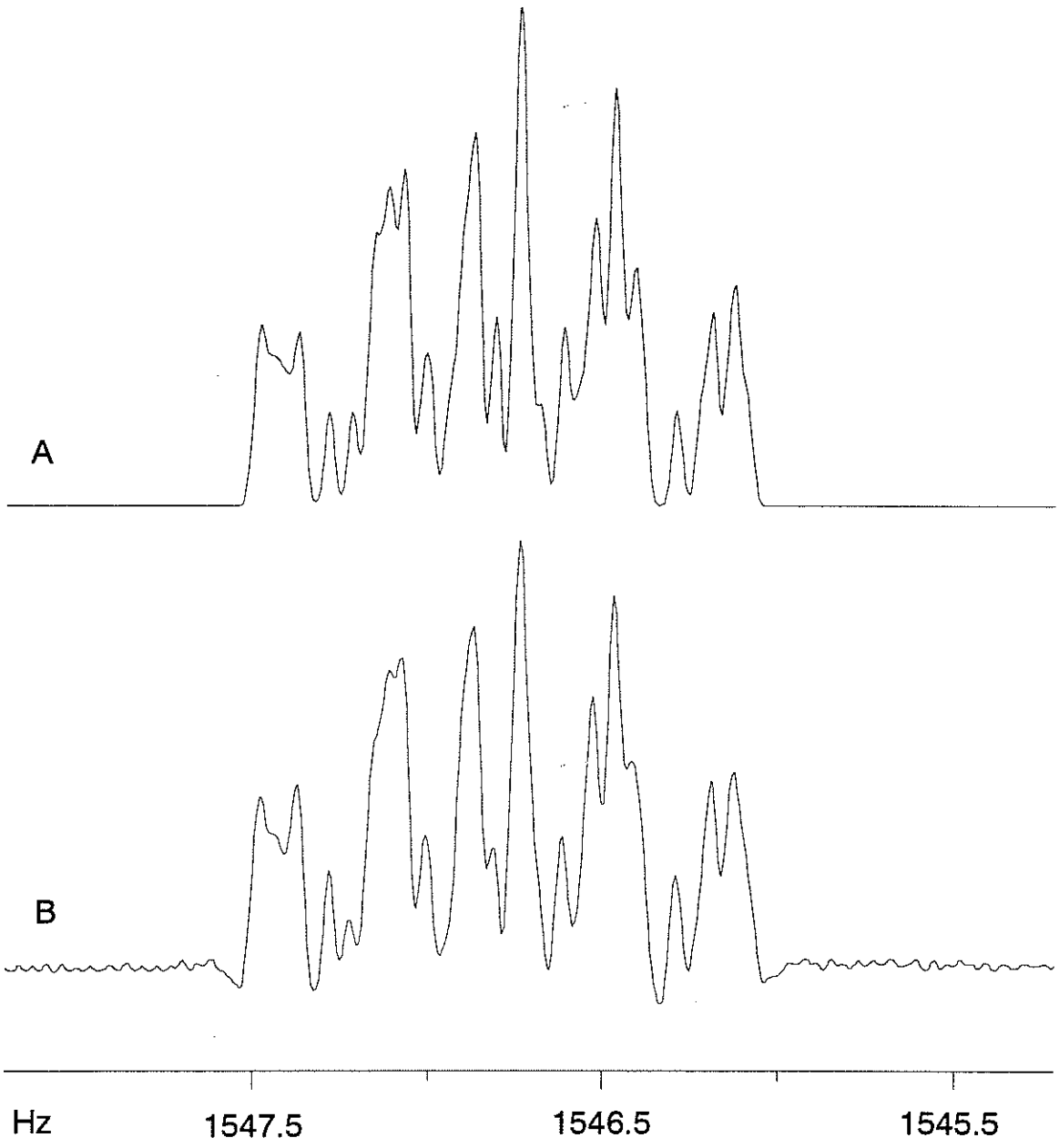

Figure 12: ^{1}H NMR spectrum of the low frequency portion of the phenylallene gamma 'doublet' in acetone-d_6. A) Theoretical spectrum with a linewidth of 0.04 Hz; B) Experimental spectrum.

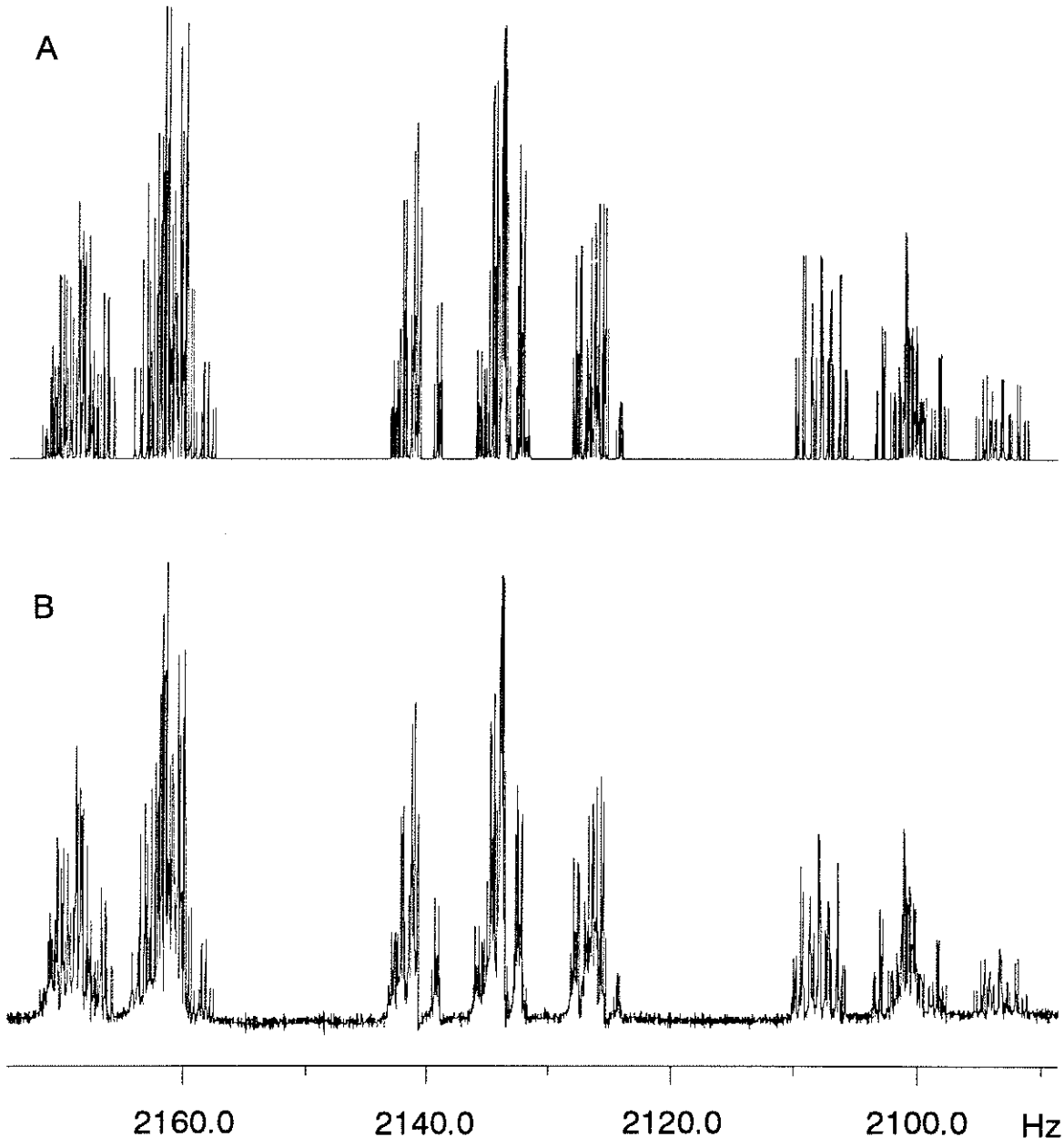

Figure 13: ^{1}H NMR spectrum of phenylallene aromatic region in benzene-d_6. A) Theoretical spectrum; B) Experimental spectrum.

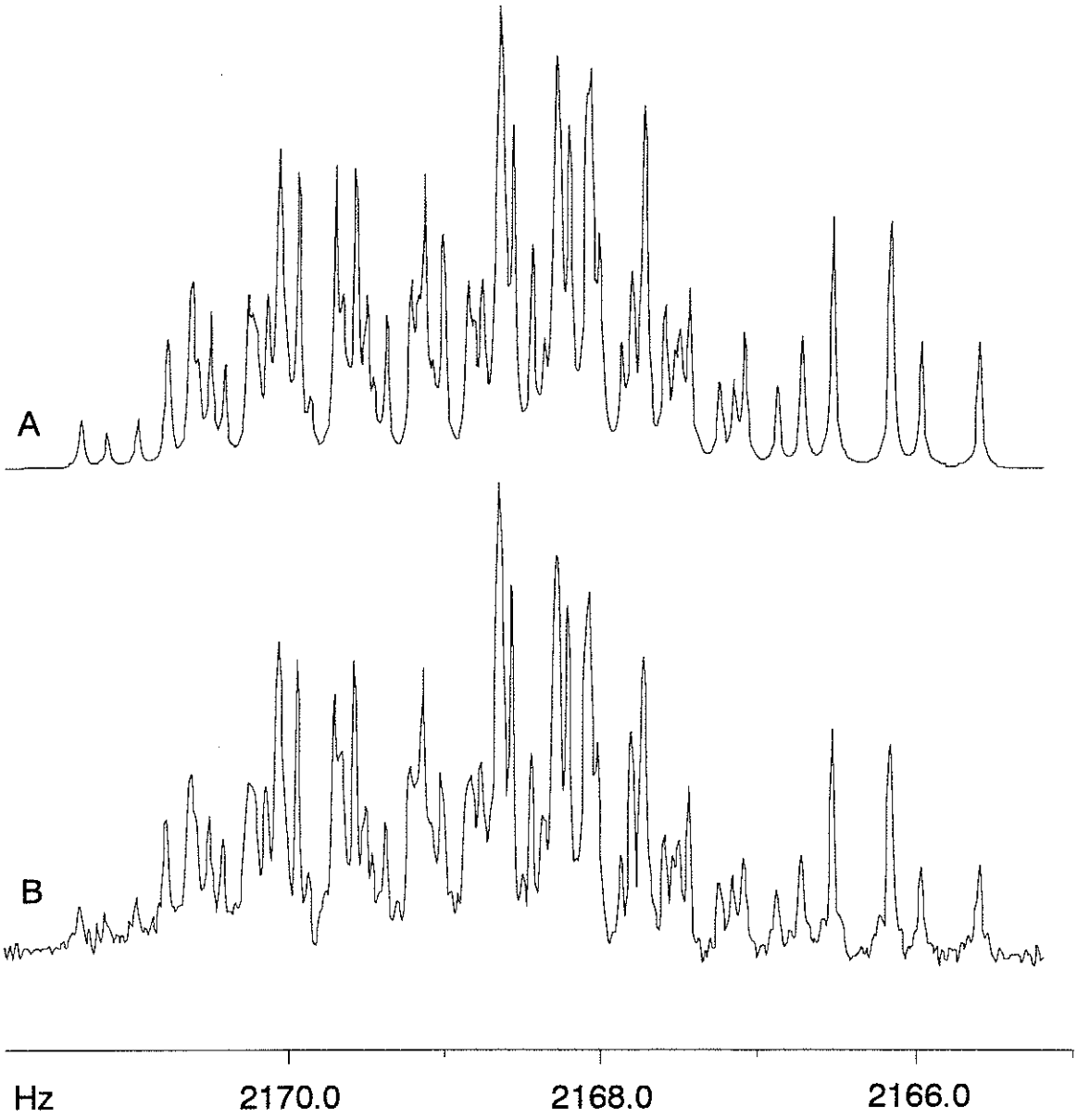

Figure 14: ^{1}H NMR spectrum of high frequency portion of phenylallene ortho 'doublet' in benzene-d_6. A) Theoretical spectrum with a linewidth of 0.035 Hz; B) Experimental spectrum.

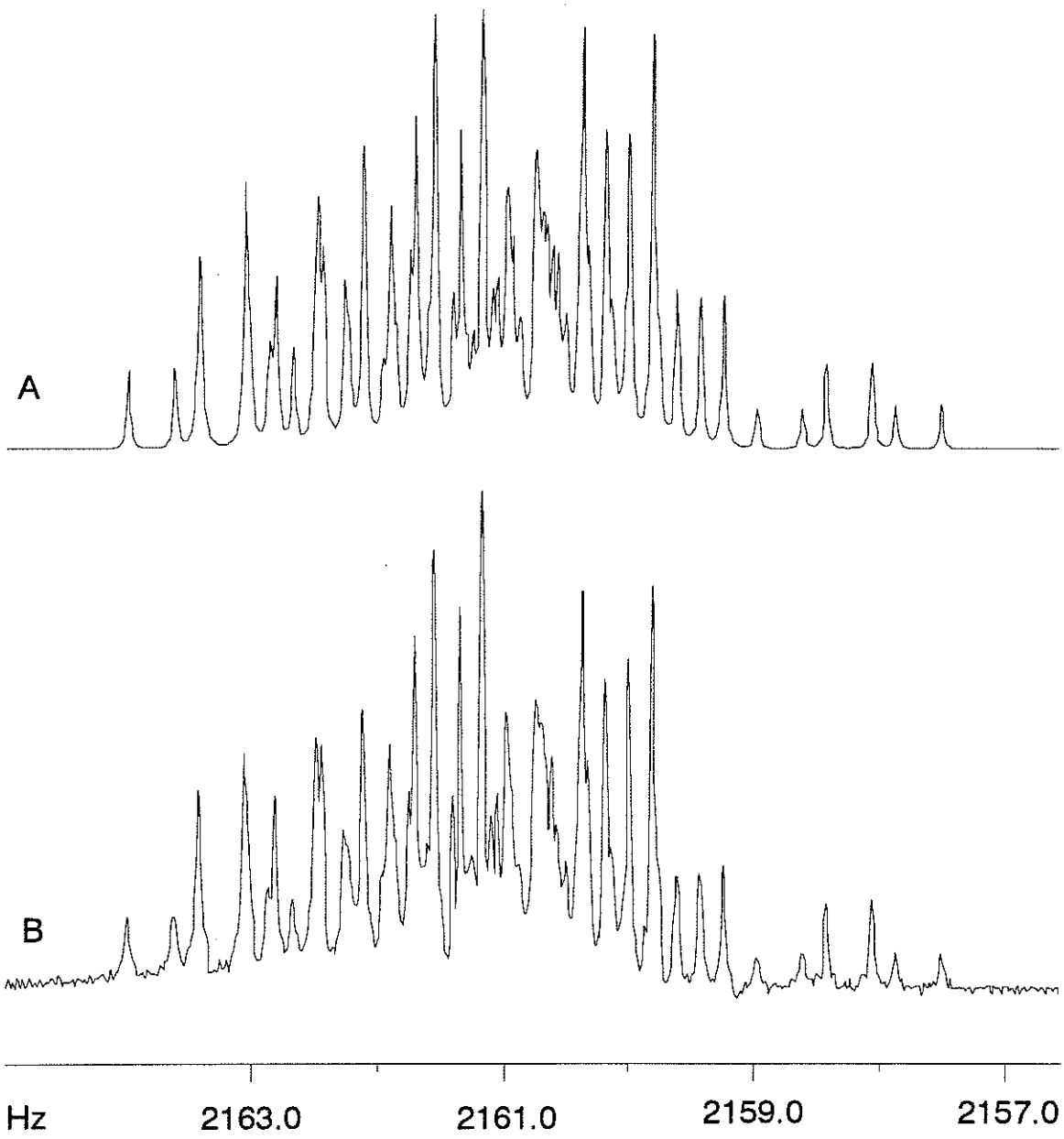

Figure 15: ^{1}H NMR spectrum of low frequency region of phenylallene ortho protons in benzene-d_6. A) Theoretical spectrum with a linewidth of 0.035 Hz; B) Experimental spectrum.

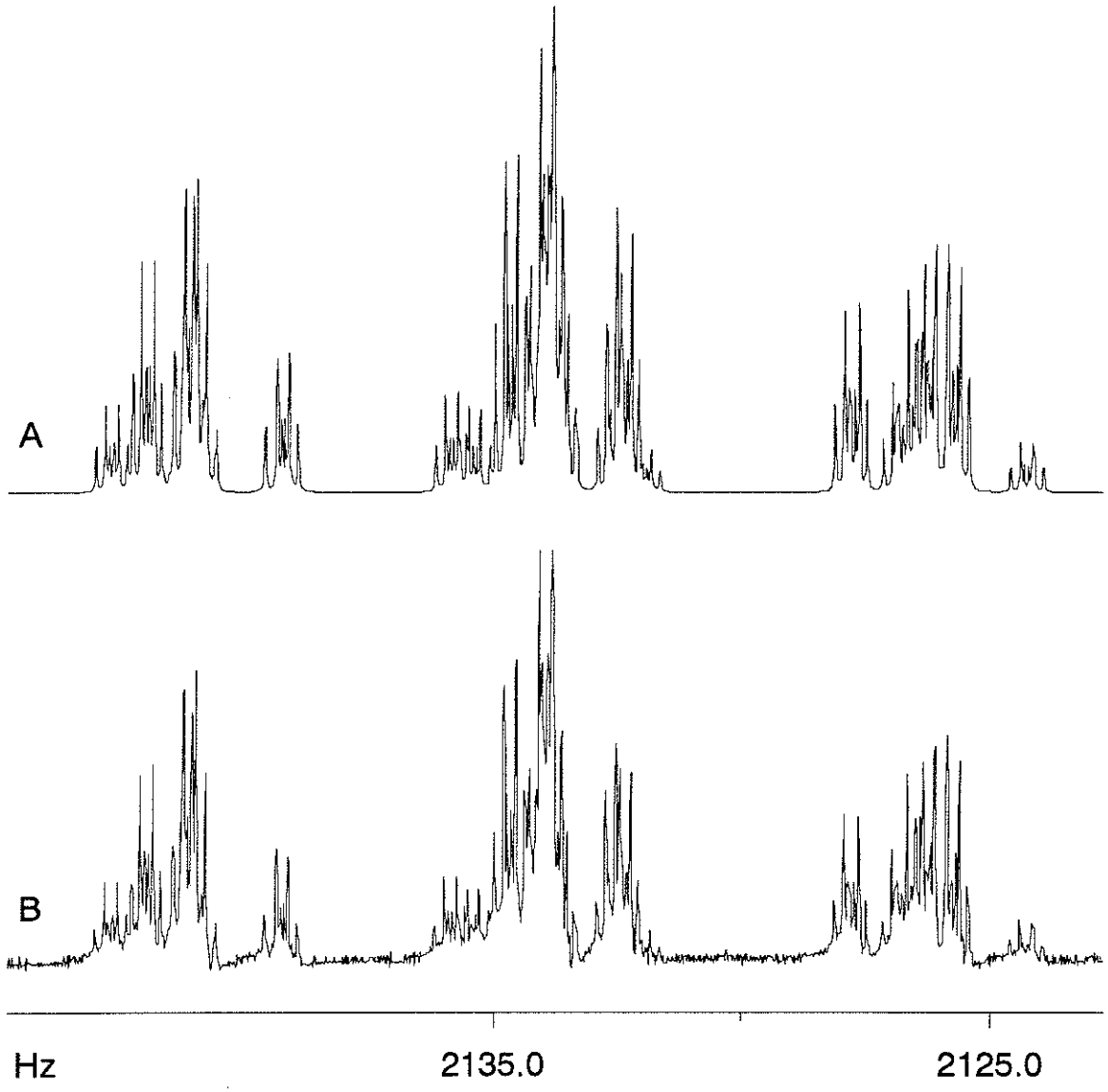

Figure 16: ^{1}H NMR spectrum of phenylallene meta protons in benzene-d_6. A) Theoretical spectrum with a linewidth of 0.035 Hz; B) Experimental spectrum.

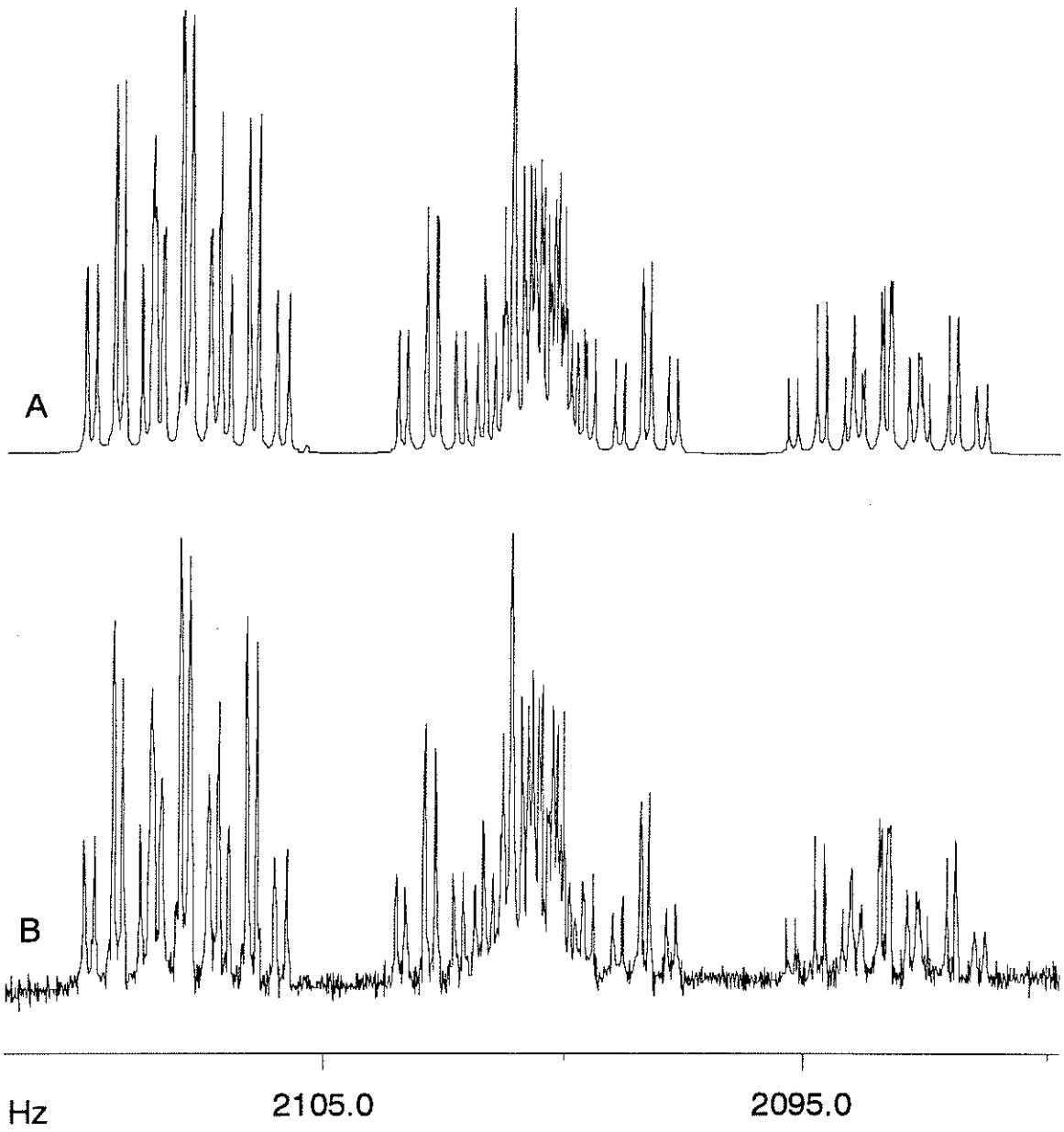

Figure 17: ^{1}H NMR spectrum of phenylallene para protons in benzene-d_6. A) Theoretical spectrum with a linewidth of 0.035 Hz; B) Experimental spectrum.

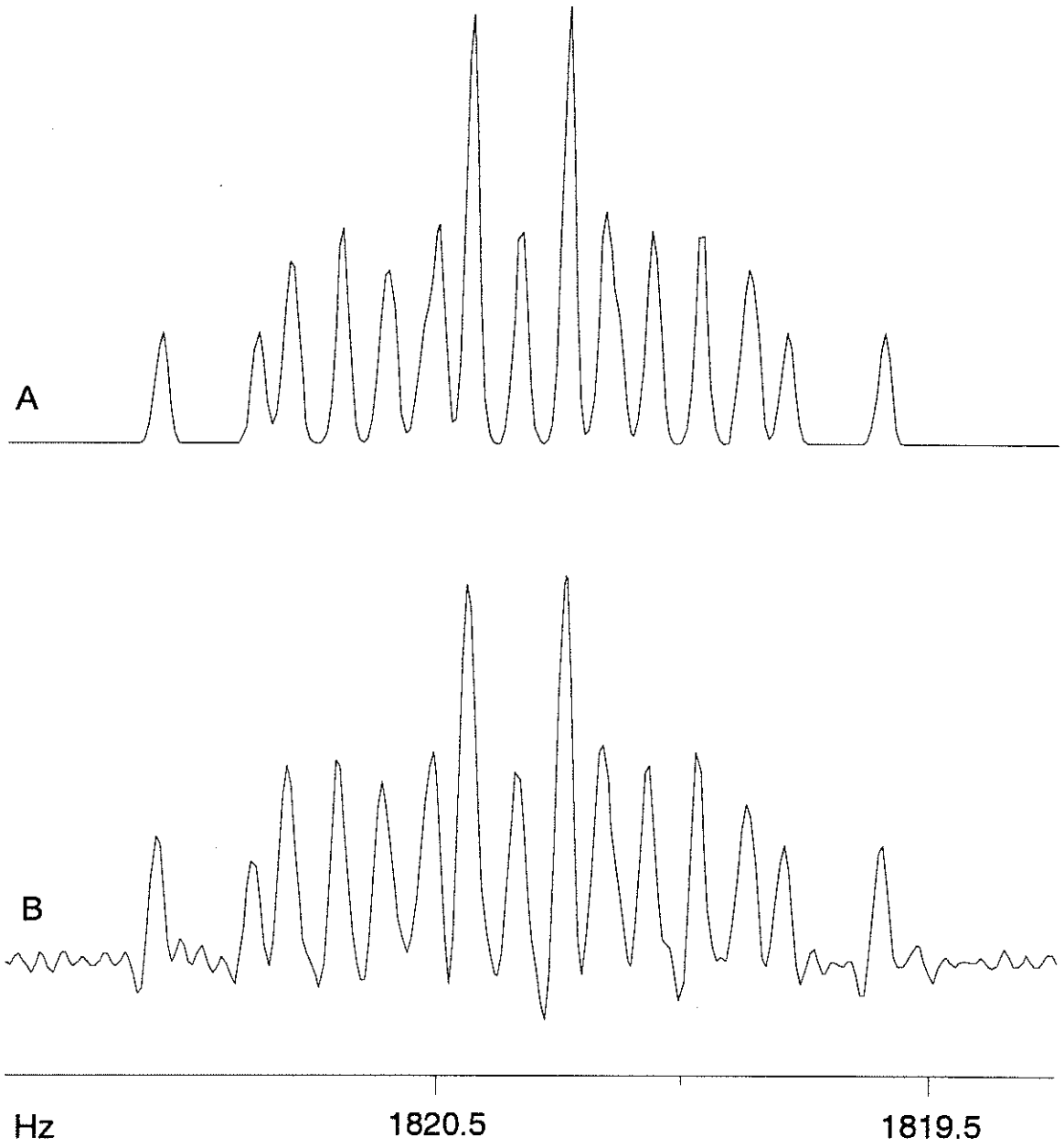

Figure 18: ^{1}H NMR spectrum of high frequency portion of phenylallene alpha 'triplet' in benzene-d_6. A) Theoretical spectrum with a linewidth of 0.035 Hz; B) Experimental spectrum.

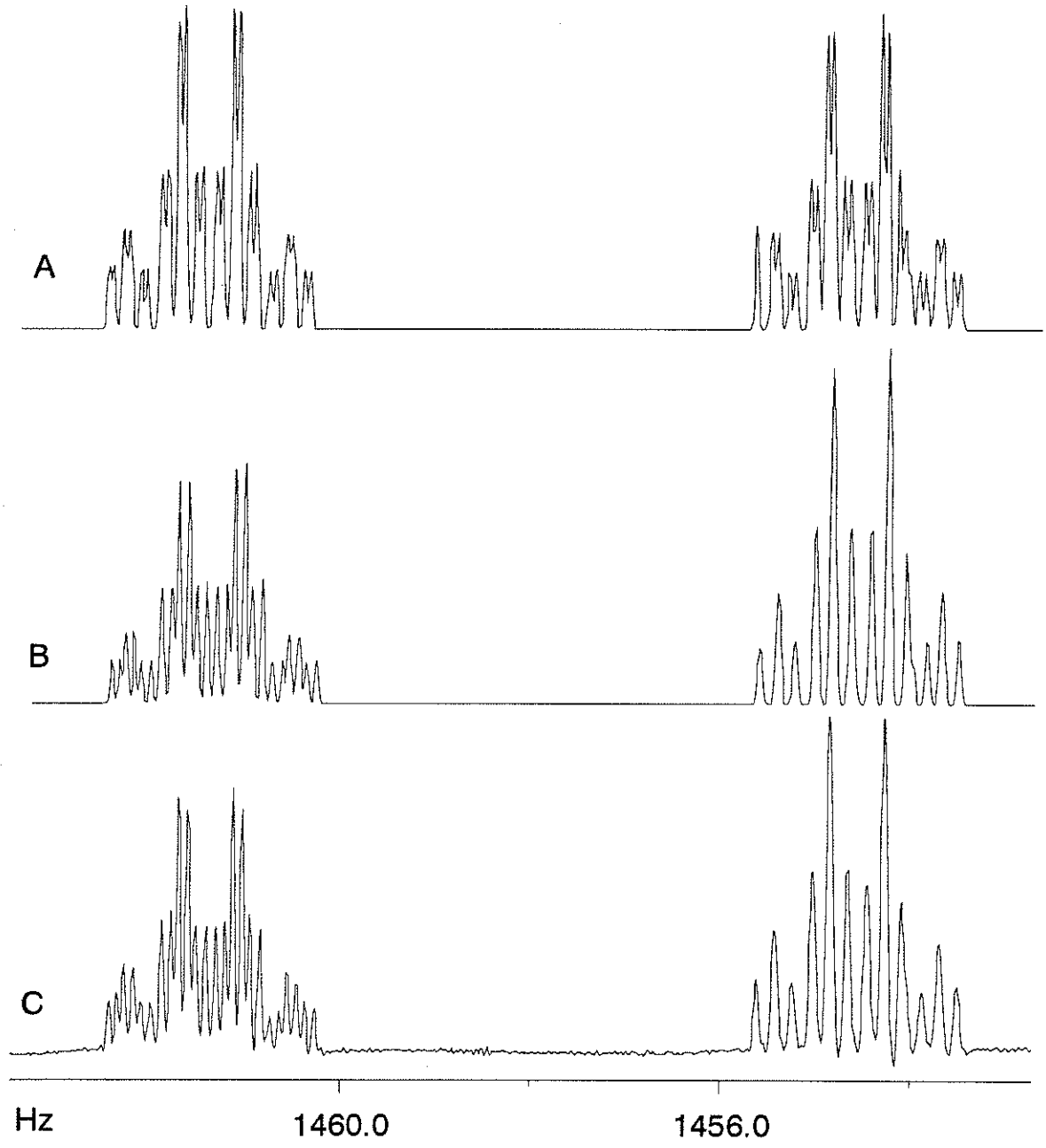

Figure 19: ^{1}H NMR spectrum of phenylallene methylene protons in benzene-d_6. A) Best fit theoretical spectrum in the absence of a dipolar coupling between these protons; B) Best fit theoretical spectrum with a positive dipolar coupling of 0.0150(4) Hz; C) Experimental spectrum.

3.1.2 Sign Determinations

The relative signs of indirect spin-spin coupling constants can be determined by double resonance experiments given favourable spectral conditions [33]. NMR transitions depend on the local magnetic environment, each transition corresponding to a specific spin orientation of other coupled nuclei. Spin states can be assigned labels, following the convention that for a positive sign, the spin state of the high frequency transition is labelled "+" and the low frequency transition is labelled "–". Weak irradiation of a particular transition will perturb only transitions, observed in the spectra of other nuclei, which share a common energy level. Since the high-resolution NMR Hamiltonian is symmetric with respect to the reversal of all signs, only *relative* signs can be determined in this way.

Figure 20 shows the labelling of the gamma proton spin states for each transition of the alpha proton given that the four-bond coupling between them, $^4J_{\alpha\gamma}$, is negative [43, 44, 45]. Present in each portion of the 'triplet' are small splittings arising from couplings to ring protons (see Figure 18). Weakly irradiating the peak bands for a given spin state of the gamma protons will result in the decoupling (or perturbation) of only those transitions associated with that given gamma spin state. Figure 21 illustrates the collapse of the doublet in the para proton spectrum related to the gamma protons by a negative coupling. Had $^8J_{4\gamma}$ been positive, the doublet at 2095.4 Hz would have collapsed. A second experiment (not shown) verified this sign. Similar procedures were carried out to determine the relative signs for $^7J_{3\gamma}$ and $^6J_{2\gamma}$ (Figures 22 and 23).

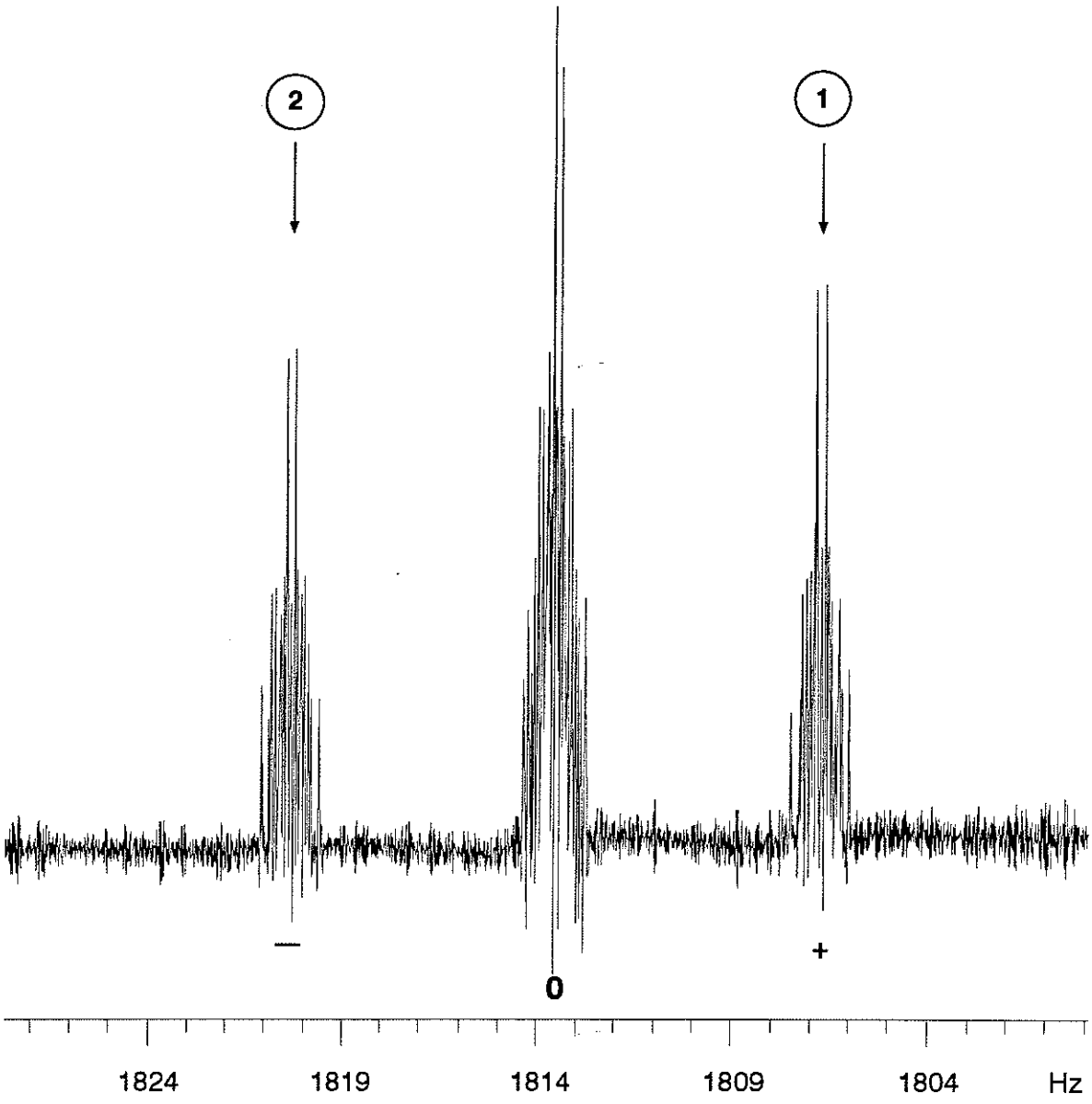

Figure 20: ^{1}H NMR spectrum of the alpha proton in phenylallene in benzene-d_6 solution with gamma proton spin states labelled according to convention given that $^4J_{\alpha\gamma}$ is negative (see text for details). Frequencies of irradiation in experiments 1 and 2 are indicated by arrows.

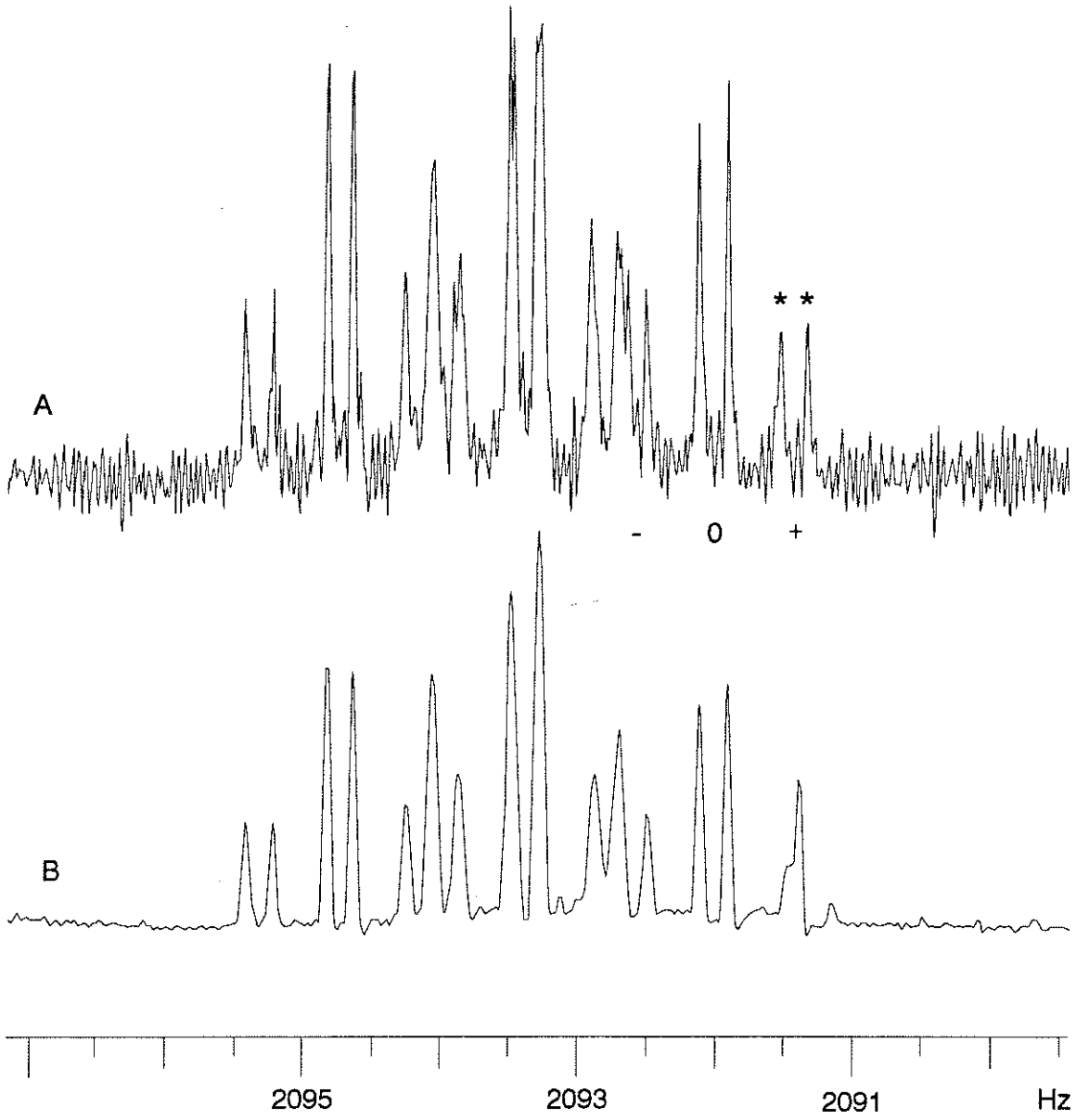

Figure 21: Sign determination of $^{8}J_{4\gamma}$. A) ^{1}H NMR spectrum of the low frequency portion of the para proton 'triplet' in phenylallene; B) The same region while weakly irradiating the alpha proton for a positive spin state of the gamma protons (experiment 1 in figure 20). Given signs are based on a negative $^{8}J_{4\gamma}$ and confirmed by the collapse of the starred doublet. The apparent difference in the noise level is due to differing levels of resolution enhancement.

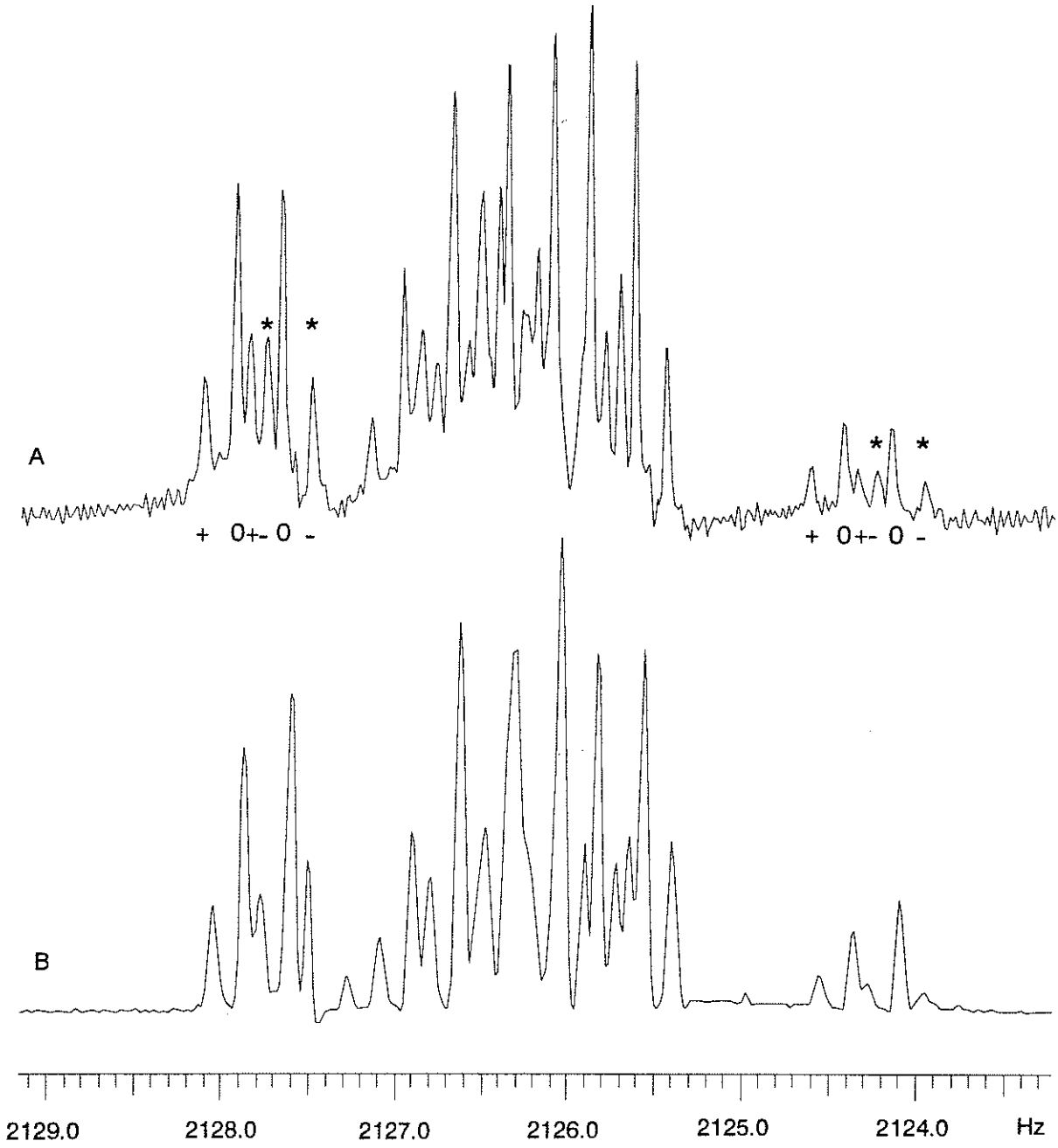

Figure 22: Sign determination of $^{7}J_{3\gamma}$. A) ^{1}H NMR spectrum of the low frequency portion of the meta proton 'triplet' in phenylallene; B) The same region while weakly irradiating the alpha proton for a negative spin state of the gamma protons (experiment 2 in figure 20). Given signs are based on a positive $^{7}J_{3\gamma}$ and confirmed by the collapse of the starred doublets.

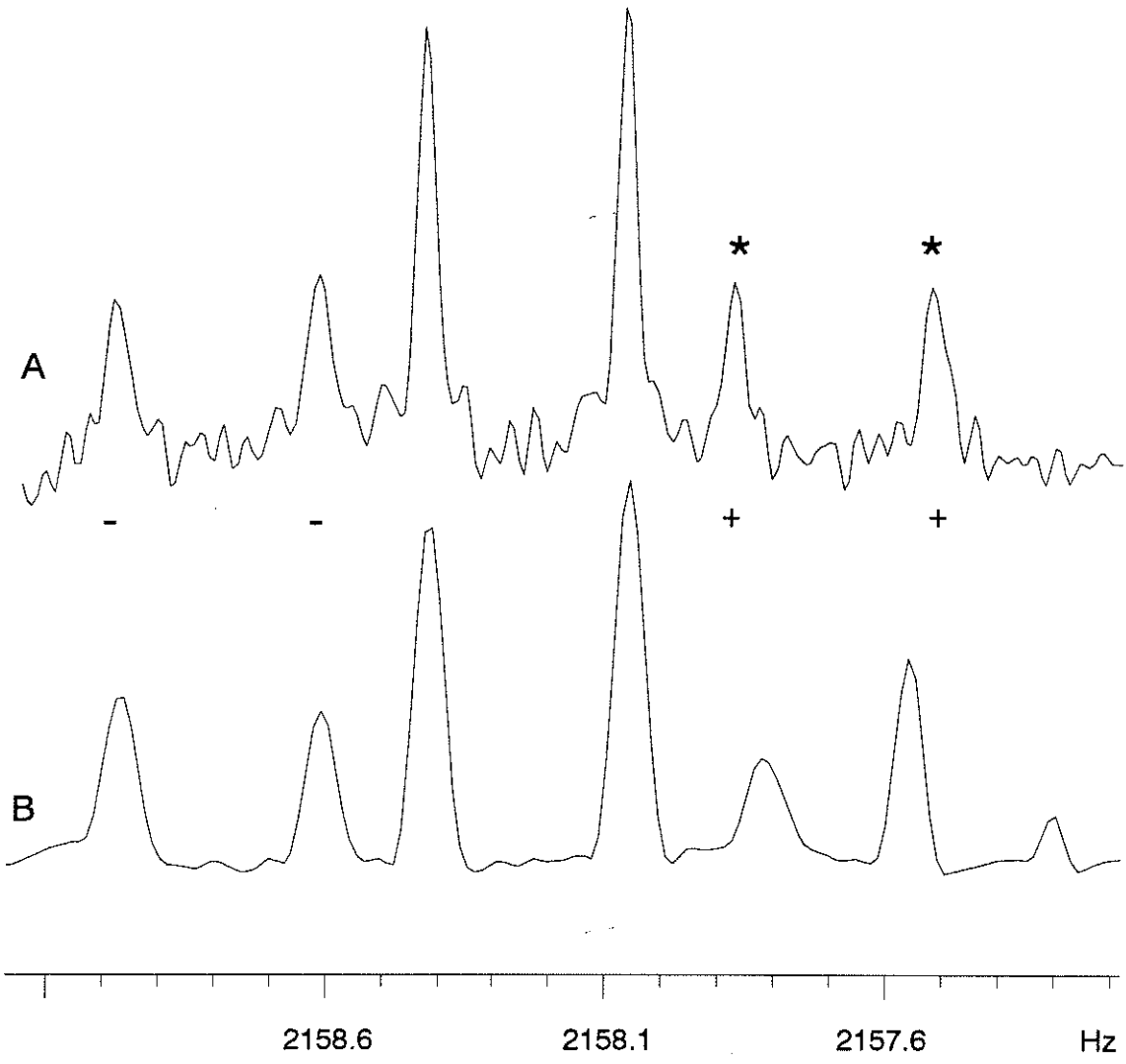

Figure 23: Sign determination of $^{6}J_{2\gamma}$. A) ^{1}H NMR spectrum of the low frequency portion of the ortho proton 'doublet' in phenylallene; B) The same region while weakly irradiating the alpha proton for a positive spin state of the gamma protons (experiment 1 in figure 20). Given signs are based on a negative $^{6}J_{2\gamma}$ and and confirmed by the perturbation of the starred doublets.

3.1.3 Carbon-13 NMR

Carbon-13 NMR data for the sidechain in phenylallene are listed in Tables 4 and 5. Figures 24 through 30 showcase selected spectral regions and theoretical fits. The signs of coupling constants within the allenyl group (Table 4) are known [46], whereas those of the intergroup coupling constants (Table 5) are based on theory or analogous compounds.

Spectra of phenylallene in acetone-d_6 solution with decoupled ring protons (Figures 24 to 26) were analysed as arising from an AB_2X spin system, where X represents the alpha, beta or gamma carbon. Fully coupled ^{13}C NMR spectra of the phenylallene sidechain in benzene-d_6 solution (Figure 28 to 30) were analysed as $ABB'CC'MXY_2$ spin systems, where M is the appropriate sidechain carbon. Good fits were obtained for these cases, given the spectral complexity and poor signal-to-noise ratio. Fully coupled spectra of C_β, acquired in both solvents, proved more difficult to analyse. A satisfactory fit for the benzene-d_6 solution was obtained, but the extreme second-order character of the ortho and meta protons in acetone-d_6 solution precluded an acceptable analysis of C_β in this solvent. The spectral consequences of virtual coupling show that the associated coupling constants, $^4J(H_2, C_\beta)$ and $^5J(H_3, C_\beta)$, have opposite signs.

One striking observation is the *decrease* in $^1J(H_\alpha, C_\alpha)$ and $^1J(H_\gamma, C_\gamma)$, of 3.9 and 1.0 Hz on moving from the benzene-d_6 solution to the polar acetone-d_6 solution. The neat compound, containing also 10% v/v benzene-d_6 and 5% v/v TMS, yields a $^1J(H_\alpha, C_\alpha)$ of 161.5(3) Hz [46], which lies in between the values determined in acetone-d_6 and benzene-d_6 solutions. In most cases, an *increase* is observed in passing to a more polar environment [47, 48, 49], as understood by models in which the electric field from the solvent causes a redistribution of charge in the whole molecule containing the C–H bond [47]. If, however, charge redistribution is localized in the bond, a decrease is indeed predicted [47]. Why this should be the case for the allenyl moiety is unknown, and would benefit from further study for a number of its

derivatives.

Solvent perturbations of other spectral parameters in Table 4 are also observed. Two- and three-bond carbon-hydrogen coupling constants shift by a few percent. Such perturbations have not been previously reported. Carbon-13 NMR chemical shifts in the allenyl group display solvent effects as large as 0.54 *ppm* and vary in sign. Different yet, are those shifts reported for a 2 M solution of phenylallene in $CDCl_3$ [50]. Chemical shift computations of the free molecule would be of interest, and appear possible, judging from satisfactory results for allene [51].

Table 4: Selected ^{13}C NMR spectral parameters in phenylallene

Parameter[a]	acetone-d_6	benzene-d_6
$\nu(C_\alpha)^b$	94.273	94.391
$\nu(C_\beta)$	210.404	209.868
$\nu(C_\gamma)$	78.887	78.605
$^1J(H_\alpha, C_\alpha^c)$	158.65	162.53
$^1J(H_\gamma, C_\gamma)$	167.25	168.23
$^2J(H_\alpha, C_\beta)$	– 3.27	– 3.45
$^2J(H_\gamma, C_\beta)$	– 4.46	– 4.46
$^3J(H_\gamma, C_\alpha)$	8.08	8.16
$^3J(H_\alpha, C_\gamma)$	6.99	7.18

a) Chemical shifts are in *ppm*, to high frequency of the TMS resonance at 75.48 MHz; J couplings are in Hz. b) Standard deviations as given by the spectral analysis are less than 0.01 Hz. c) Signs within the allenyl fragment are known [46].

Table 5: Long-range $^nJ_{H,C}$ (Hz) in phenylallene from ^{13}C NMR spectra.

Parameter[a]	benzene-d_6	*Parameter*	benzene-d_6
$^3J(H_2, C_\alpha)^b$	(+)5.36	$^6J(H_3, C_\gamma)$	(–)0.04(2)
$^4J(H_2, C_\beta)$	(–)0.62	$^5J(H_4, C_\alpha)$	(+)0.91
$^5J(H_2, C_\gamma)$	(+)0.43	$^6J(H_4, C_\beta)$	(–)0.42
$^4J(H_3, C_\alpha)$	(+)0.80	$^7J(H_4, C_\gamma)$	(+)0.28
$^5J(H_3, C_\beta)$	(+)0.22		

a) Standard deviations as given by the spectral analysis are less than 0.01 Hz unless otherwise indicated. b) Signs in parentheses are based on theory or analogous compounds.

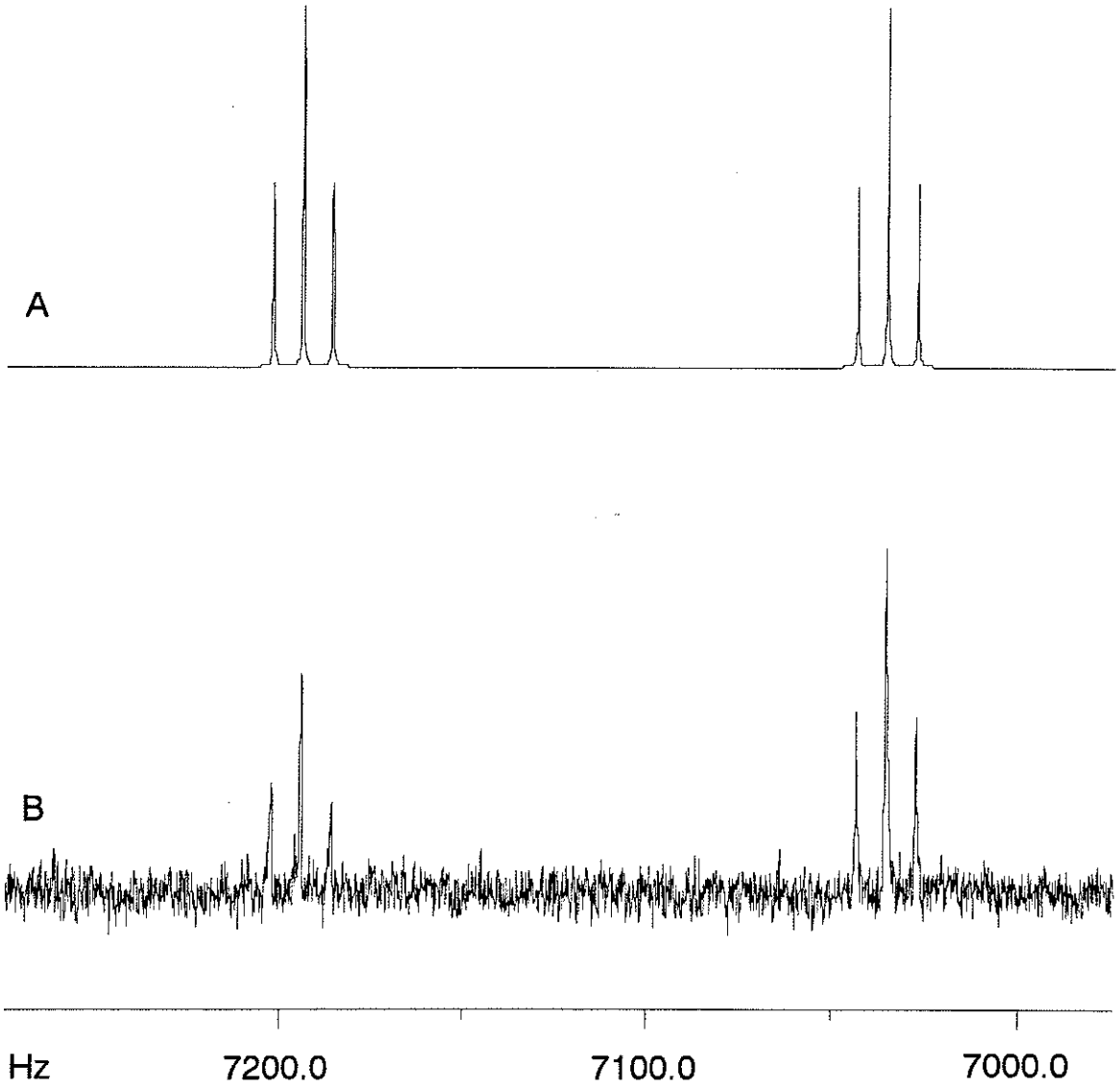

Figure 24: ^{13}C NMR spectrum of phenylallene alpha carbon in acetone-d_6 with ring protons decoupled. A) Theoretical spectrum with a linewidth of 0.2 Hz; B) Experimental spectrum.

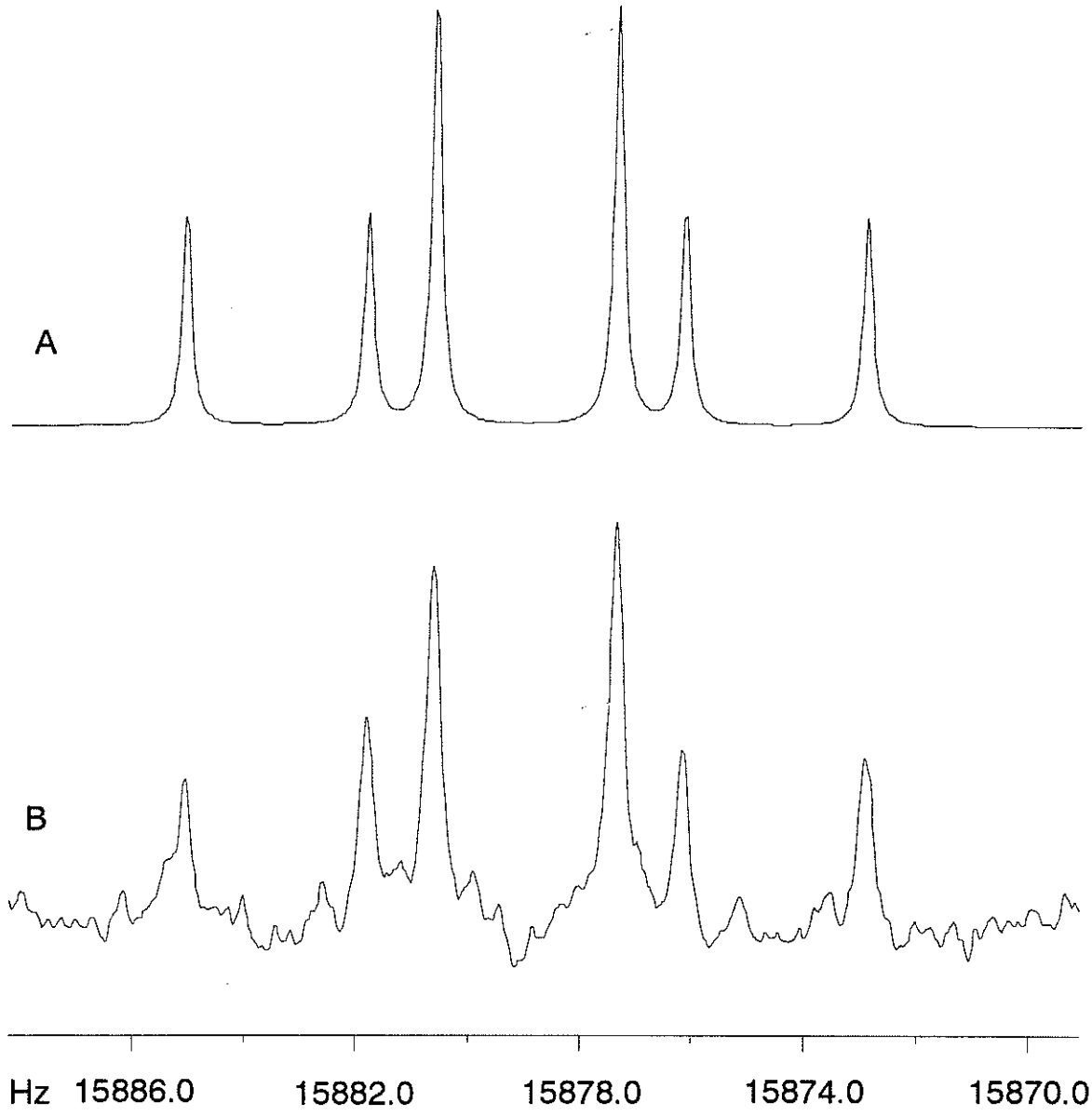

Figure 25: ^{13}C NMR spectrum of phenylallene beta carbon in acetone-d_6 with ring protons decoupled. A) Theoretical spectrum with a linewidth of 0.2 Hz; B) Experimental spectrum.

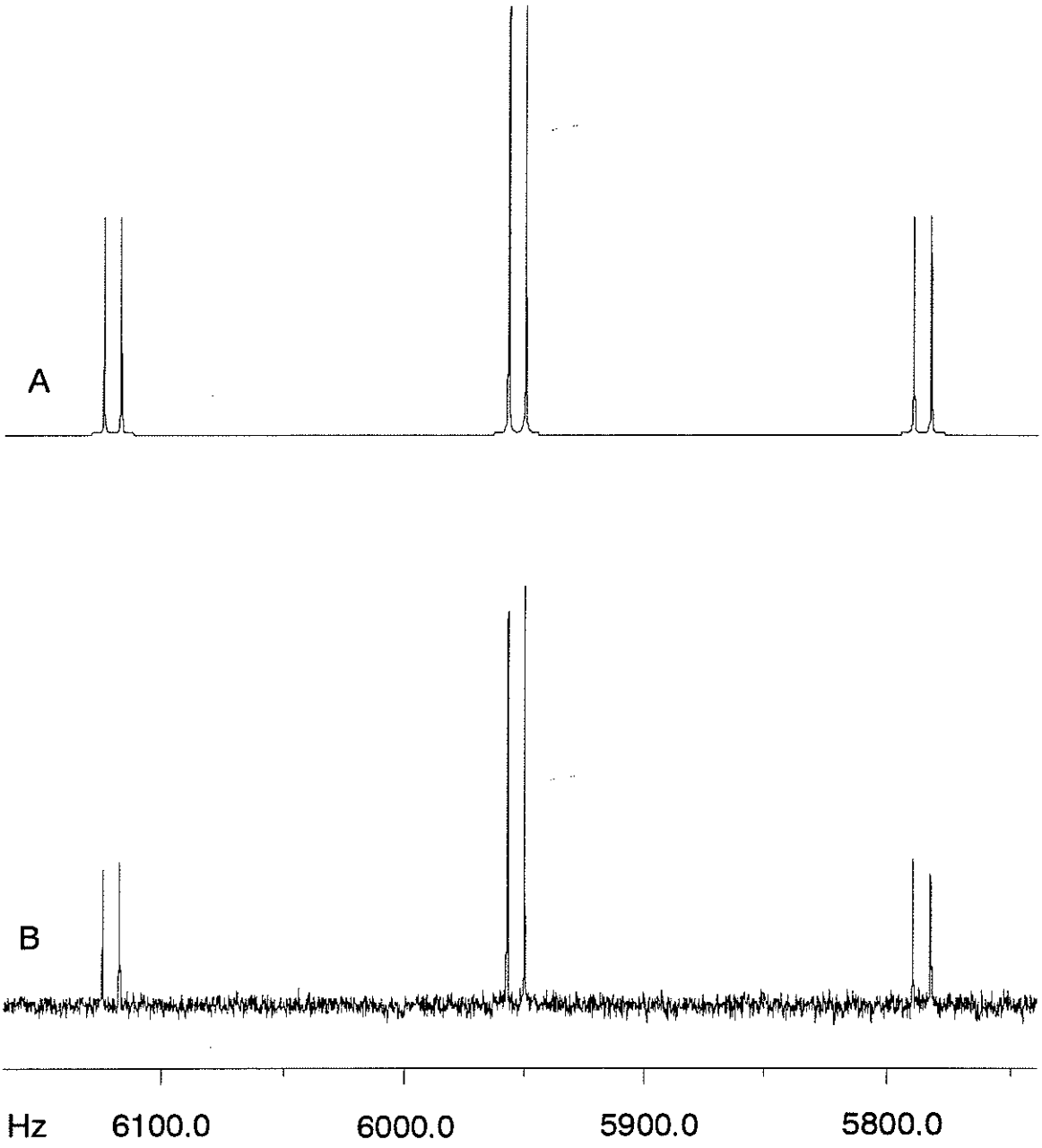

Figure 26: ^{13}C NMR spectrum of phenylallene gamma carbon in acetone-d_6 with ring protons decoupled. A) Theoretical spectrum with a linewidth of 0.2 Hz; B) Experimental spectrum.

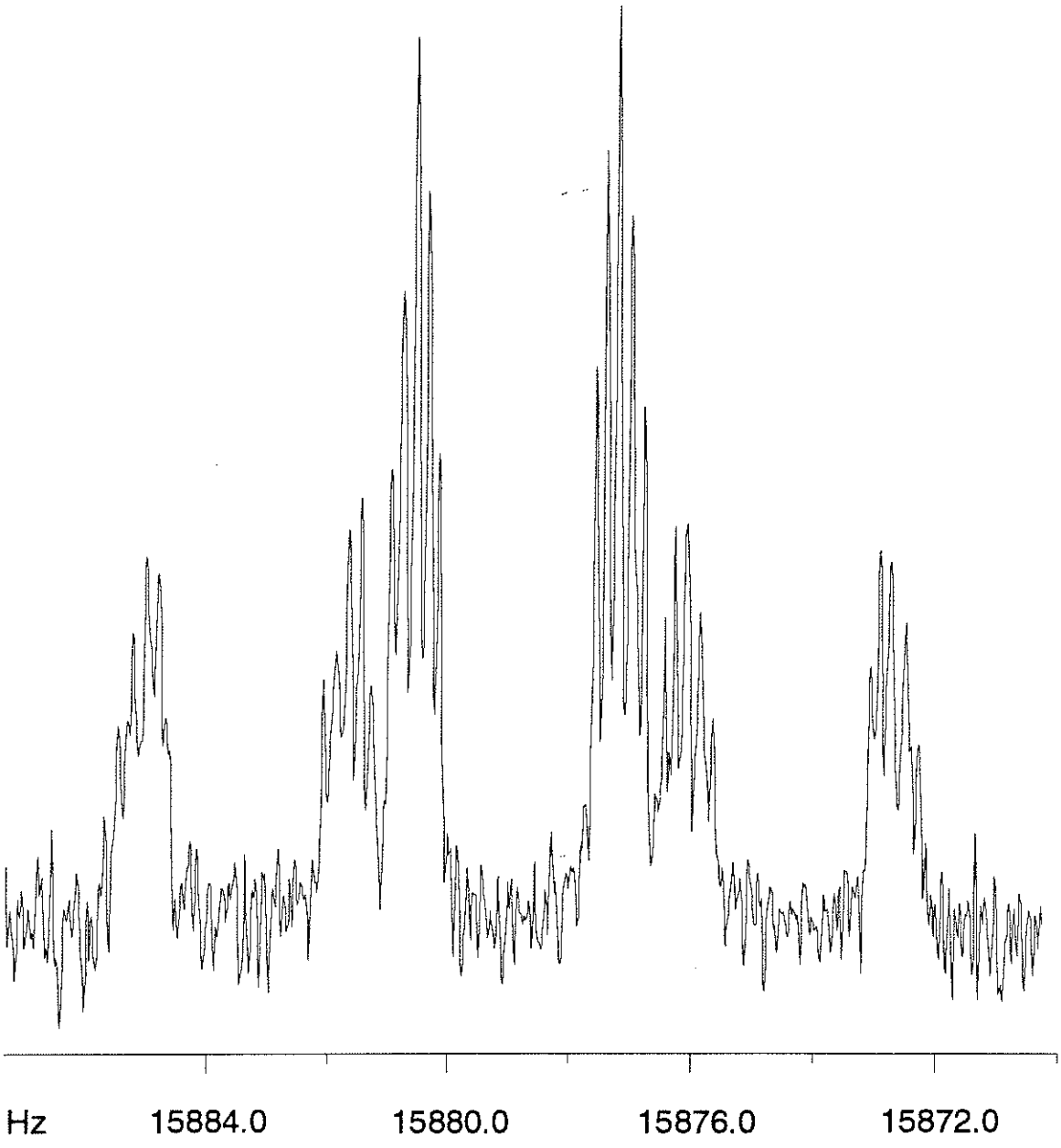

Figure 27: ^{13}C NMR spectrum of fully coupled phenylallene beta carbon in acetone-d_6.

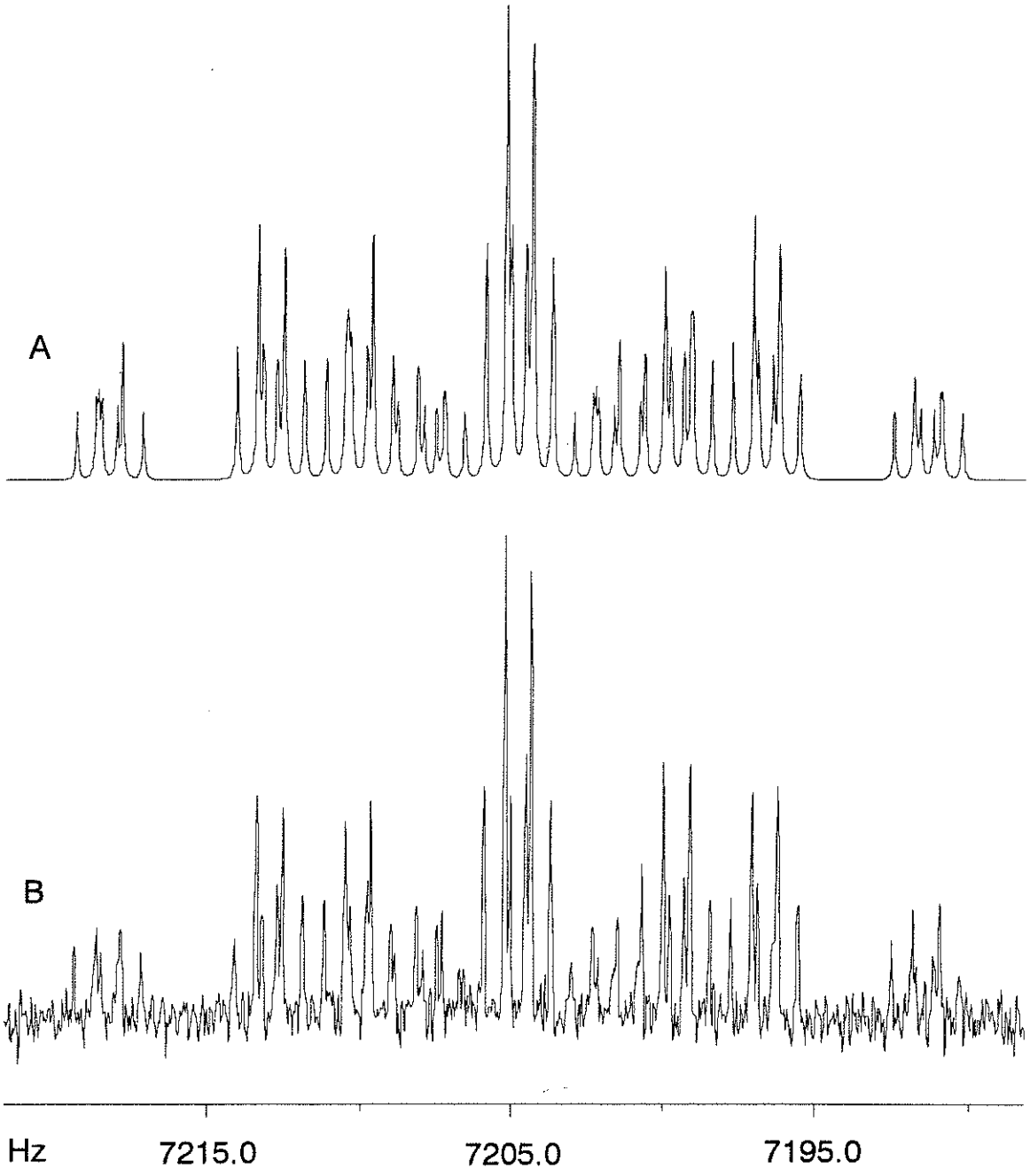

Figure 28: ^{13}C NMR spectrum of the high frequency portion of the fully coupled phenylallene alpha carbon 'doublet' in benzene-d_6. A) Theoretical spectrum with a linewidth of 0.08 Hz; B) Experimental spectrum.

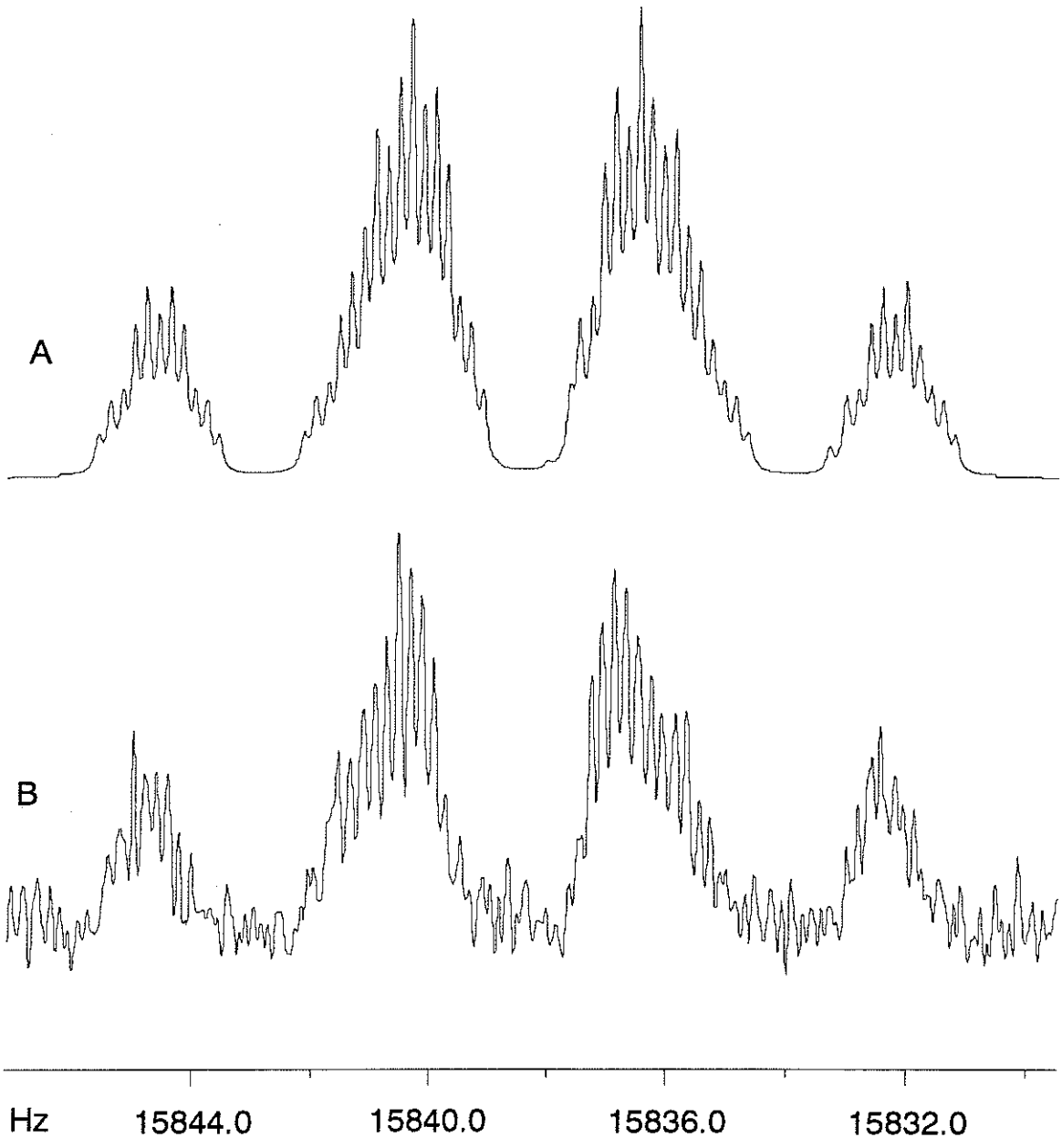

Figure 29: ^{13}C NMR spectrum of fully coupled phenylallene beta carbon in benzene-d_6. A) Theoretical spectrum with a linewidth of 0.13 Hz; B) Experimental spectrum. (Poor spectral appearance is due to distortions introduced at the reproduction stage.)

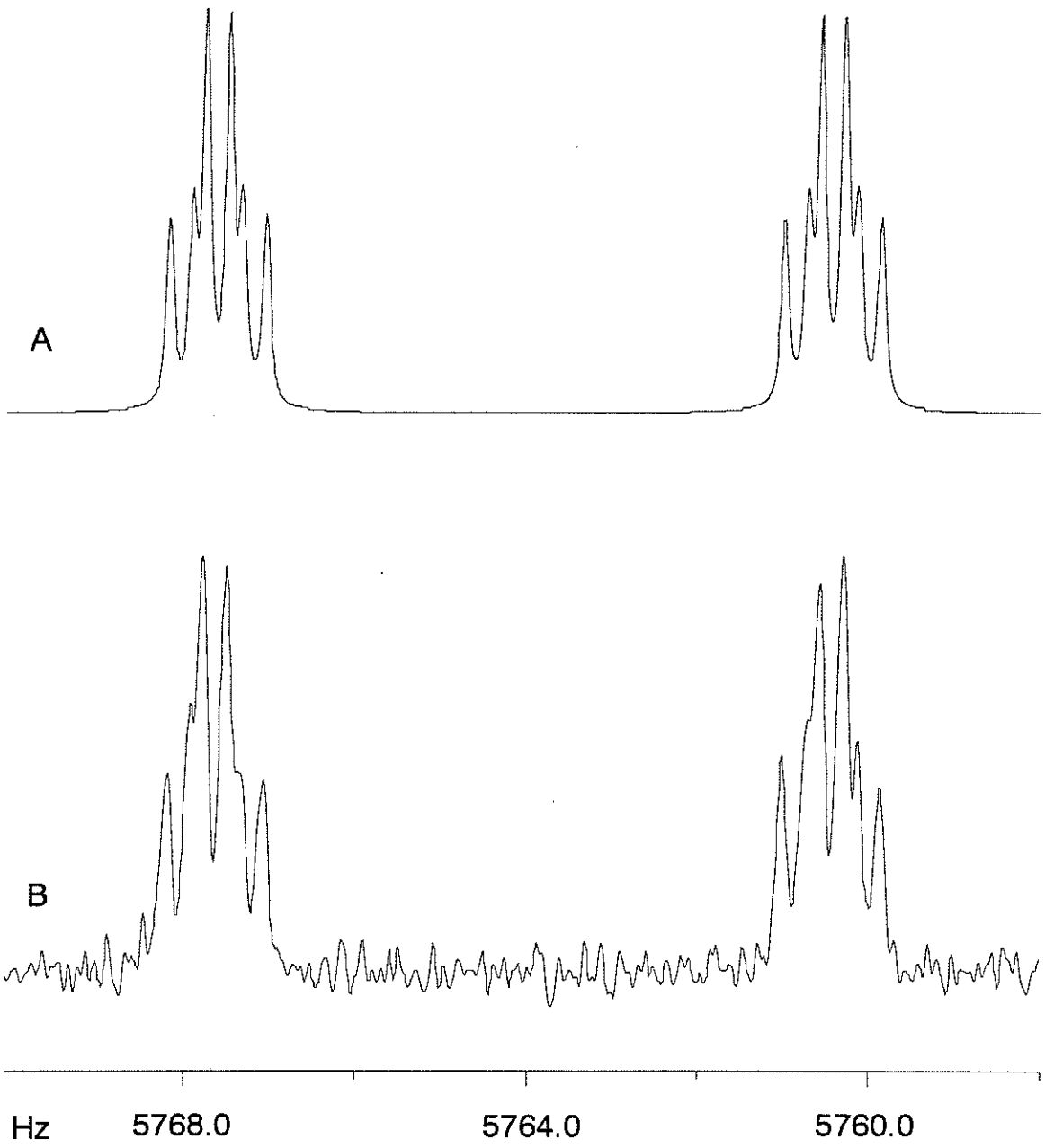

Figure 30: ^{13}C NMR spectrum of the low frequency portion of the fully coupled phenylallene gamma carbon 'triplet' in benzene-d_6. A) Theoretical spectrum with a linewidth of 0.08 Hz; B) Experimental spectrum.

3.1.4 Molecular Orbital Computations

The theoretical energies, computed for various angles of the torsion, θ , are reproduced in Table 6. For each basis set, these energies were fit to the potential function of equation 1, yielding the twofold and fourfold components listed in Table 7. Table 7 also compares these values with similar computations on styrene [9, 10, 11]. Figure 31 illustrates the shapes and relative magnitudes of the various computed potentials for phenylallene.

Not included in Table 7 are the potential functions for styrene and phenylallene as computed using the AM1 algorithm. Phenylallene computations give a barrier height of 7.42(1) $kJ\,mol^{-1}$, and an AM1 value for the height of styrene's potential is 6.07 $kJ\,mol^{-1}$ [52]. Scaling factors relating AM1 barriers to experimental barriers have been investigated by Meier et al. [52], who suggest that for styrene, the AM1 barrier must be multiplied by 2.1. The average scale factor over a survey of eight similarly conjugated molecules is 1.9 ± 0.25. Applying these empirically-determined factors to phenylallene AM1 data gives a twofold potential of 15.6 and 14.1 ± 1.9 $kJ\,mol^{-1}$, respectively. These values are reasonably close to the MP2/6-31G* barrier height of 16.0 $kJ\,mol^{-1}$ (Table 6).

As discussed in section 1, the experimental barrier height in styrene is commonly taken to be 12.8(1) or 13.8(2) $kJ\,mol^{-1}$, determined by supersonic jet fluorescence spectroscopy [4] or microwave spectroscopy [5]. It is apparent from Table 7 that the 6-31G value of 13.2 $kJ\,mol^{-1}$ [10] agrees best with these values, wheras a larger basis set, 6-31G*, gives an unacceptably low barrier [11]. From the viewpoint of the unknown barrier in phenylallene, it is interesting that each basis set yields a barrier higher by nearly 4.0 $kJ\,mol^{-1}$ than for styrene (Figure 32). This difference can be considered a rough estimate of the destablization of planar styrene due to steric repulsion between the ortho and β-*cis* C–H bonds (Figure 1). Moreover, in contrast to styrene, where the MP2/6-31G* barrier is 1.1 $kJ\,mol^{-1}$ lower than the HF/6-31G* barrier [11], the MP2/6-31G* computation does not alter the barrier in

phenylallene. Since the origin of this barrier reduction in styrene is likely the tendency of MP2 calculations to lengthen C–H bonds, thus *increasing* steric strain, the absence of this effect in phenylallene lends credence to the importance of the steric factor. This approximation is also consistent with that obtained by Bothner-By *et al.* [16], in their analysis of deuterium quadrupolar splittings of partially aligned styrene-α-d. Their inclusion of a $\cos^{12}\theta$ term in a trial potential energy function to model the steric repulsion energy suggested an upper limit of 4.2 $kJ\,mol^{-1}$.

According to the potentials in Table 7, the expectation values of $\langle\cos^2\theta\rangle$ at 300 K are 0.90 and 0.83 for 6-31G level computations of phenylallene and styrene, respectively, implying somewhat lower conjugation in the latter. Supporting this notion, the chemical shifts of the C_4 nuclei, often taken to be indicative of the extent of π electron transfer, are 128.5, 127.6 and 126.6 *ppm* for benzene, styrene and phenylallene [53][6]. As expected from the $\langle\cos^2\theta\rangle$ values, unity corresponding to most effective π overlap, the allenyl group transfers slightly more electron density to the phenyl ring than does the vinyl group. The para proton of phenylallene is also more shielded, by 0.03 *ppm*, than in styrene, in acetone-d_6 solution[7]. This argument does not address the intrinsic π donation characteristics of the vinyl and allenyl groups, indeed assuming them to be about equal; it rather suggests that steric forces, which act conformationally to somewhat inhibit π conjugation in styrene, are absent in phenylallene.

The MP2/6-31G* (frozen-core) structure of the planar and perpendicular conformers of phenylallene may be of interest to molecular spectroscopists (Figures 33 and 34). The computed rotational constants are 4.57923, 0.99314 and 0.82072 GHz for planar phenylallene, and 4.18214, 0.967747 and 0.867967 GHz for the perpendicular conformer at the equilibrium geometry. The height of the internal rotational barrier is calculated as 16.0 $kJ\,mol^{-1}$, so that the planar conformer is presumably the more

[6]Reference [53] does not appear to give the ^{13}C NMR chemical shifts for phenylallene, although they are cited in reference [54] as coming from the former.

[7]The shift for styrene was measured at a concentration of 16 *mol*% [25], whereas that for phenylallene was at 5.1 *mol*%.

relevant of the two. There are some significant changes predicted in the bond angles at the first exocyclic carbon atom on twisting the sidechain out of plane, which imply a small measure of repulsion in the planar form. The exocyclic Csp^2–Csp^2 bond length increases by nearly 0.02 Å in the perpendicular form, likely from the reduction of conjugational forces. Comparison of the planar conformer with an MP2/6-31G* structure of allene [55], in which the C=C bond length is 1.313 Å, suggests a slight lengthening of the C_α–C_β bond. This lengthening may imply some delocalization into the C_1–C_α bond.

Table 6: Theoretical conformational energies ($kJ\ mol^{-1}$) for phenylallene

$\theta°$	*AM1*	*STO-3G*	*6-31G*	*6-31G**	*6-31G***	*MP2/6-31G**
0.0	0.000	0.000[a]	0.000	0.000	0.000	0.000[b]
15.0	0.375	1.125	0.868	0.786	0.782	—
30.0	1.524	4.383	3.441	3.145	3.131	—
45.0	3.312	9.250	7.434	6.858	6.836	—
60.0	5.282	14.543	11.984	11.146	11.117	—
75.0	6.806	18.671	15.697	14.694	14.660	—
90.0	7.415	20.289	17.215	16.158	16.122	16.040[b]

a) The total computed energies for the planar conformer with STO-3G to MP2/6-31G* bases were −341.182752, −345.295485, −345.414641, −345.429114, and −346.543821 au, in that order. b) These represent correlation-gradient (post-HF geometry optimization) calculations.

Table 7: Theoretical internal rotational potentials ($kJ mol^{-1}$) for phenylallene (PHA) and styrene (STY)

	STO-3G		*6-31G*		*6-31G**		*6-31G***
Parameter	*PHA*	*STY*[a]	*PHA*	*STY*[b]	*PHA*	*STY*[c]	*PHA*
V_2	20.26(2)	16.28(8)	17.16(1)	13.19(15)	16.07(1)	12.016(8)	16.06(1)
V_4	− 0.88(2)	− 3.00(7)	− 1.15(1)	− 3.18(15)	− 1.22(1)	− 3.127(8)	− 1.20(1)
$\langle \sin^2 \theta \rangle$	0.075	0.130	0.095	0.167	0.103	0.183	0.103
$\langle \theta \rangle$	13.0	17.9	14.8	21.0	15.5	22.3	15.5

a) STO-3G barrier for styrene taken from reference [9]. b) 6-31G barrier for styrene from reference [10]. c) 6-31G* styrene barrier derived from data reported in reference [11]. A slightly better fit is obtained if a sixfold component of − 0.11 $kJ\ mol^{-1}$ is included.

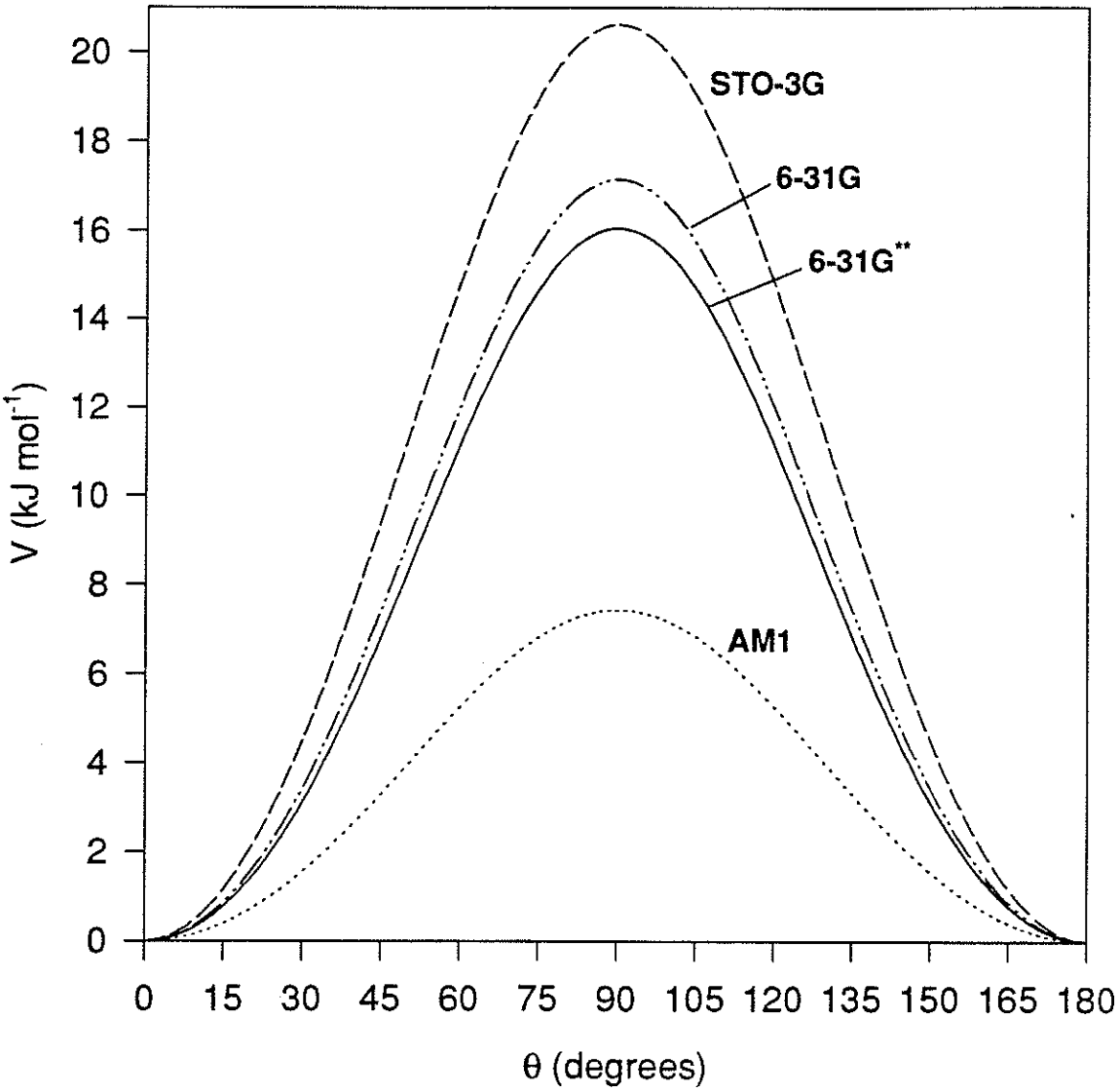

Figure 31: Theoretical internal rotational potentials for phenylallene computed using the indicated basis sets. The 6-31G* and 6-31G** potentials differ by only about 10 $J\,mol^{-1}$ and are indistinguishable at this scale.

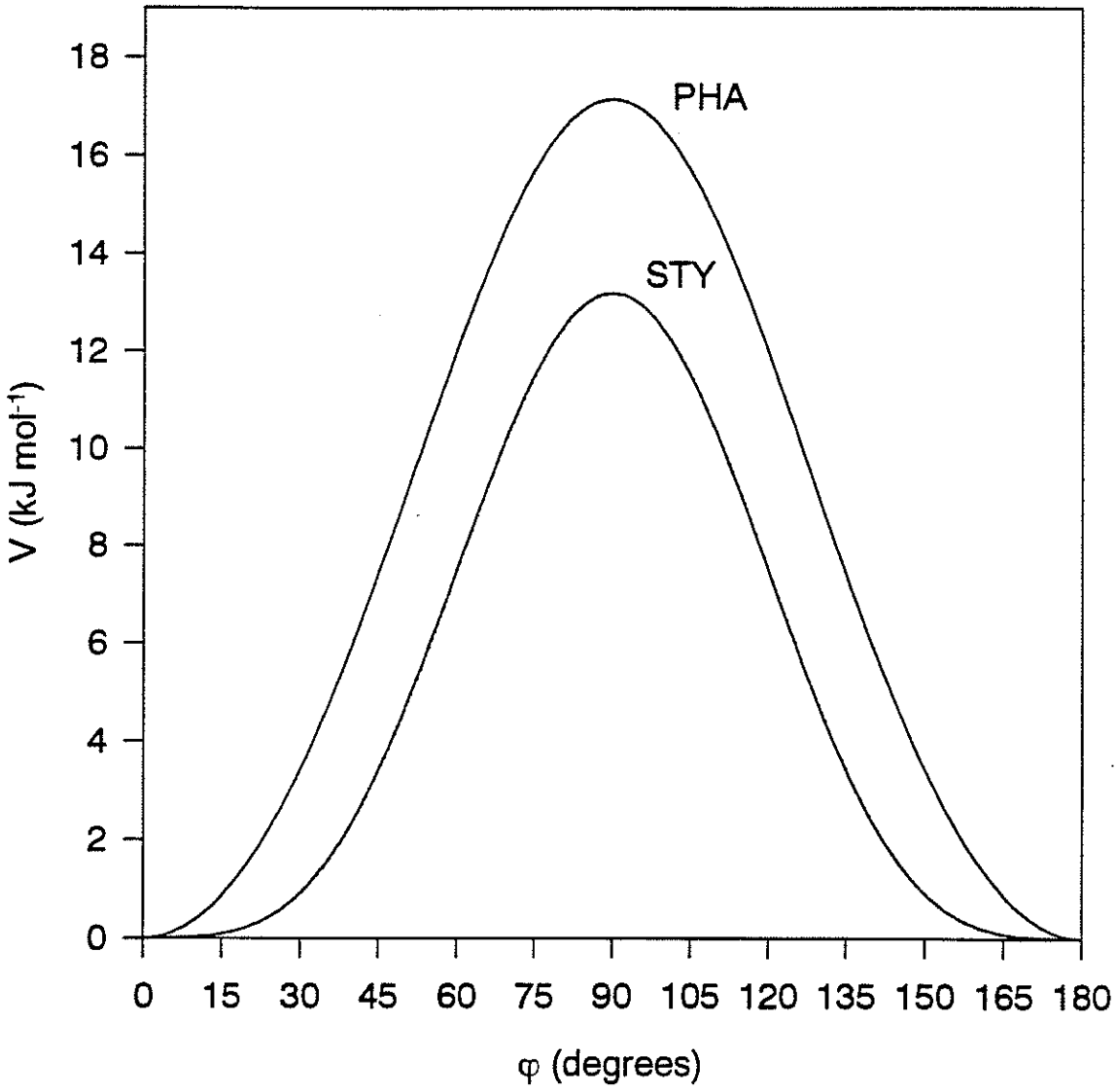

Figure 32: Comparison of the 6-31G level internal rotational potentials in phenylallene and styrene. The angle, ϕ, represents torsion about the exocyclic Csp^2–Csp^2 bond.

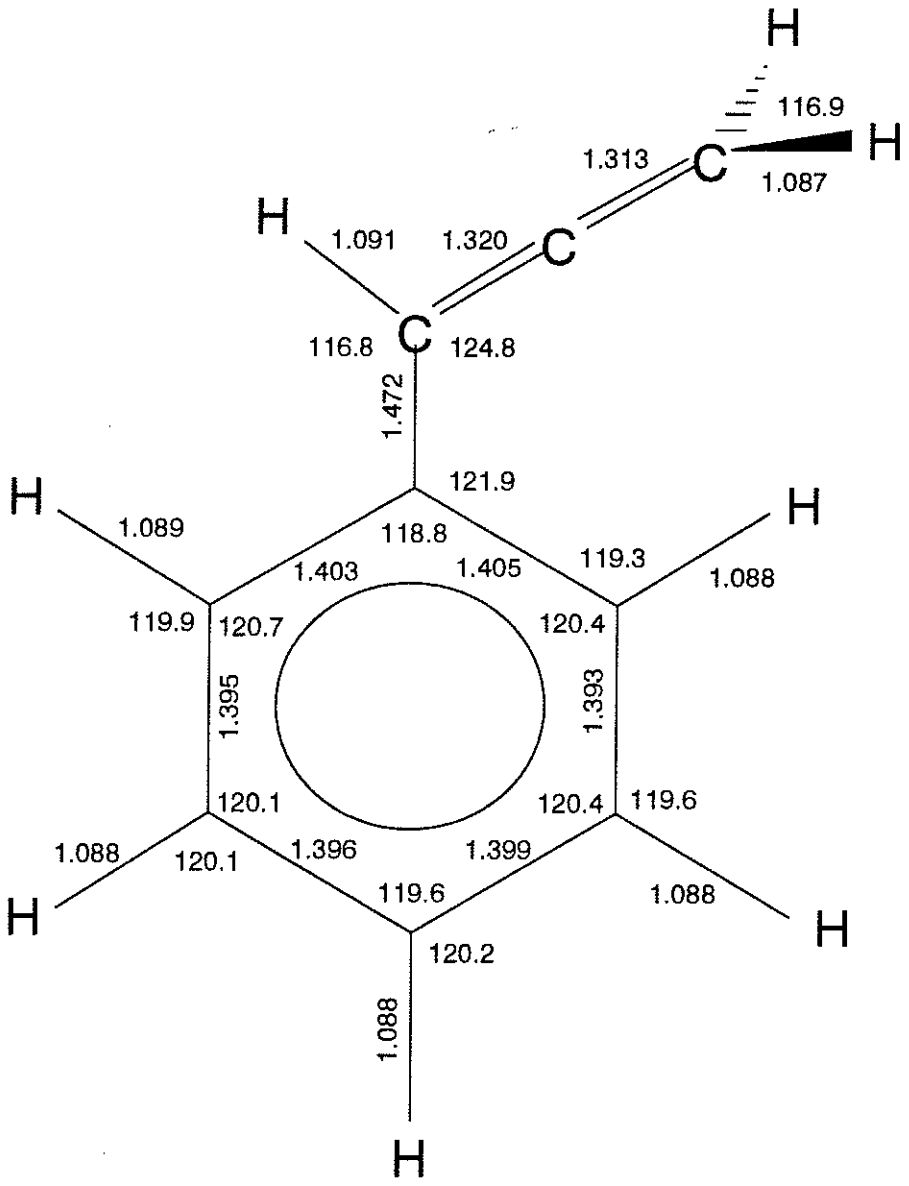

Figure 33: Computed MP2/6-31G* structure of planar phenylallene.

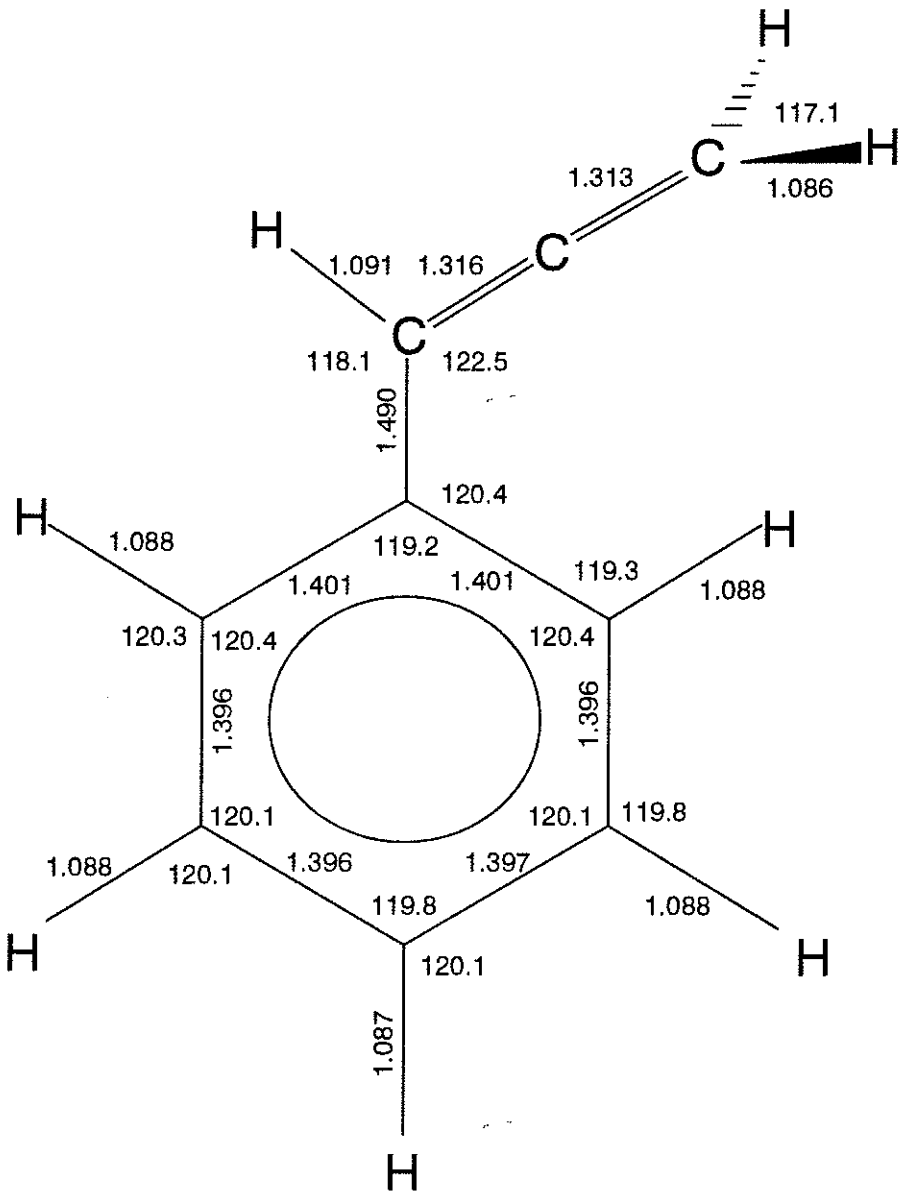

Figure 34: Computed MP2/6-31G* structure of *perpendicular* phenylallene. Note that the sidechain is not drawn in projection, it being more convenient to indicate bond parameters in the structure as drawn.

3.1.5 Long range coupling constants, ${}^{n}J(H_{ring}, H_{allenyl})$

INDO MO FPT computations [20, 21] yielded ${}^{n}J(H_{ring}, H_{allenyl})$ as a function of the torsion angle, θ, for the 6-31G** structures. Computed values were fit to plausible functions of θ, as summarized in Table 8. Figures 35 and 37 depict these functions graphically. In all functional relationships discussed, ${}^{n}J$ are in units of Hz. Errors associated with the coefficients, A to D, are less than 0.01 Hz, unless otherwise indicated.

Included in Table 8 is a factor by which theoretical ${}^{n}J$ couplings must be scaled to reproduce the experimental values. From MO computations of the internal rotational potential, $\langle \sin^2 \theta \rangle$ is assumed to be 0.103, and for an evenfold potential, $\langle \sin^2(\theta/2) \rangle$ is 0.5. It is notable that INDO MO FPT calculations are notorious for overestimating contributions arising from σ electrons. This is especially evident for couplings with a potentially all-*trans* pathway. The factor in ${}^{5}J_{3,\alpha}$, for instance, is smaller than for ${}^{8}J_{4,\gamma}$. Other such scaling factors can also be understood in this way.

The gamma protons

Theoretically, the eight-bond coupling to the gamma protons can be written:

$$ {}^{8}J_{4,\gamma} = -0.79(1) + 0.73(3) \sin^2 \theta. $$

An equivalent expression, more illustrative for dissecting spin transmission mechanisms, is

$$ {}^{8}J_{4,\gamma} = -0.06 \sin^2 \theta - 0.79 \cos^2 \theta. $$

This latter representation strongly implies the coupling mechanism mediated by π electrons, as shown in Figure 36. Specifically, the diagram in this figure depicts the benzene plane lying perpendicular to the page, so that its $2p\pi$ orbitals are situated in the plane of the page. Thus, for planar phenylallene, the interproton methylene vector is also parallel to the page. Uncrossed arrows denote electron spin states, and crossed arrows indicate the spin state of the proton. Since there is no π electron

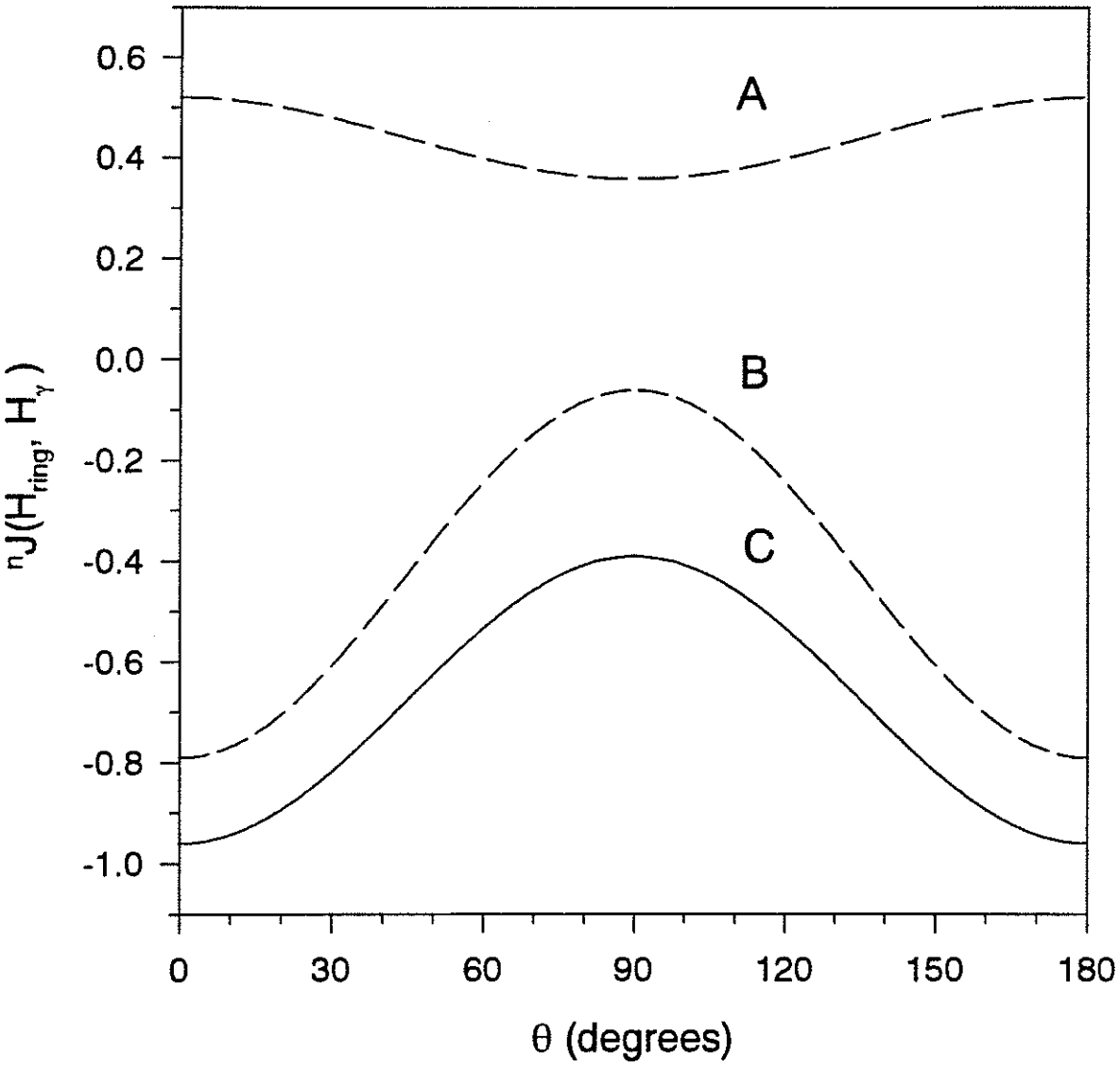

Figure 35: INDO MO FPT calculations of $^nJ(H_{ring}, H_\gamma)$: A) $^7J_{3,\gamma}$; B) $^8J_{4,\gamma}$; C) $^6J_{2,\gamma}$.

Table 8: INDO MO FPT computations of intergroup ${}^{n}J_{H,H}$ (Hz) in HF/6-31G** structure of phenylallene. Planar molecule, $(\theta = 0°)$ is depicted in Figure 3.

Coupling	B[a]	C[b]	D[c]	*Factor*[d]
${}^{4}J_{2,\alpha}$	− 1.22	− 0.50	− 0.19	0.56
${}^{6}J_{2,\gamma}$	− 0.39(2)	− 0.96	—	0.64
${}^{5}J_{3,\alpha}$	0.36	0.25	0.81	0.42
${}^{7}J_{3,\gamma}$	0.36	0.52	—	0.41
${}^{6}J_{4,\alpha}$	− 1.009(1)	− 0.228(1)	—	0.69
${}^{8}J_{4,\gamma}$	− 0.06	− 0.79(3)	—	0.85

a) Coefficient of $\sin^2\theta$; b) Coefficient of $\cos^2\theta$; c) Coefficient of $\sin^2(\theta/2)$; d) Factor by which the theoretical coupling must be multiplied to reproduce experiment (see text).

density at the nucleus, nuclear spin information is transmitted via the familiar σ-π spin polarization mechanism. The relationship between the H_4 nuclear spin state and the C_4 electron spin state is defined by the hyperfine interaction parameter, Q^H_{CH}. In general, the first symbol in the subscript represents the atom carrying the unpaired spin, the two subscripts together indicate the bond being spin polarized, and the superscript designates the nucleus coupled to the unpaired electron. Q^H_{CH} is negative, leading to a parallel orientation of the π electon at C_4. The electron spin correlation along the extended π system gives rise to the indicated spin state at C_β. This spin state is, in turn, related to that of H_γ by another σ-π, or *hyperconjugative* interaction, Q^H_{CCH}, which is known to be positive. By this simple mechanism, H_4 and H_γ can be seen to have parallel spins, thus defining a negative ${}^{8}J_{4,\gamma}$.

Intuitively, one can appreciate that as θ increases from zero, the π electron spin correlation decreases, vanishing when θ reaches 90° . The computed angle dependence of ${}^{8}J_{4,\gamma}$ agrees with this model. The semiempirical, INDO MO FPT computational

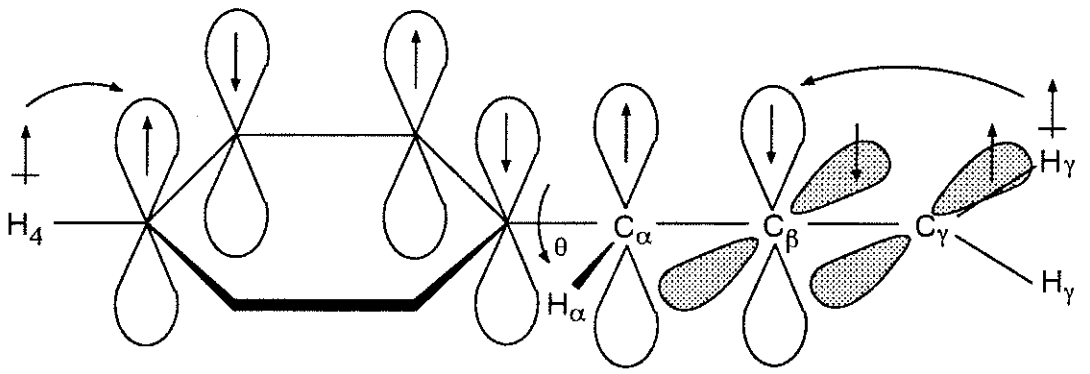

Figure 36: Spin state transmission in phenylallene

scheme predicts the qualitative conformational dependence of long range coupling constants rather well [57], especially for pure π electron mechanisms, but is not expected, in general, to provide quantitative results. One approach to a calibration of the computations, for the present molecule, is to compare the measured ${}^4J_{\alpha,\gamma}$ of $-6.83(2)$ Hz, also a π electron coupling constant [45], with the computed number. The theoretical ${}^4J_{\alpha,\gamma}$ varies less than 5% with rotation about θ , with an average value of -8.0 Hz. The resulting ratio is 0.85. Of course, this approach does not account for computational errors at the C_4 site, nor the computation of the π electron spin correlation at the C_1 and C_α sites. Judging from the success of similar computations for ${}^7J_{4,\beta}$ in styrene, however, which is also a pure π electron coupling constant, this calibration seems reasonable [18, 24, 25]. If the above expression is reduced by this factor,

$$ {}^8J_{4,\gamma} = -0.67(1) + 0.62(2)\sin^2\theta. $$

Considering the average value of ${}^8J_{4,\gamma}$ obtained in the two solvents, -0.607 Hz (Table 2), this relationship predicts $\langle\sin^2\theta\rangle$ to be 0.102(4) at 300 K.

It so happens that this expectation value agrees exactly with those computed for the free molecule from the 6-31G* and 6-31G** potentials (Table 7). It is also true that ${}^8J_{4,\gamma}$ is essentially the same in both the polar and non-polar solvent. Naturally, it does not follow that the internal rotational potential of phenylallene is independent

of solvent, yet this certainly appears to be the case for some non-polar molecules. The potential in ethylbenzene, for instance, seems to be solvent-independent [58]. By contrast, the internal rotational potential in the relatively polar benzyl fluoride, changes by 2 $kJ\,mol^{-1}$ in passing from CS_2 to acetone-d_6 solution [59]. Its dipole moment is 1.77 D in benzene solution [60], whereas the computed dipole moments for phenylallene planar and perpendicular conformers are 0.078 and 0.076 D at the 6-31G** level. Furthermore, spin-spin coupling constants in styrene and a number of its derivatives have been interpreted on the basis of such an invariance [23, 24]. From these considerations, the ensuing discussion of lrJs in phenylallene is predicated on the assumption that the internal potential is unaltered by the solvents used.

The seven-bond coupling to H_γ, from the meta position of phenyl ring, is 0.206 Hz. Based on the diagram in Figure 36, it seems unlikely that this coupling constant is transmitted by a mechanism other than the π electron system delineated for $^8J_{4,\gamma}$. The positive sign of $^7J_{3,\gamma}$, as determined by spin tickling experiments and verified by the sign of $D_{\gamma,\gamma}$, can be explained by the anti-parallel spin orientations depicted in Figure 36. The magnitude of $^7J_{3,\gamma}$ is about one-third of that for $^8J_{4,\gamma}$. This can be understood from the notion that spin correlation for atoms belonging to different classes (starred or unstarred) is larger in magnitude than between atoms of the same class [19, 61]. A suggestive set of numbers is the Hückel bond orders for the carbons of benzene: $\frac{2}{3}$ for ortho-bonded carbons and zero for meta.

The INDO MO FPT results, given by

$$^7J_{3,\gamma} = 0.52\cos^2\theta + 0.36\sin^2\theta,$$

do not conform to the mechanism postulated above, leading to a large coupling, 0.36 Hz, for the perpendicular conformer. On this model, one expects $^7J_{3,\gamma}$ to become very small, or indeed, vanish completely, at $\theta = 90°$. Confirmation of this prediction would require a derivative of phenylallene characterized by a large average torsion angle.

In terms of the present model, the ratio $^7J_{3,\gamma}/^8J_{4,\gamma} = -0.34$ is a measure of

the proportion of the π electron contributions, at meta and para sites, to coupling constants involving nuclei in the sidechain of benzene derivatives. There has been some uncertainty about this ratio, for example, in toluene [62] and other alkyl benzene derivatives [63]. The utility of such a measurement lies in the fact that some coupling constants, particularily $^5J(H_{meta}, CH)$, can have substantial stereospecific σ components which may be useful for determining conformational populations [63, 64]. Subtraction of a known π electron component can increase the precision of this determination.

One striking feature of $^6J_{2,\gamma}$ is its near equality with $^8J_{4,\gamma}$. Average values from the two solutions are $-0.581(3)$ and $-0.607(4)$ Hz, respectively. The implication, that the π electron contributions to these coupling constants are effectively equal, is unexpected from the viewpoint of the bond orders available from molecular orbital theory, where ^nJ is proportional to the square of a mobile bond order [65, 66, 67, 68]. However, other formulations, based on valence bond theory [61, 66], find ^nJ proportional to a bond order, variously defined [66, 69]. Some theoretical developments do, indeed, predict nearly equal contributions of the π electron contributions to the coupling constants between ortho and between para protons in benzene [19].

The INDO MO FPT computation for this coupling yields

$$^6J_{2,\gamma} = -0.96\cos^2\theta - 0.39\sin^2\theta.$$

After reduction by a factor of 0.85, as for $^8J_{4,\gamma}$, this expression implies a coupling of -0.33 Hz in the perpendicular conformer. In the absence of an additional mechanism which is operative in this conformation, the INDO MO FPT result is inexplicable.

The alpha proton

The coupling constant, ${}^6J_{4,\alpha}$, in styrene consists of two components, one due to a π electron mechanism analogous to the one in Figure 36 and the other arising from a σ-π mechanism. The former depends on $\cos^2\theta$, and the latter on $\sin^2\theta$ [18]. Two empirical developments of this relationship have produced somewhat different potentials:

$$ {}^6J_{4,\alpha} = -0.149\cos^2\theta - 0.597\sin^2\theta \ \ [24], $$

and

$$ {}^6J_{4,\alpha} = -0.130\cos^2\theta - 0.800\sin^2\theta \ \ [27]. $$

If these expressions are applied to phenylallene, with a $\langle\sin^2\theta\rangle$ of 0.103, as above, they predict ${}^6J_{4,\alpha}$ as -0.195 Hz and -0.199 Hz, respectively. The average of the experimental values is $-0.212(1)$ Hz (Table 2).

INDO MO FPT computations for phenylallene overestimate the magnitudes of the coefficients, as for styrene [24], yielding

$$ {}^6J_{4,\alpha} = -0.228(1)\cos^2\theta - 1.009(1)\sin^2\theta. $$

Reduction of both terms by a factor of 0.69 produces agreement with the experimental value:

$$ {}^6J_{4,\alpha} = -0.157(1)\cos^2\theta - 0.696(1)\sin^2\theta. $$

INDO's prediction of ${}^5J_{3,\alpha}$ for phenylallene demonstrates the abovementioned tendency for overestimates of σ electron pathways. Similar overestimates are calculated for toluene [62, 64] and benzaldehyde [70], to name only two. Specifically, for phenylallene, INDO MO FPT computes

$$ {}^5J_{3,\alpha} = 0.25\cos^2\theta + 0.36\sin^2\theta + 0.81\sin^2(\theta/2). $$

The calculated value, given the appropriate angular terms, is 0.67 Hz, contrasting with the measured coupling of 0.284(2) Hz. An adjusted expression, which better conforms to the empirical data and current understanding of spin information transmission, can be developed as follows. The foregoing discussion of long range spin-spin

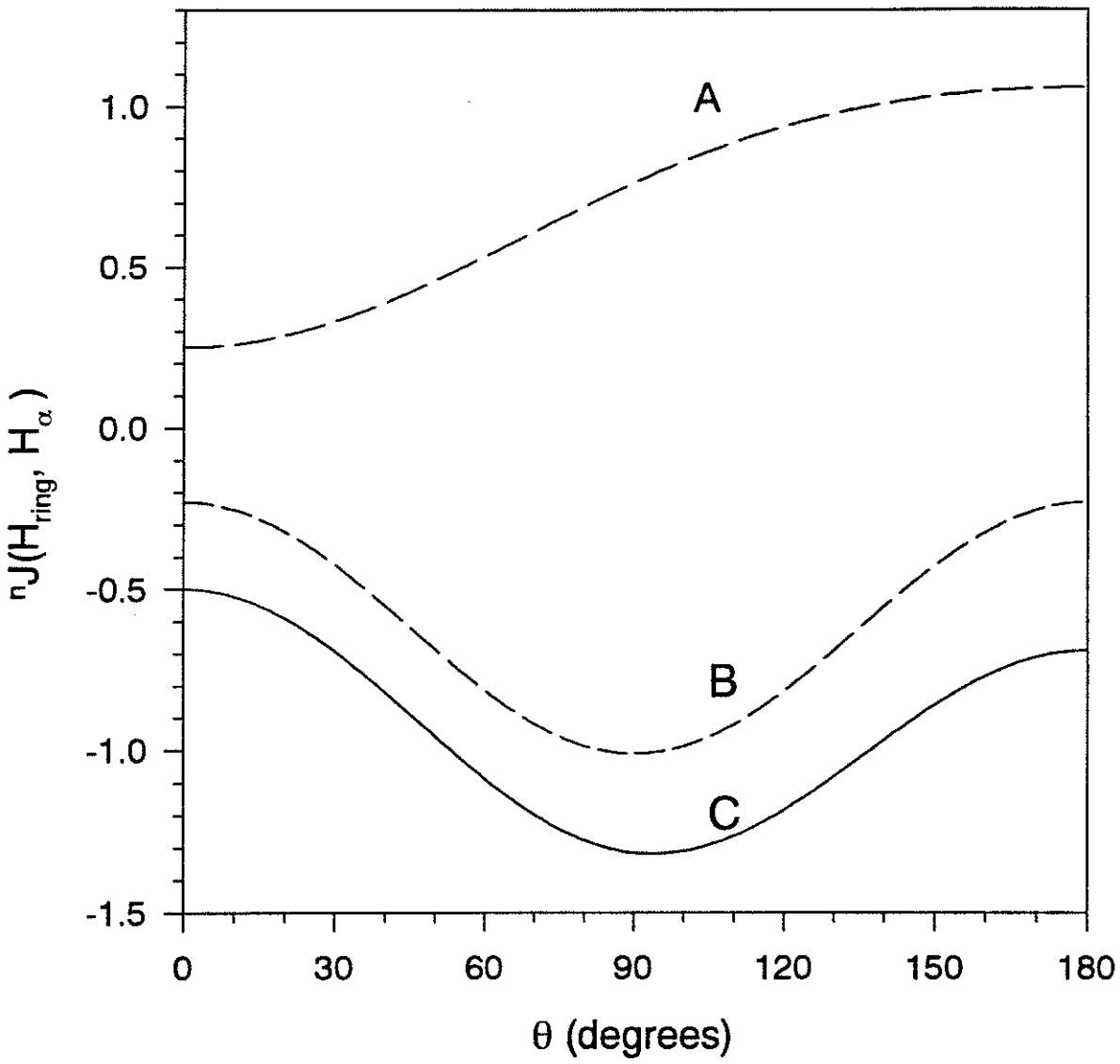

Figure 37: INDO MO FPT calculations of ${}^{n}J(H_{ring}, H_{\alpha})$: A) ${}^{5}J_{3,\alpha}$; B) ${}^{6}J_{4,\alpha}$; C) ${}^{4}J_{2,\alpha}$.

couplings to the gamma protons derived the ratio of π and σ-π electron contributions to meta and para positions for the planar molecule to be 34%. By scaling the expression for ${}^6J_{4,\alpha}$ by 0.34, one obtains coefficients of 0.053 and 0.237 Hz, respectively. Combining these estimates with the experimental value, one obtains

$$^5J_{3,\alpha} = 0.05\cos^2\theta + 0.24\sin^2\theta + 0.42\sin^2(\theta/2),$$

where the coefficient of $\sin^2(\theta/2)$ has been reduced by 0.5.

For benzaldehyde and toluene derivatives, there is evidence that ${}^5J$ effectively vanishes for the planar conformation in which the coupling is not an all-*trans* pathway [71, 72]. One might intuit that, because this is true for the sidechain Csp^2 in benzaldehyde, it should also be true for phenylallene. However, ${}^6J$ is undetectable in benzaldehyde [73], corresponding to the large internal barrier, and implying a negligible π electron component in ${}^5J$ at $\theta = 0^\circ$.

Finally, theory yields

$$^4J_{2,\alpha} = -0.50\cos^2\theta - 1.22\sin^2\theta + 0.19\sin^2(\theta/2).$$

Assuming that the σ electron contribution, in $\sin^2(\theta/2)$, is less reliably given than the π electron pathways, a single scaling factor is not meaningful. Rather, since the π electron contribution appears to be equal to ortho and para sites for ${}^{6,8}J_\gamma$, the coefficients of ${}^6J_{4,\alpha}$ can be imported into this expression for ${}^4J_{2,\alpha}$ and the σ contribution evaluated according to the measured value. This empirical procedure yields

$$^4J_{2,\alpha} = -0.16\cos^2\theta - 0.70\sin^2\theta + 0.32\sin^2(\theta/2).$$

3.1.6 Long range coupling constants, ${}^{n}J({}^{1}H_{ring}, {}^{13}C_{allenyl})$

Computed values for the nine ${}^{n}J({}^{1}H_{ring}, {}^{13}C_{allenyl})$s were obtained using HF/6-31G level geometries by the INDO MO FPT formalism, exactly as above (see section 3.1.5). Table 9 compiles the resulting coefficients and Figures 38, 39 and 40 display the angular dependencies. The 6-31G** geometries were used in the previous section to evaluate long range interproton coupling constants, while long range carbon-hydrogen couplings were obtained from computations on 6-31G geometries. This inconsistency will not alter the qualitative functional relationships presented here, since only semiquantitative agreement of the coefficients, A to D, with experiment would be anticipated, at best.

The para proton

Coupling of the alpha carbon to the proton in the para position is computed to obey the expression,

$$^{5}J(H_4, C_\alpha) = 1.23 - 0.33 \sin^2 \theta.$$

As with proton-proton coupling constants, the INDO MO FPT calculations overestimate certain contributions and must be scaled appropriately. In this case, multiplying all terms by 0.76 reproduces the experimental value of 0.91 Hz. This coupling constant is larger than the corresponding couplings in toluene of 0.65 Hz [74] and in benzoic acid of 0.5 Hz [75]. In toluene, ${}^{5}J(H_4, C_\alpha)$ has been interpreted as a σ-π interaction, proportional to $Q^{H}_{CH} Q^{C}_{CC}$. Both hyperfine interactions are negative, and refer to π electron spin densities on the contiguous aromatic carbon atoms [74]. In phenylallene, however, the alpha carbon is sp^2 hybridized, so that an additional hyperfine interaction comes from π electron spin density on C_α (Figure 36). This contribution can be thought of as involving parameters describing the polarization by the π density on C_α of those orbitals centered on C_α and containing s character [76]. The net result is a negative contribution to ${}^{5}J(H_4, C_\alpha)$. As the conformation passes from planar to perpendicular, INDO predicts a decrease of 0.33 Hz, corresponding

to the eventual cessation of spin correlation between the π electrons on C_1 and C_α.

For ${}^6J(H_4, C_\beta)$, the computed numbers are reproduced by the function

$$ {}^6J(H_4, C_\beta) = -0.47 \sin^2\theta - 0.66 \cos^2\theta. $$

This representation emphasizes the possible π electron and hyperconjugative components. Scaling this expression to agree with the measured value of $(-)0.42\ Hz$, gives

$$ {}^6J(H_4, C_\beta) = -0.31 \sin^2\theta - 0.43 \cos^2\theta. $$

If this is true, then the σ-π hyperfine interaction parameter, $Q^{Csp}_{CCC_{sp}}$, is positive, and proportional to $\sin^2\theta$. Its magnitude is 44% of Q^H_{CCH}, the hyperfine parameter characterizing ${}^6J_{4,\alpha}$. The π contribution to ${}^6J(H_4, C_\beta)$ is predicted to decrease more rapidly than the σ-π term as the torsion angle increases.

The seven bond coupling constant, ${}^7J(H_4, C_\gamma)$, is $0.28\ Hz$, experimentally. This being a coupling transmitted via spin correlation in the extended system, the INDO expression can be scaled in the usual way to give

$$ {}^7J(H_4, C_\gamma) = 0.31 \cos^2\theta + 0.03 \sin^2\theta. $$

According to Hund's rule, the electron correlation at C_β favours a parallel orientation, as depicted in Figure 36. Hence, the positive coupling constant can be considered the result of the positive product, $Q^H_{CH} Q^{C_\gamma}_{CC_\gamma}$, outweighing the negative contribution proportional to $Q^H_{CH} Q^{C_\gamma}_{C_\gamma}$. As with ${}^8J(H_4, H_\gamma)$, ${}^7J(H_4, C_\gamma)$ should essentially vanish when the π electron conjugation between aromatic and allenic groups is absent in the perpendicular conformer.

Table 9: INDO MO FPT computations of intergroup ${}^{n}J_{C,H}$ (Hz) in HF/6-31G structure of phenylallene. Planar molecule, $(\theta = 0°)$ is depicted in Figure 3.

Coupling	A[a]	B[b]	C[c]	D[d]	*Factor*[e]
${}^{3}J(H_2, C_\alpha)$	4.55	—	0.77	1.05	0.93
${}^{4}J(H_2, C_\beta)$	—	– 0.63	– 0.76	– 0.26	0.71
${}^{5}J(H_2, C_\gamma)$	—	0.36	0.66	0.06	0.65
${}^{4}J(H_3, C_\alpha)$	0.71	—	– 0.13	– 0.17	—
${}^{5}J(H_3, C_\beta)$	—	0.34	0.42	0.45	—
${}^{6}J(H_3, C_\gamma)$	—	– 0.18	– 0.31	0.10	—
${}^{5}J(H_4, C_\alpha)$	1.23	– 0.33	—	—	0.76
${}^{6}J(H_4, C_\beta)$	—	– 0.47	–0.66	—	0.66
${}^{7}J(H_4, C_\gamma)$	—	0.05	0.52	—	0.59

a) Constant term; b) Coefficient of $\sin^2\theta$; c) Coefficient of $\cos^2\theta$; d) Coefficient of $\sin^2(\theta/2)$; e) Factor by which the theoretical coupling must be multiplied to reproduce experiment (see text).

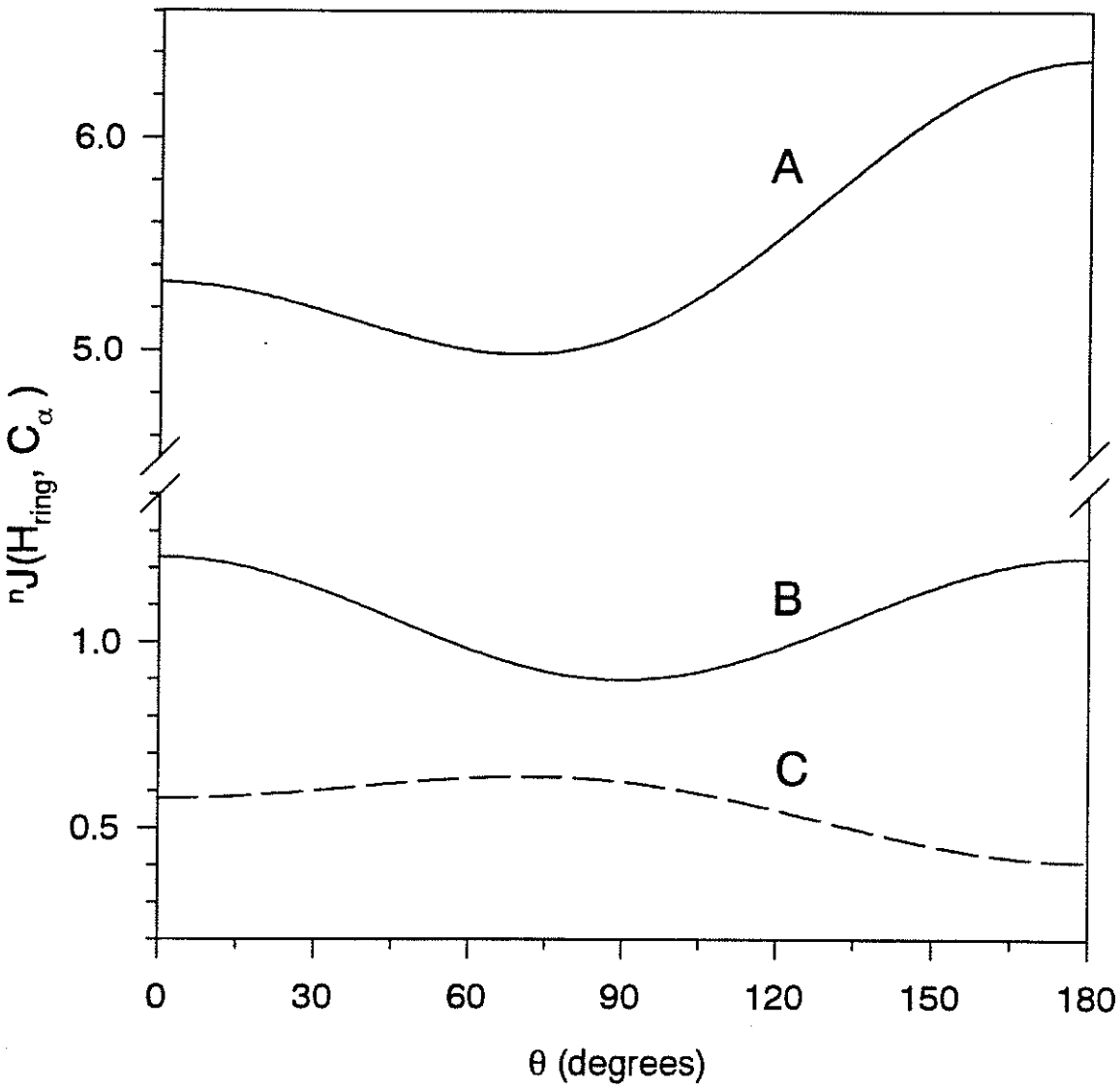

Figure 38: INDO MO FPT coupling expressions: A) $^3J(H_2, C_\alpha)$; B) $^5J(H_4, C_\alpha)$; C) $^4J(H_3, C_\alpha)$.

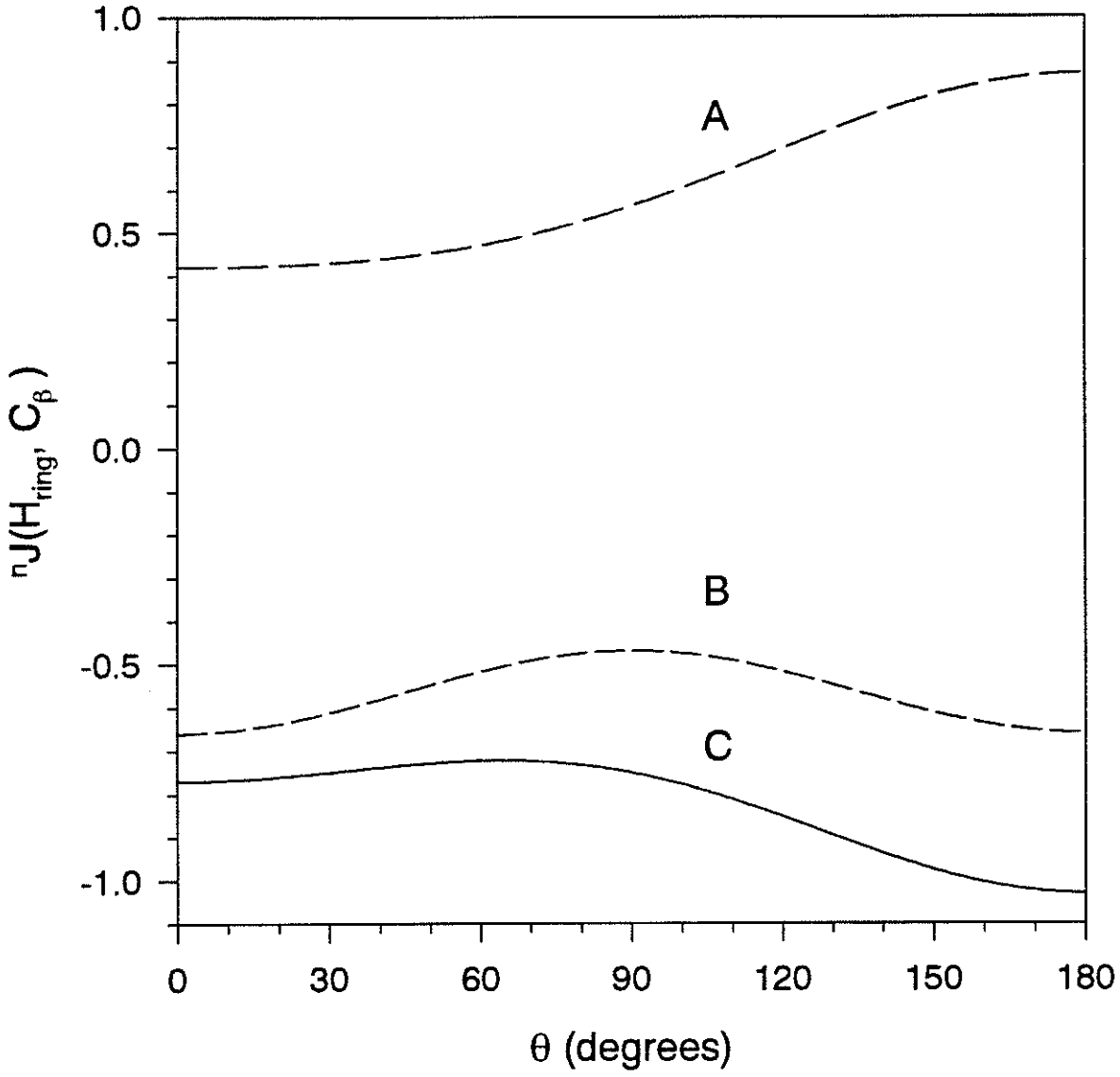

Figure 39: INDO MO FPT coupling expressions: A) ${}^{5}J(H_3, C_\beta)$; B) ${}^{6}J(H_4, C_\beta)$; C) ${}^{4}J(H_2, C_\beta)$.

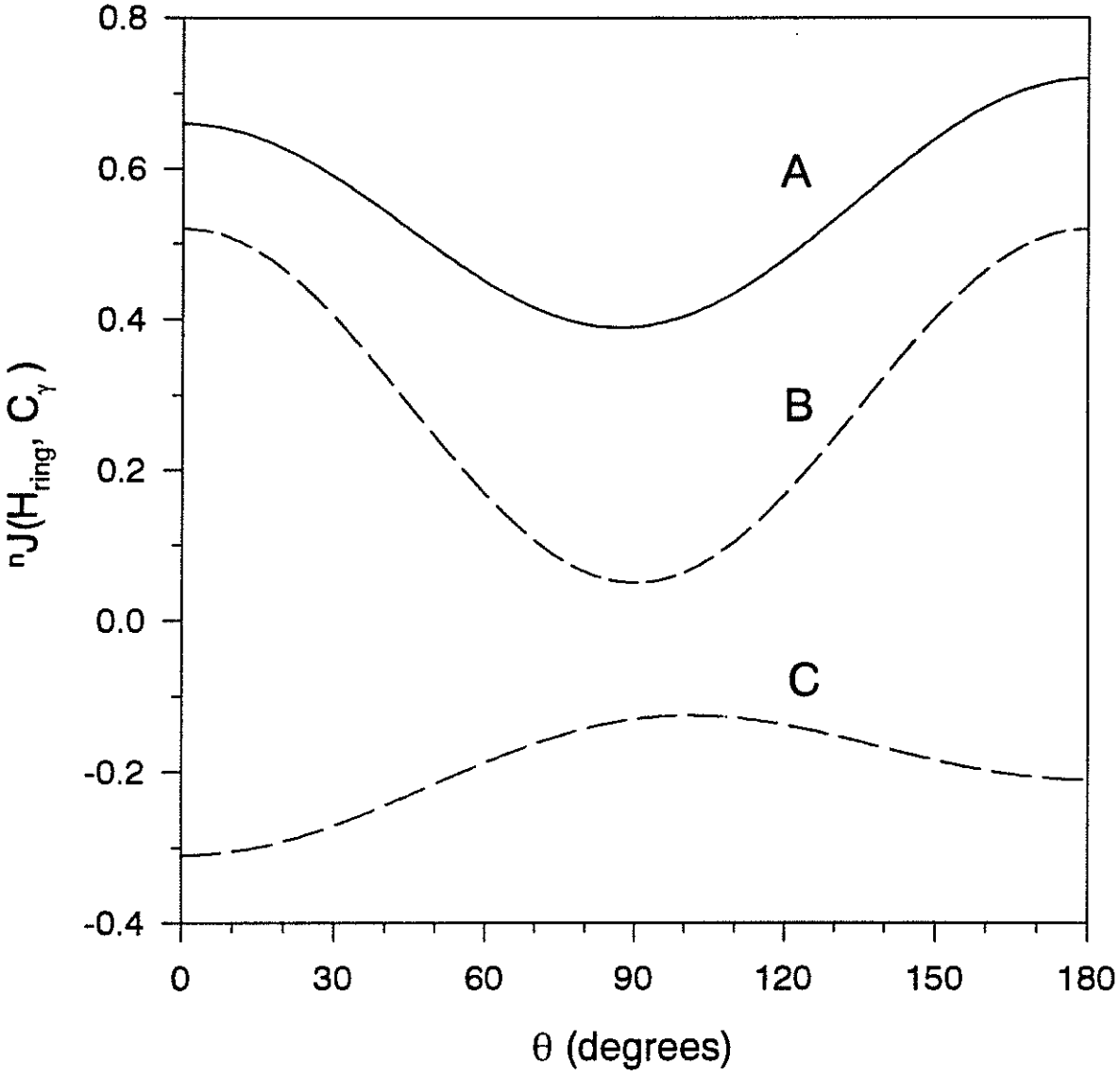

Figure 40: INDO MO FPT coupling expressions: A) $^5J(H_2, C_\gamma)$; B) $^7J(H_4, C_\gamma)$; C) $^6J(H_3, C_\gamma)$.

The ortho protons

The theoretical vicinal coupling constant, ${}^3J(H_2, C_\alpha)$, follows the expression

$$ {}^3J(H_2, C_\alpha) = 4.55 + 0.77\cos^2\theta + 1.05\sin^2(\theta/2), $$

suggesting a π electron contribution of 0.77 Hz. The term in $(\sin^2(\theta/2))$ may represent a substituent effect from C_β. Utilizing the computed geometric terms, this function predicts ${}^3J(H_2, C_\alpha)$ as 5.76 Hz, not substantially different than the measured value of 5.36 Hz. The analogous coupling in toluene is only 4.62 Hz. Part of this difference must be due to a π electron contribution in phenylallene, obviously absent in toluene, through the partial double bond connecting C_α to the ring. Probably factoring into the observed difference as well, is the greater length of this bond in toluene.

INDO calculates

$$ {}^4J(H_2, C_\beta) = -0.63\sin^2\theta - 0.76\cos^2\theta - 0.26\sin^2(\theta/2). $$

Lacking any means of assessing the π electron components of this coupling, relative to other sites, the entire expression must be scaled by 0.71 to reach agreement with the measured -0.62 Hz.

For ${}^5J(H_2, C_\gamma)$, the INDO numbers are best represented by

$$ {}^5J(H_2, C_\gamma) = 0.36\sin^2\theta + 0.66\cos^2\theta + 0.06\sin^2(\theta/2). $$

The usual π electron component, signified by the term in $\cos^2\theta$, appears to be present, but the meaning of the $\sin^2\theta$ term is not immediately apparent. It cannot be a σ-π contribution of the kind involved in ${}^6J(H_4, C_\beta)$, for that would require ${}^7J(H_4, C_\gamma)$ to also have a substantial value in the perpendicular conformation, which it does not have. Multiplication of the above expression by 0.65 brings it into accord with the measured coupling constant of 0.43 Hz.

The meta protons

The theoretical formulation of ${}^4J(H_3, C_\alpha)$ follows the relationship

$$ {}^4J(H_3, C_\alpha) = 0.71 - 0.13\cos^2\theta - 0.17\sin^2(\theta/2), $$

implying a contribution of -0.13 Hz from the π electrons in the fully conjugated planar conformer, and, perhaps, a negative substituent perturbation with a maximum magnitude for the all-*trans* extension of the C_α–C_β. The experimental value is 0.80 Hz — larger, surprisingly, than the 0.51 Hz predicted theoretically. This is the only instance where such an inversion occurs, suggesting that INDO *underestimates* the σ electron component of ${}^4J(H, C)$ for the familiar W configuration of the intervening bonds in an aromatic system.

In ${}^5J(H_3, C_\beta)$, INDO's usual overestimate is again evident, citing

$$ {}^5J(H_3, C_\beta) = 0.42\cos^2\theta + 0.34\sin^2\theta + 0.45\sin^2(\theta/2). $$

This relationship purports a value of 0.63 Hz, while the observed value is less than half as large.

Finally for phenylallene, ${}^6J(H_3, C_\gamma)$ computes as

$$ {}^6J(H_3, C_\gamma) = -0.31\cos^2\theta - 0.18\sin^2\theta + 0.10\sin^2(\theta/2). $$

The positive σ electron term has a precedent in one of similar magnitude predicted for the all-*trans* ${}^6J(H_5, H_9)$ in styrene [18] (see Figure 1), and confirmed in 3-fluorostyrene [23]. The predicted value of ${}^6J(H_3, C_\gamma)$ in phenylallene, however, is -0.25 Hz, in poor agreement with the measured coupling of $\pm 0.04(2)$ Hz. In order to assess which term, or *terms*, are faulty in the theory, would require a phenylallene derivative characterized by a large effective torsion angle.

3.2 2-Formylstyrene

3.2.1 Proton NMR

Proton NMR data from the 2-formylstyrene solutions described in Table 1 are detailed in Tables 10 to 12. Chemical shifts and coupling constants are given in units of *hertz (Hz)*. Numbers in parentheses, where given, are standard deviations in the last significant digit, as given by the NUMMRIT analysis. All other standard deviations are less than 0.001 Hz. Molecular structure and numbering are given in Figure 41. The spectra were treated as arising from an ABCDEFGX spin system. Representative examples of spectral fits are displayed in Figures 42 to 63.

Some unique spectral features arise from the strong deshielding of H_7 (*vide infra*), juxtaposing its spectrum with spectra of two of the aromatic protons. The proximity of their chemical shifts, for example, produces severe spectral congestion and overlapping peaks (Figure 47). Additionally, second order effects combine with a very small coupling to the formyl proton in acetone-d_6, to produce an unusual aromatic spectrum for H_5 (Figure 45 and 46). Measured chemical shifts are accounted for qualitatively in Section 3.2.4.

Signs of coupling constants were determined unambiguously from the spectral analysis. Some imperfections in the agreement between the experimental and calculated spectra are observed. Figure 52, for example, displays the ^{1}H NMR spectrum of the formyl proton in acetone-d_6 solution. At high magnification corresponding to about 0.3 Hz/cm, it can be seen that two of the theoretical peaks are split by about 0.02 Hz, but appear experimentally as single peaks. Different combinations of signs for $^6J_{8,10}$, $^6J_{9,10}$ and $^5J_{7,10}$ lead to further disagreement in this region, as well as in the H_8 and H_9 regions. Moreover, introduction of a small dipolar coupling constant between H_7 or H_8 and H_{10} does not improve the fit. A similar discrepency is apparent for the formyl proton in a solution of CS_2/C_6D_{12} (Figure 63). With this evidence, the given signs are taken to be unequivocal and it is unlikely that the magnitudes used to reproduce experimental data differ sufficiently from the *true* values to affect their

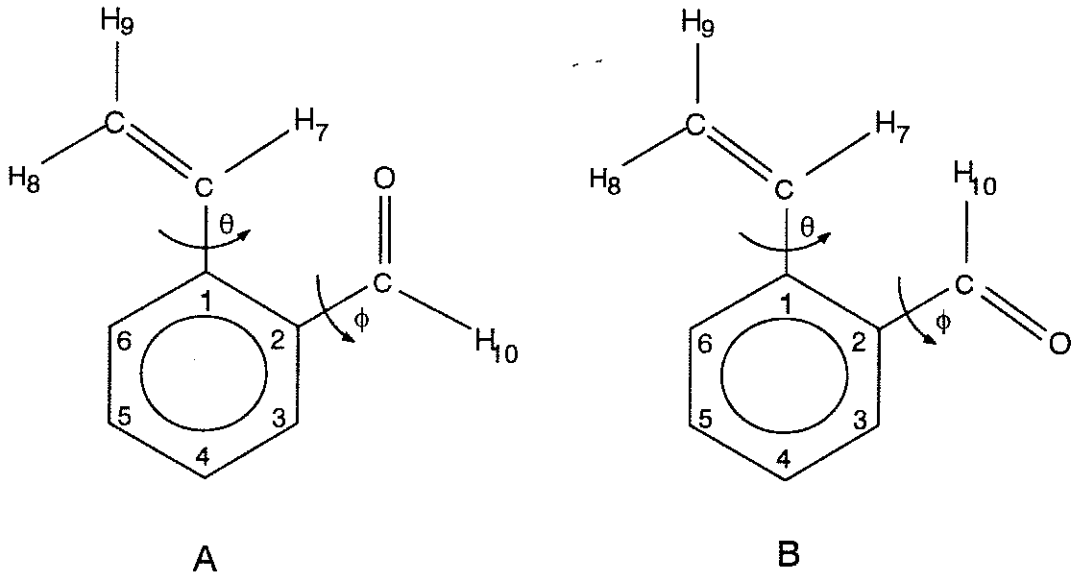

Figure 41: Molecular structure and numbering scheme for 2-formylstyrene conformers **A** and **B** drawn in the planar conformation where $\theta = 0°$.

use in the text.

The solvent-induced changes in intravinyl coupling constants, ^2J_g, ^3J_c and ^3J_t, are parallel to those measured in 3-fluorostyrene [23]. Similarly, coupling constants within the ring change with the polar solvent in analogy with both 3-fluorostyrene and 2-formylisopropylbenzene [77]. Such small changes, also measured for monosubstituted benzenes in this laboratory, follow patterns largely independent of the nature of the substituent.

Table 10: ^{1}H NMR chemical shifts and analytical statistics for 2-formylstyrene in acetone-d_6 and carbon disulphide at 300 K.

Parameter	$(CH_3)_2C{=}O^a$	$CS_2/C_6D_{12}^b$
ν_3^c	2361.030^d	2308.103
ν_4	2252.764	2201.007
ν_5	2290.354	2233.088
ν_6	2308.563	2245.712
ν_7	2302.246	2259.685
ν_8	1735.959	1686.709
ν_9	1644.871	1620.604
ν_{10}	3094.369	3052.218
Calculated Transitions	1097	1097
Assigned Transitions	803	889
Peaks Observed	549	590
Largest Difference	0.009	0.015
RMS deviation	0.004	0.006

a) 4.43 *mol%* in acetone-d_6 with TMS as an internal reference. See Table 1 for details. *b*) Prepared to 5.6 *mol%* in CS_2 also containing 10.0 % C_6D_{12} and TMS as internal reference. Some precipitate was observed in the sample tube, however, rendering the concentration uncertain. *c*) In Hz at 300.135 MHz to high frequency of internal TMS. *d*) All standard deviations less than 0.001 Hz.

Table 11: Intragroup ^{1}H NMR coupling constants (Hz) for 2-formylstyrene in acetone-d_6 and carbon disulphide at 300 K.

Parameter	$(CH_3)_2C{=}O^a$	$CS_2/C_6D_{12}^b$
^2J_g	1.291[c]	1.338
^3J_c	11.045	10.965
^3J_t	17.453	17.353
$^3J_{3,4}$	7.738	7.712
$^3J_{4,5}$	7.374	7.354
$^3J_{5,6}$	7.858	7.822
$^4J_{3,5}$	1.458	1.464
$^4J_{4,6}$	1.191	1.206
$^5J_{3,6}$	0.542	0.533

a) 4.4 *mol*% in acetone-d_6 with TMS as an internal reference. See Table 1 for details. *b*) Prepared to 5.6 *mol*% in CS_2 also containing 10.0 % C_6D_{12} and TMS as internal reference. Some precipitate was observed in the sample tube, however, rendering the concentration uncertain. *c*) All standard deviations less than 0.001 Hz.

Table 12: Long range coupling constants (Hz) of the olefinic and aldehydic protons in 2-formylstyrene at 300 K for solutions of acetone-d_6 and carbon disulphide.

Parameter	$(CH_3)_2C{=}0^a$	$CS_2/C_6D_{12}^b$	*Parameter*	$(CH_3)_2C{=}0$	CS_2/C_6D_{12}
$^4J_{6,7}$	–0.635[c]	–0.640	$^7J_{4,8}$	0.184	0.180
$^5J_{5,7}$	0.600	0.579	$^7J_{4,9}$	0.216	0.206
$^5J_{3,7}$	0.161	0.171	$^4J_{3,10}$	–0.252	–0.251
$^6J_{4,7}$	–0.344	–0.353	$^5J_{4,10}$	0.441	0.447
$^5J_{6,8}$	–0.136	–0.129	$^5J_{6,10}$	0.364	0.362
$^5J_{6,9}$	0.045	0.049	$^5J_{7,10}$	–0.163	–0.163
$^6J_{5,8}$	–0.026	–0.022(1)	$^6J_{5,10}$	–0.020	–0.027
$^6J_{5,9}$	–0.027	–0.017(1)	$^6J_{8,10}$	0.030	0.039
$^6J_{3,8}$	–0.086	–0.083	$^6J_{9,10}$	0.025	0.038
$^6J_{3,9}$	0.053	0.051			

a) 4.43 *mol*% in acetone-d_6 with TMS as an internal reference. See Table 1 for details. *b*) Prepared to 5.6 *mol*% in CS_2 also containing 10.0 % C_6D_{12} and TMS as internal reference. Some precipitate was observed in the sample tube, however, rendering the concentration uncertain. *c*) All standard deviations less than 0.001 Hz, unless otherwise indicated.

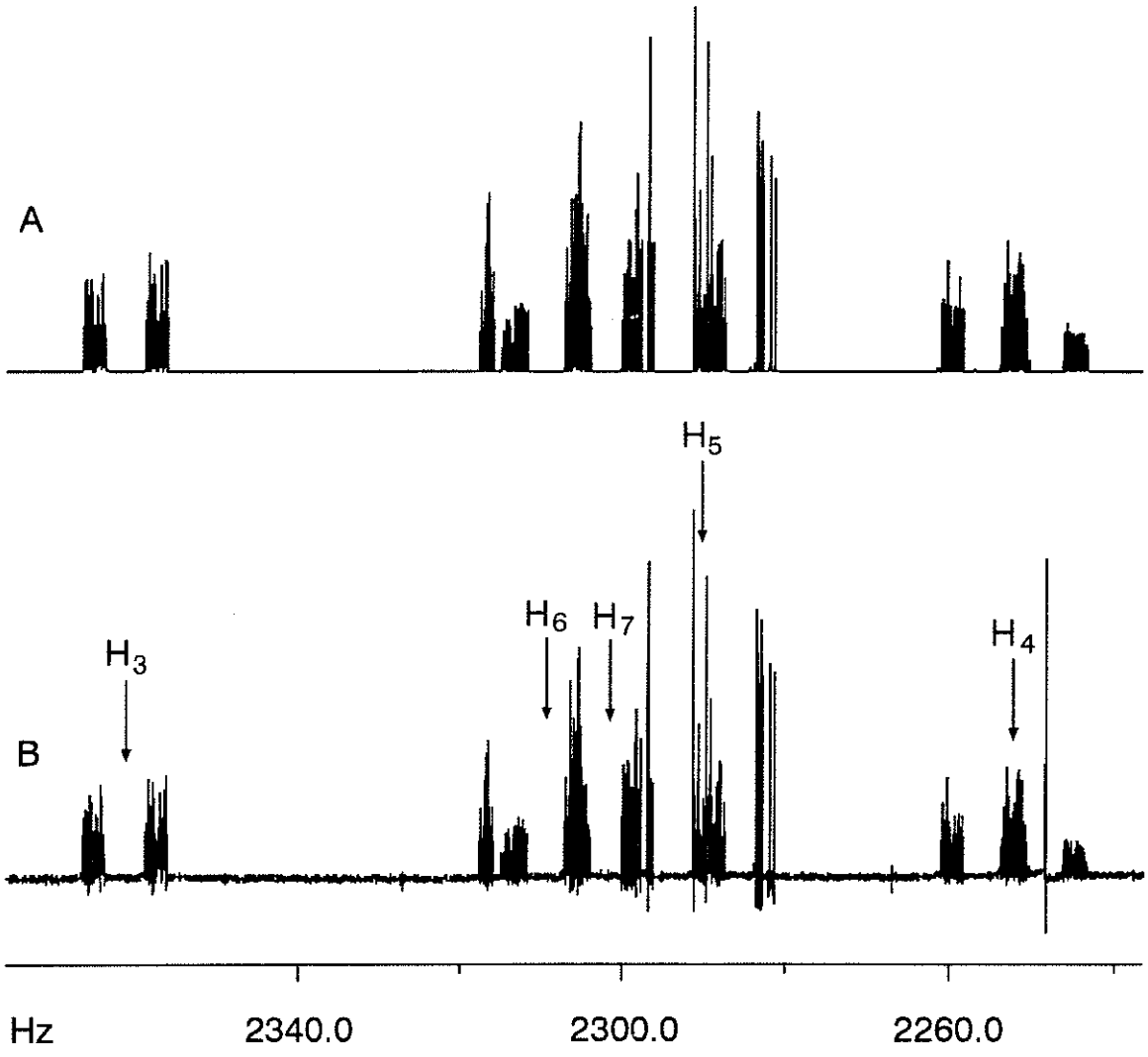

Figure 42: ^{1}H NMR spectrum of 2-formylstyrene aromatic region in acetone-d_6. A) Theoretical spectrum; B) Experimental spectrum.

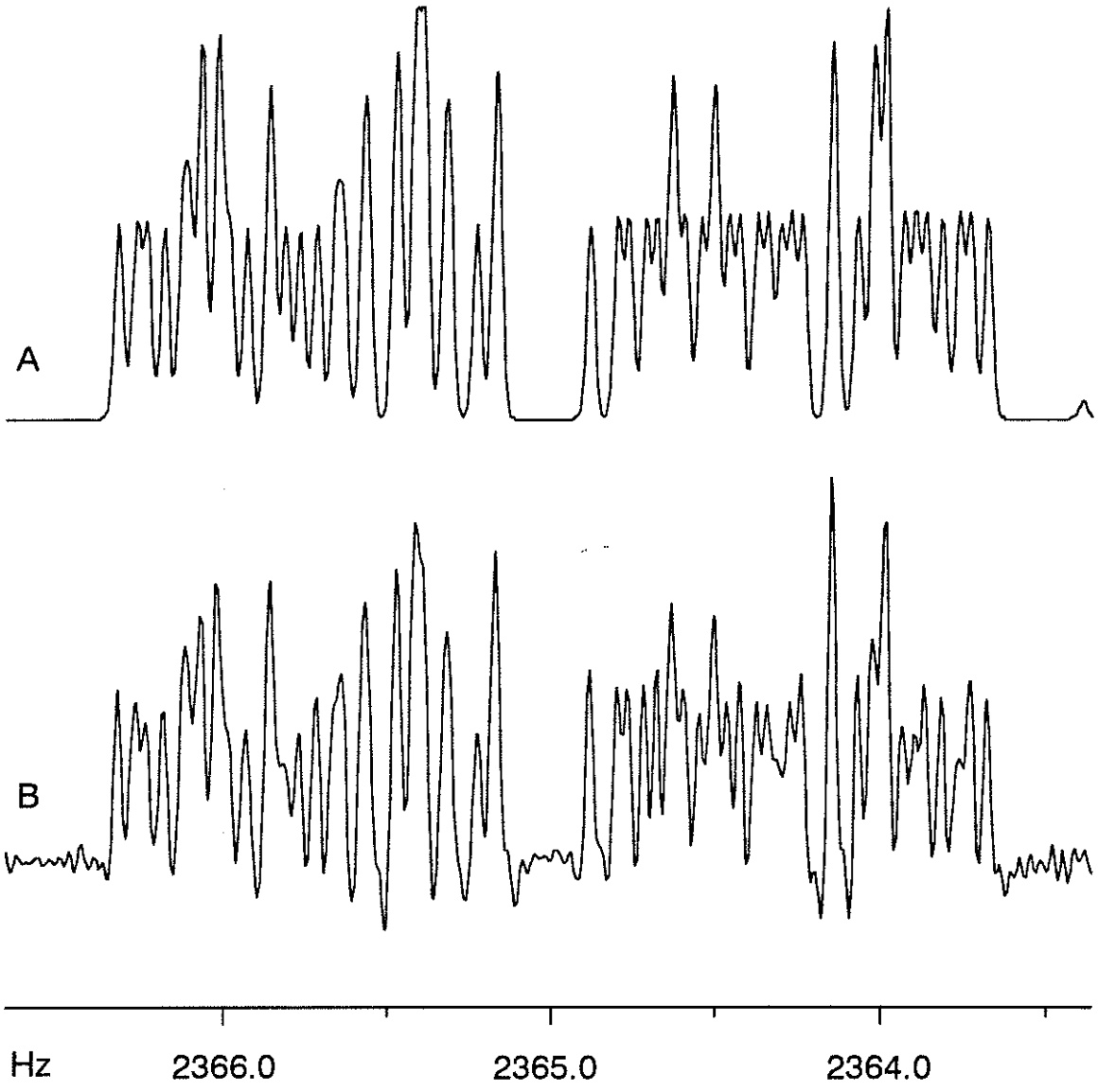

Figure 43: ^{1}H NMR spectrum of 2-formylstyrene H_3 (high frequency portion) in acetone-d_6. A) Theoretical spectrum with 30 mHz linewidth; B) Experimental spectrum.

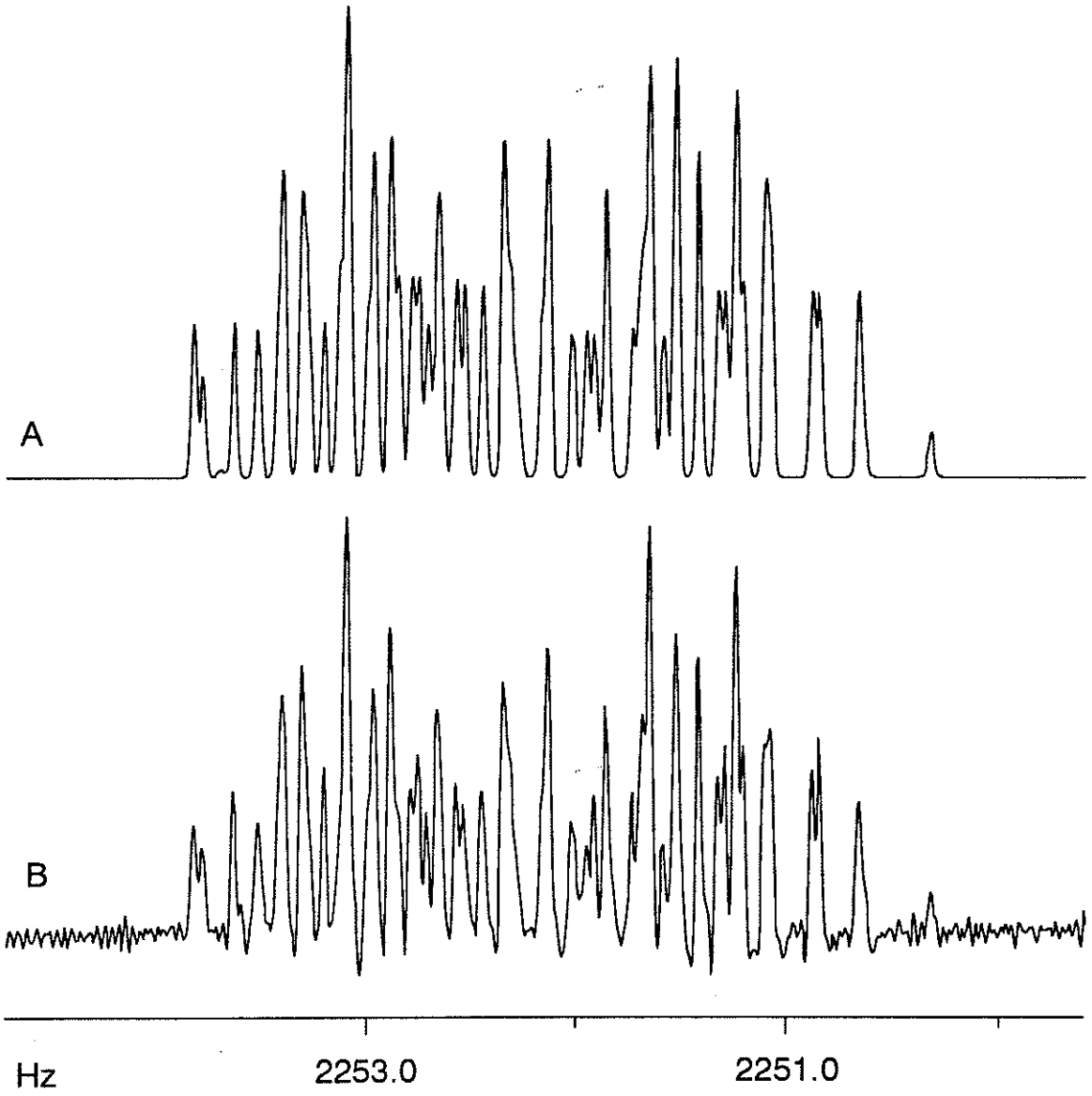

Figure 44: ^{1}H NMR spectrum of 2-formylstyrene H_4 (central portion of 'triplet') in acetone-d_6. A) Theoretical spectrum with 35 mHz linewidth; B) Experimental spectrum.

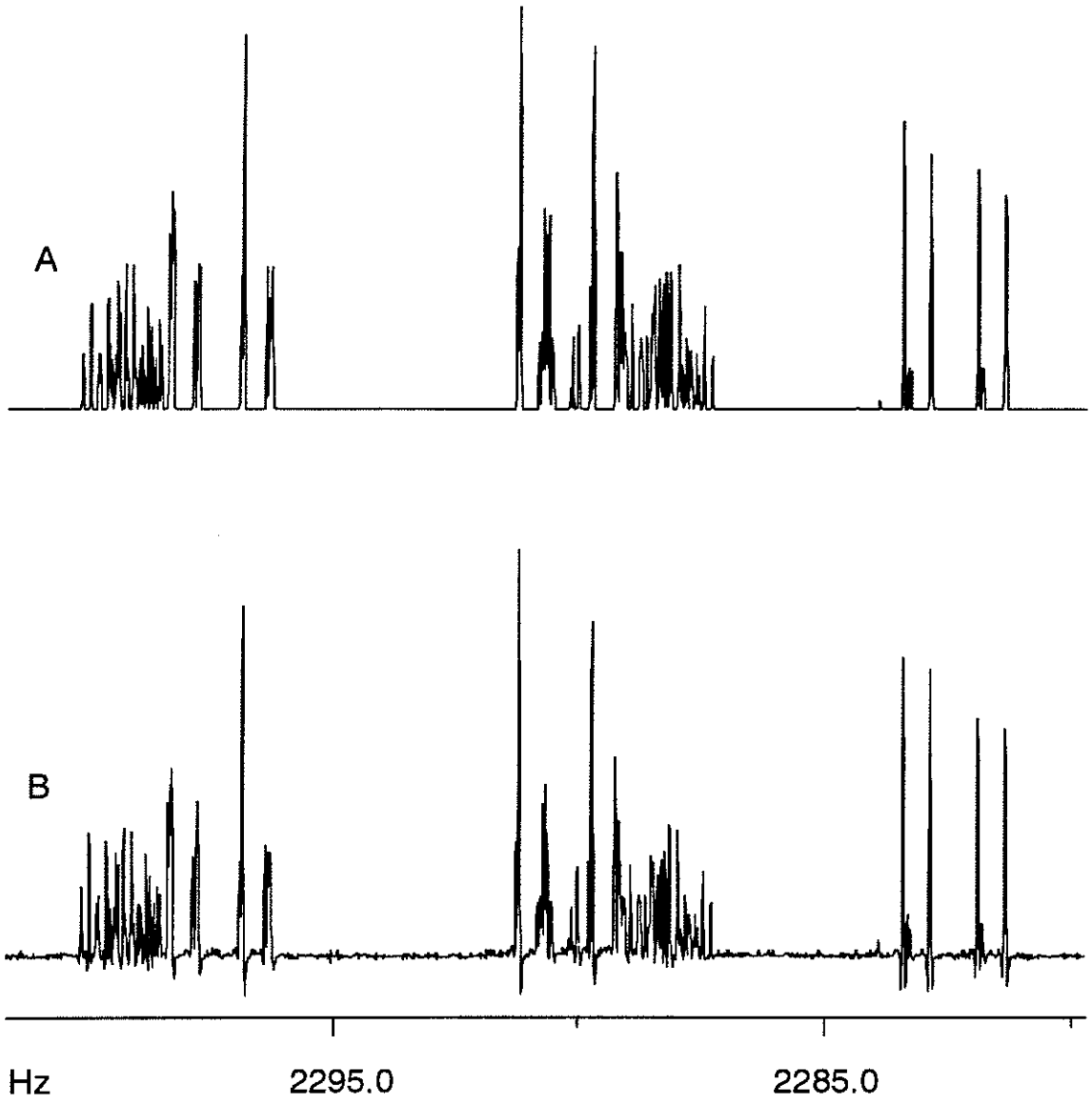

Figure 45: ^{1}H NMR spectrum of 2-formylstyrene H_5 and a portion of H_7 in acetone-d_6. A) Theoretical spectrum; B) Experimental spectrum.

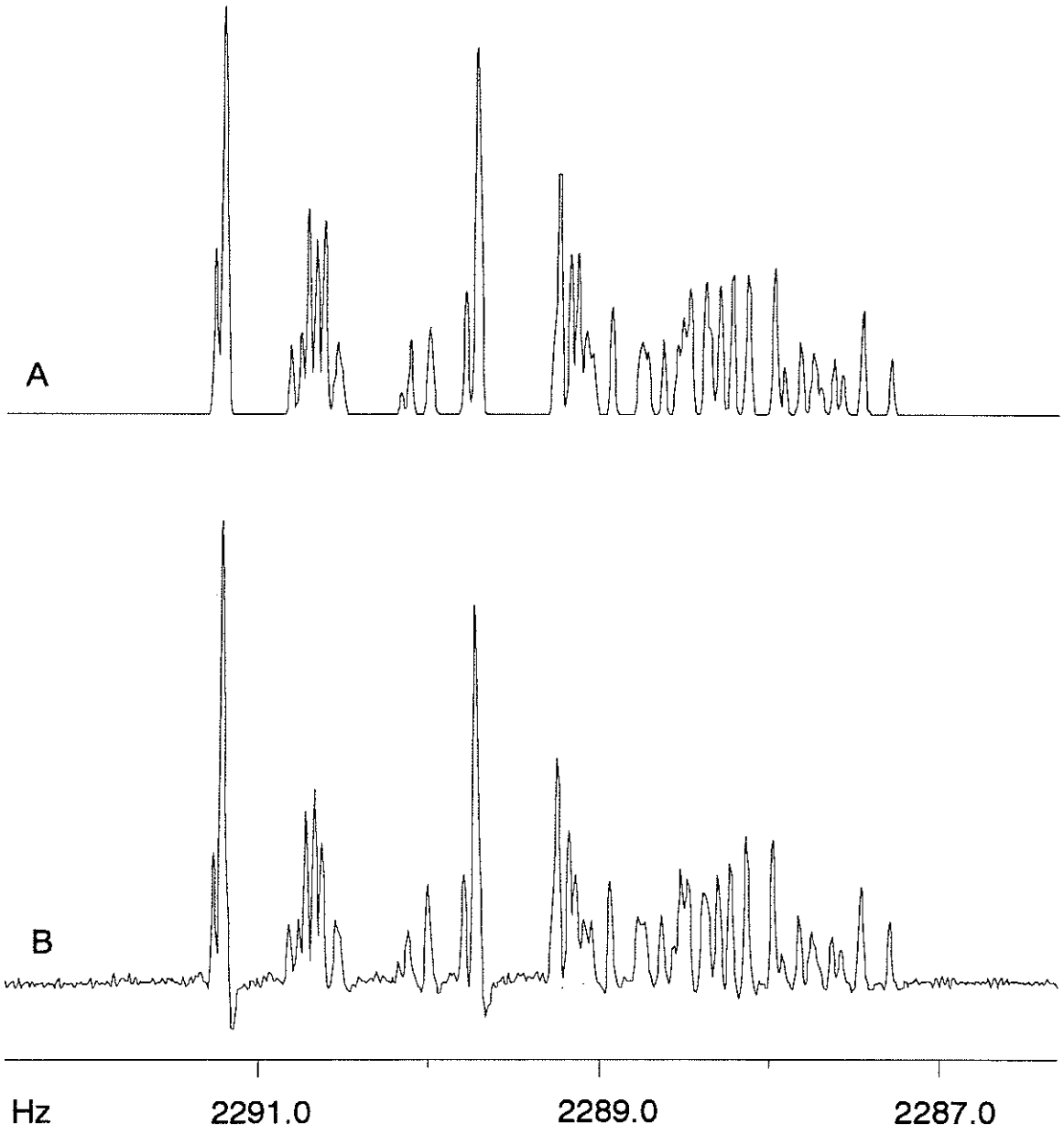

Figure 46: ^{1}H NMR spectral fragment of 2-formylstyrene overlapping H_5 and H_7 in acetone-d_6. A) Theoretical spectrum with a linewidth of 30 mHz; B) Experimental spectrum.

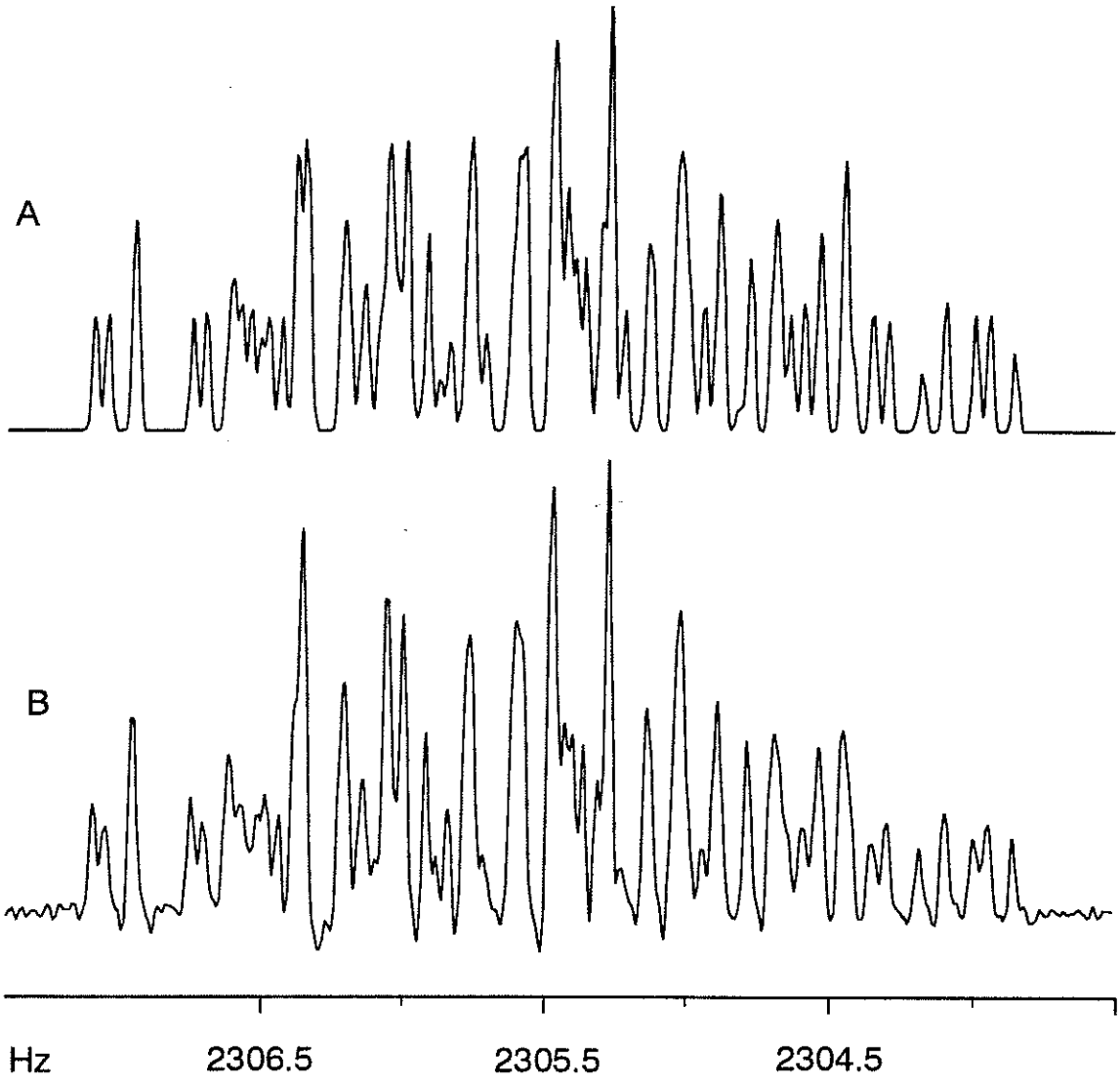

Figure 47: ^{1}H NMR spectrum of overlapping H_6 and H_7 portions of 2-formylstyrene in acetone-d_6. A) Theoretical spectrum with a linewidth of 30 mHz; B) Experimental spectrum.

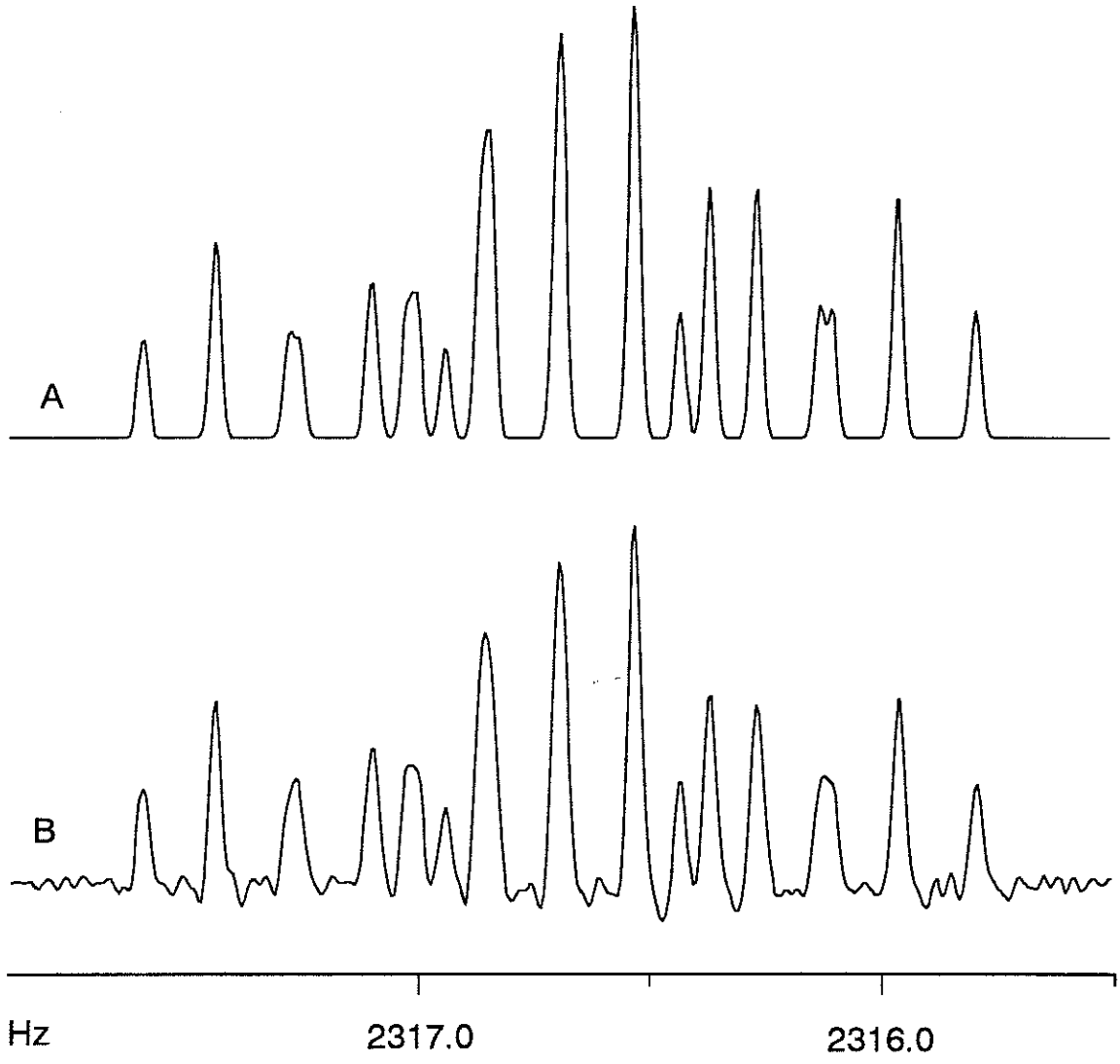

Figure 48: ^{1}H NMR spectrum of 2-formylstyrene of the high frequency portion of H_7 in acetone-d_6. A) Theoretical spectrum with a linewidth of 30 mHz; B) Experimental spectrum.

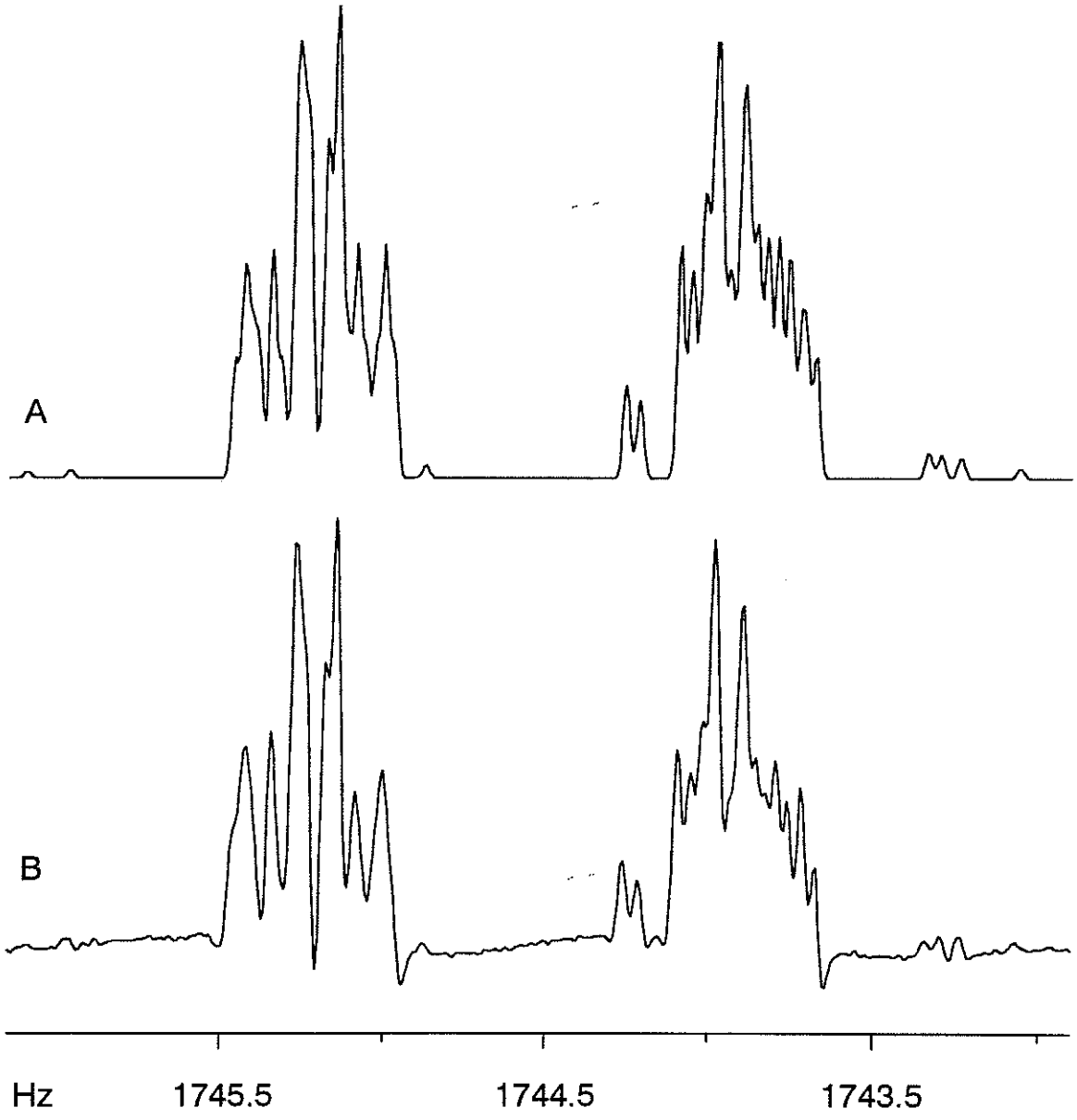

Figure 49: ^{1}H NMR spectrum of 2-formylstyrene H_8 (high frequency portion) in acetone-d_6. A) Theoretical spectrum with 30 mHz linewidth; B) Experimental spectrum.

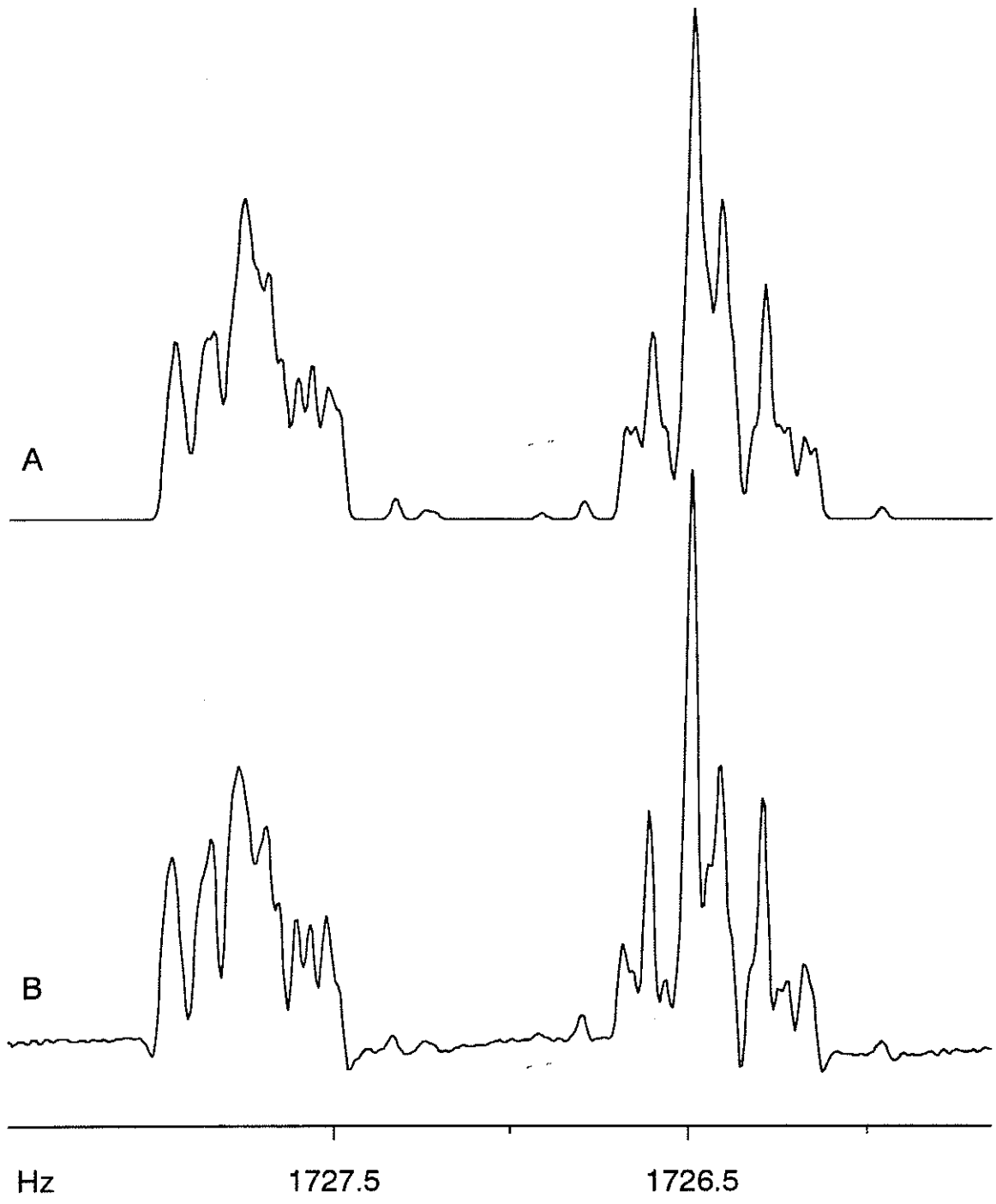

Figure 50: ^{1}H NMR spectrum of 2-formylstyrene H_8 (low frequency portion) in acetone-d_6. A) Theoretical spectrum with 30 mHz linewidth; B) Experimental spectrum.

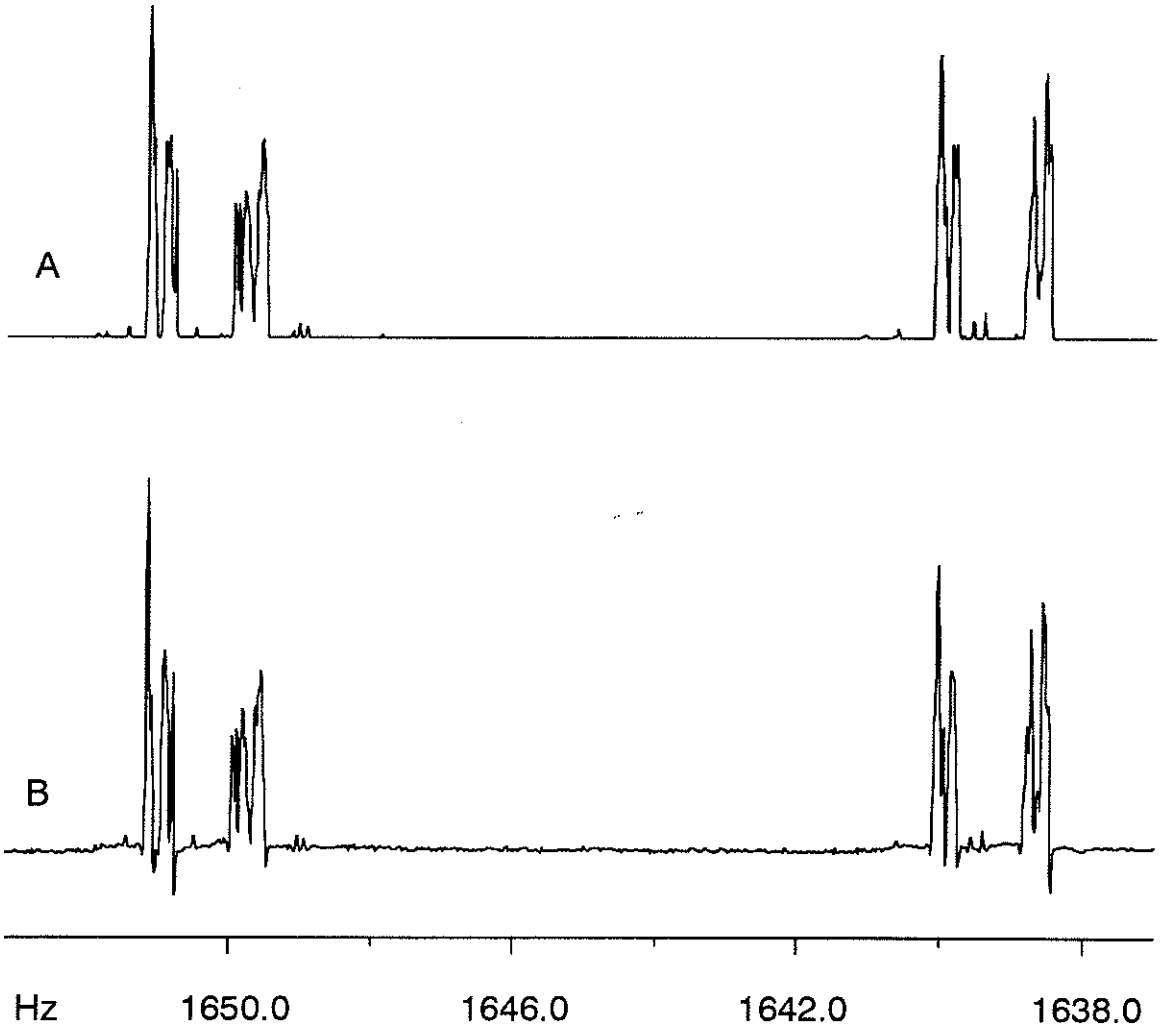

Figure 51: ^{1}H NMR spectrum of 2-formylstyrene H_9 in acetone-d_6. A) Theoretical spectrum; B) Experimental spectrum.

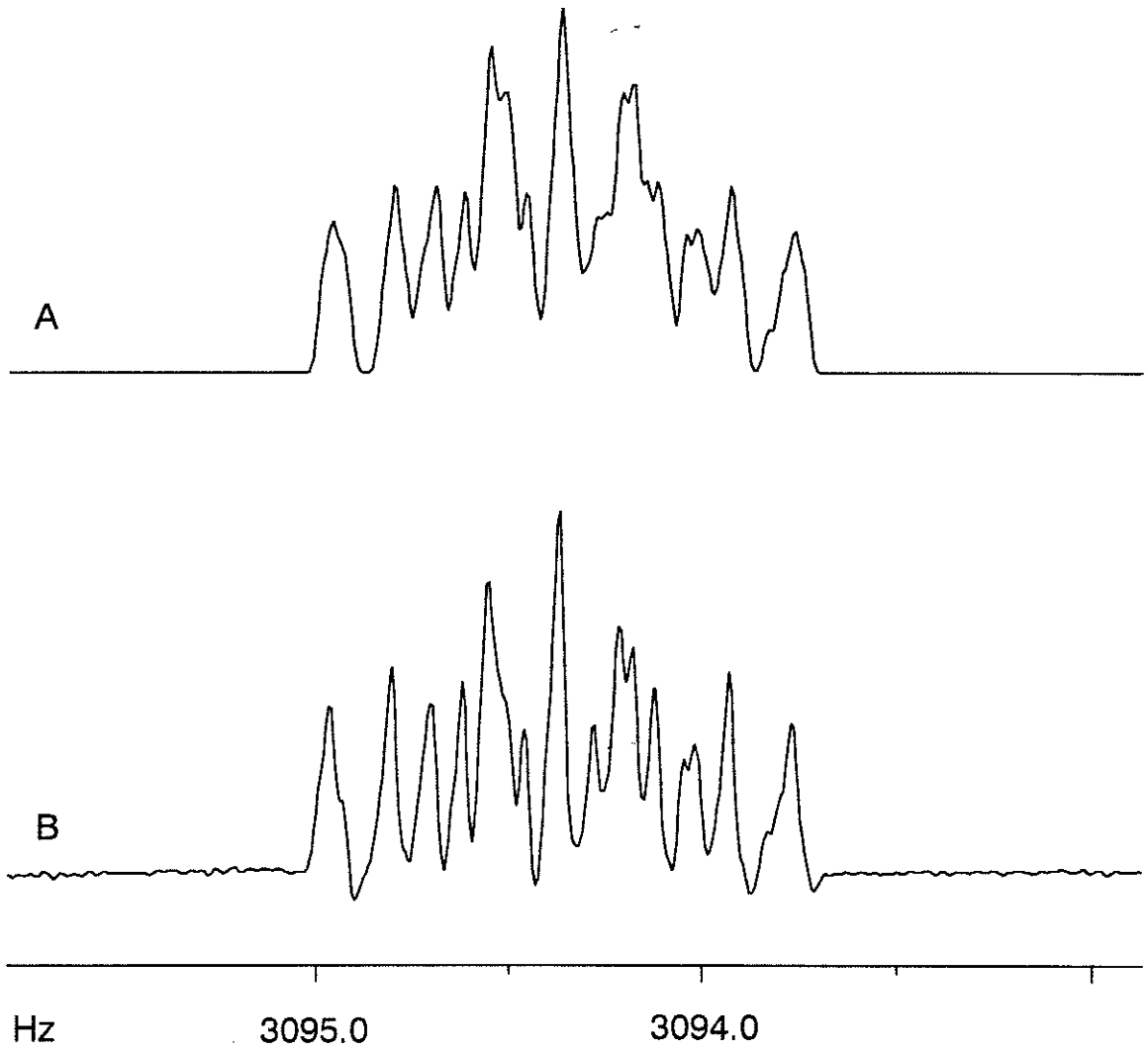

Figure 52: ^{1}H NMR spectrum of the 2-formylstyrene aldehydic proton in acetone-d_6. See text for a discussion of imperfect agreement with experiment. A) Theoretical spectrum with linewidth of 35 mHz; B) Experimental spectrum.

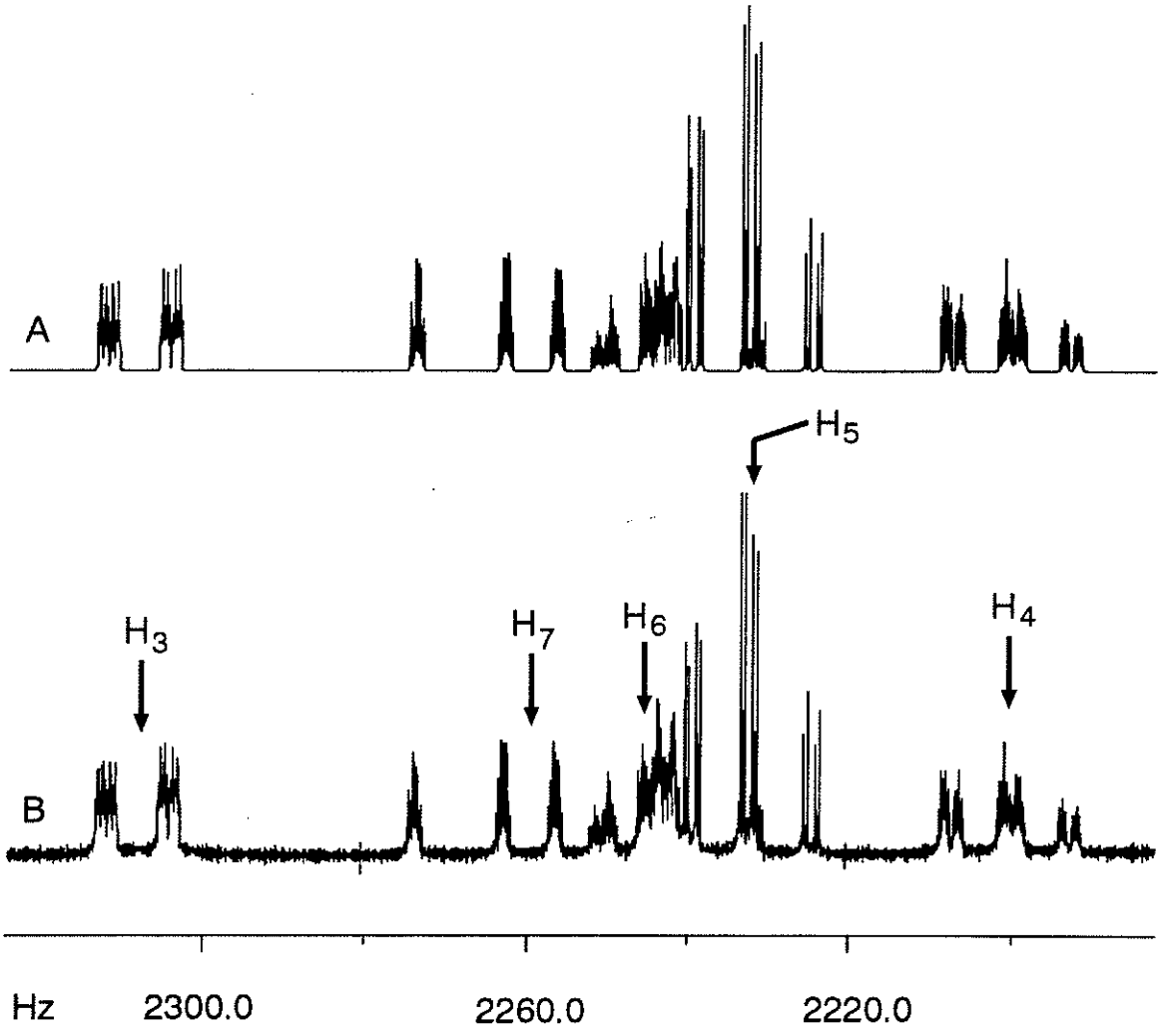

Figure 53: ^{1}H NMR spectrum of 2-formylstyrene aromatic region in CS_2/C_6D_{12}. A) Theoretical spectrum; B) Experimental spectrum.

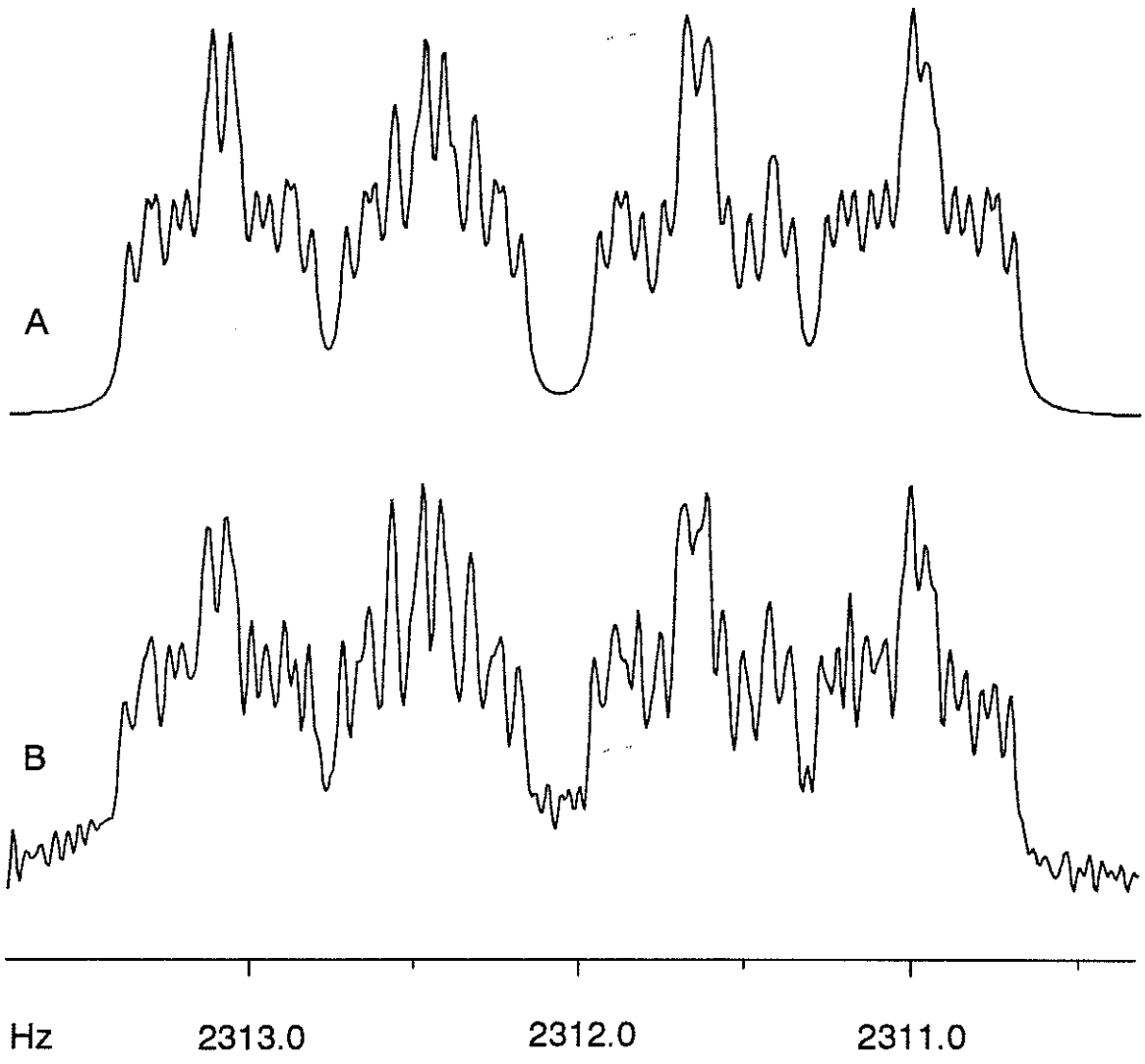

Figure 54: ^{1}H NMR spectrum of 2-formylstyrene H_3 (high frequency portion) in CS_2/C_6D_{12}. A) Theoretical spectrum with 40 mHz linewidth; B) Experimental spectrum.

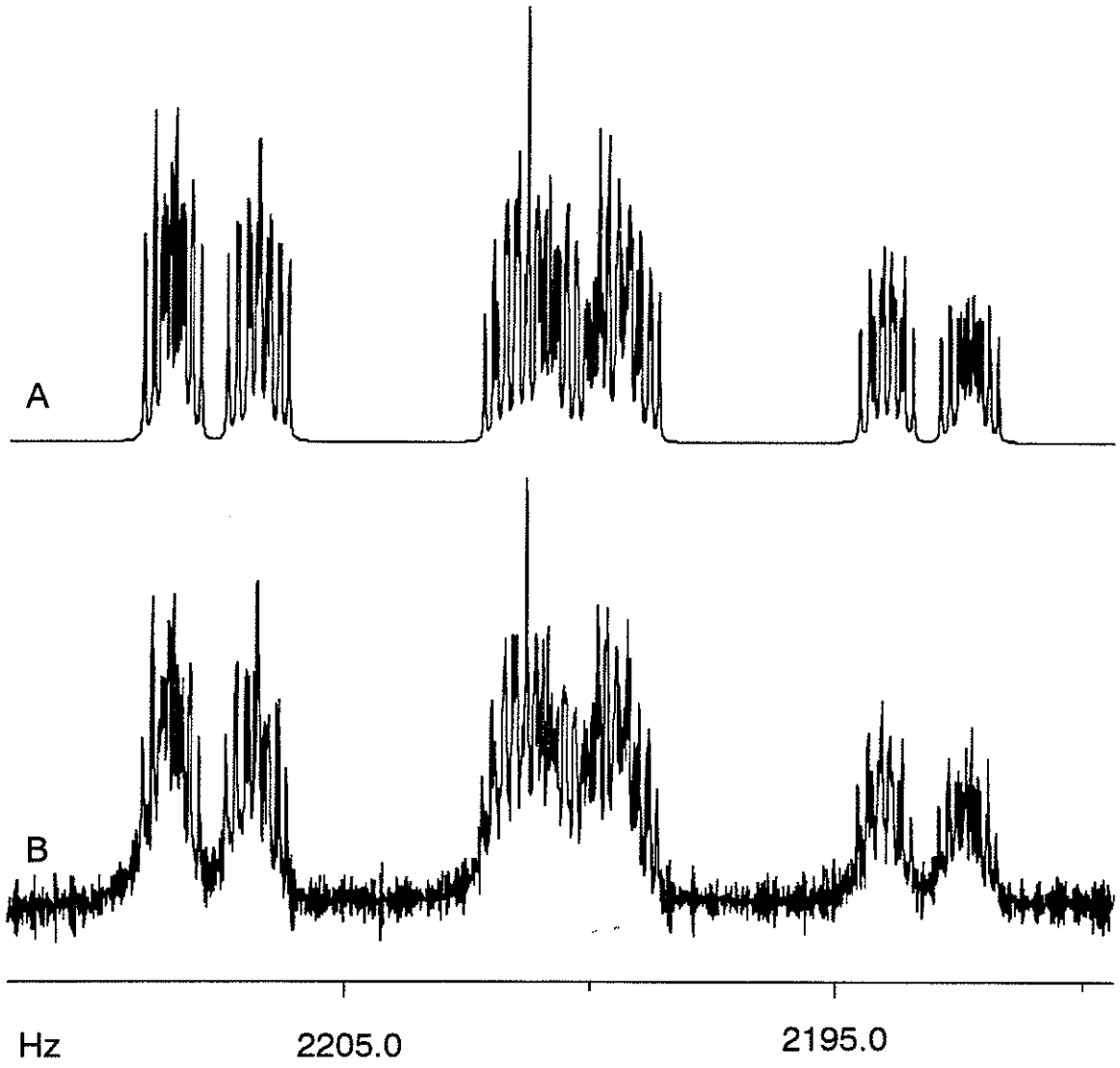

Figure 55: ^{1}H NMR spectrum of 2-formylstyrene H_4 in CS_2/C_6D_{12}. A) Theoretical spectrum; B) Experimental spectrum.

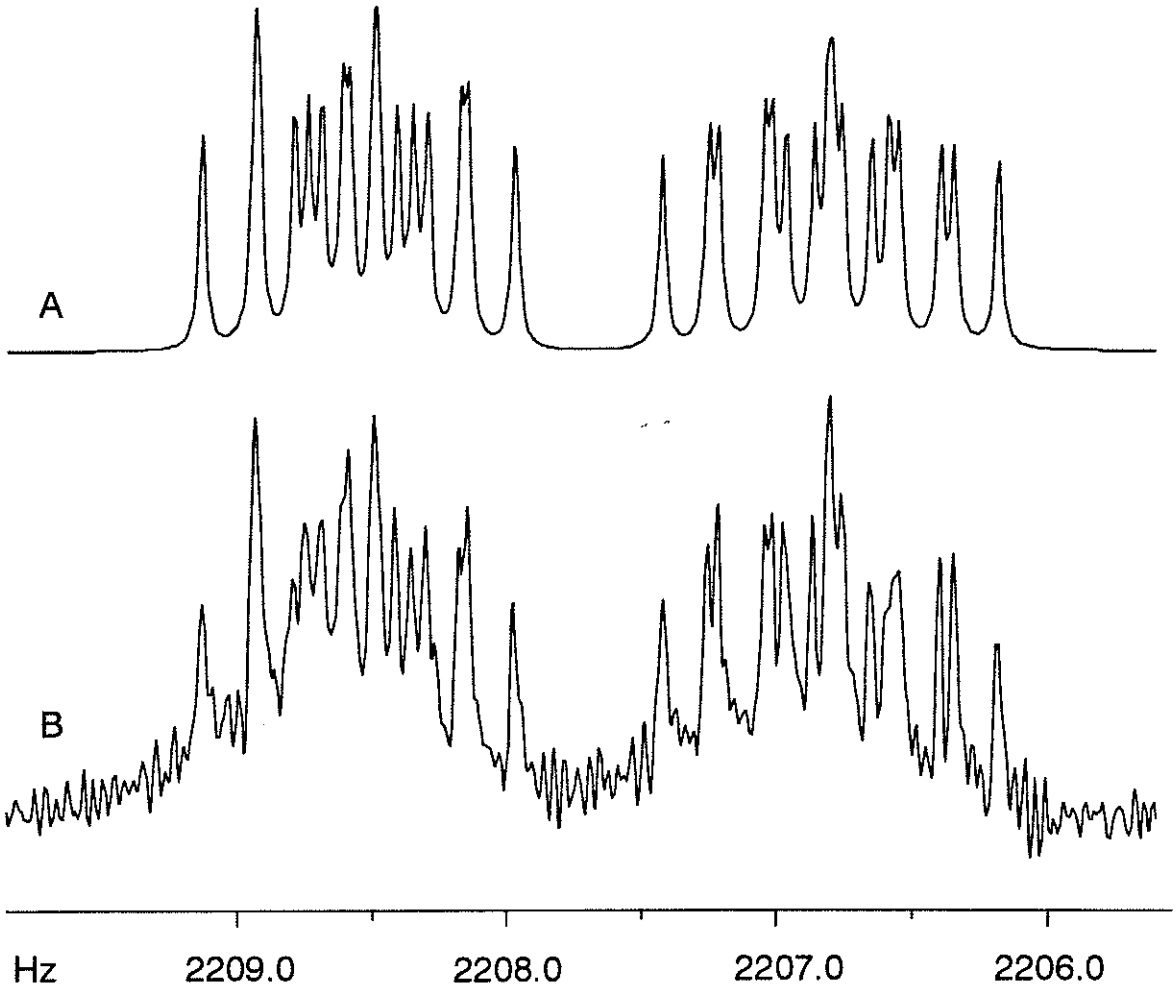

Figure 56: ^{1}H NMR spectrum of 2-formylstyrene H_4 (high frequency portion) in CS_2/C_6D_{12}. A) Theoretical spectrum with 30 mHz linewidth; B) Experimental spectrum.

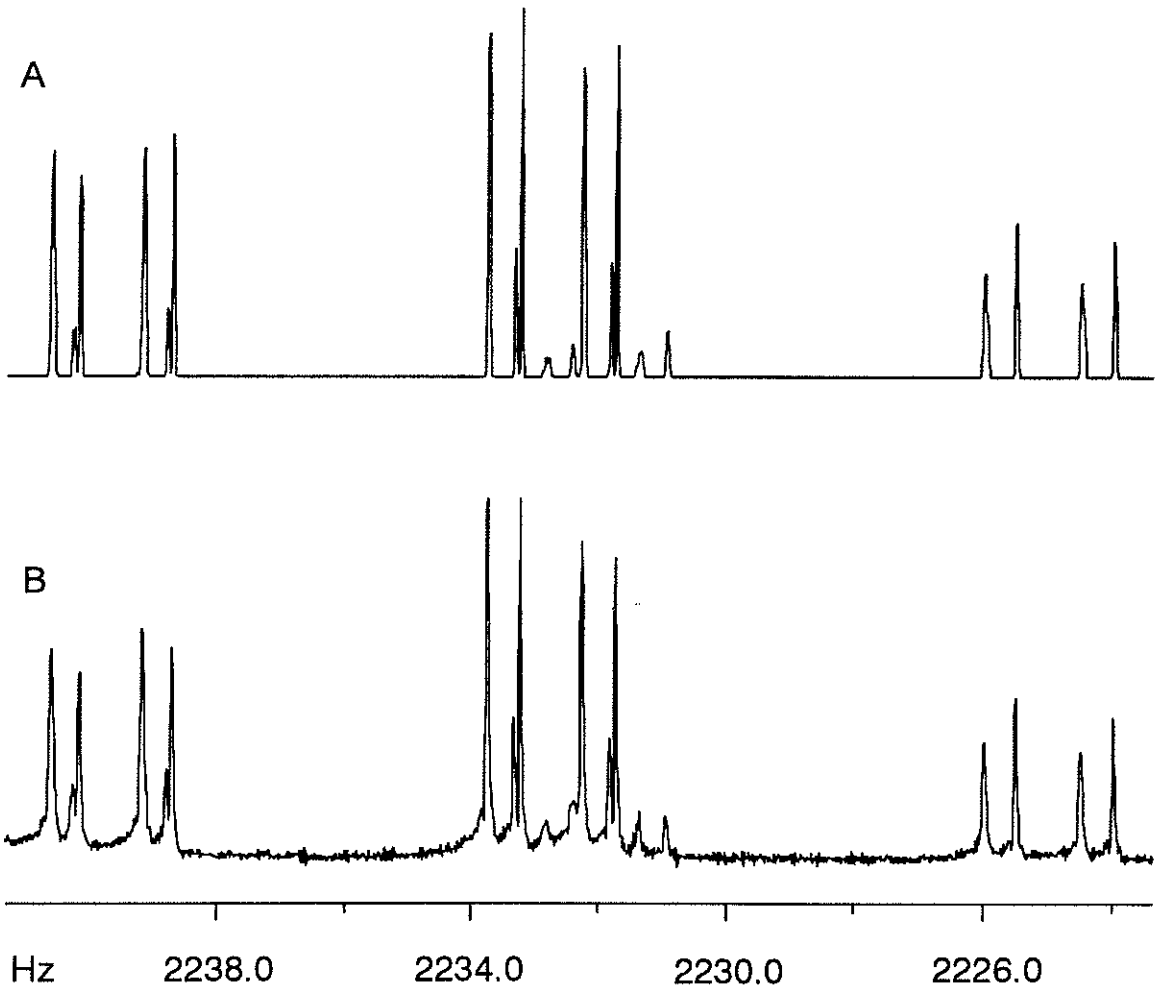

Figure 57: ^{1}H NMR spectrum of 2-formylstyrene H_5 in CS_2/C_6D_{12}. A) Theoretical spectrum with linewidth of 35 mHz; B) Experimental spectrum.

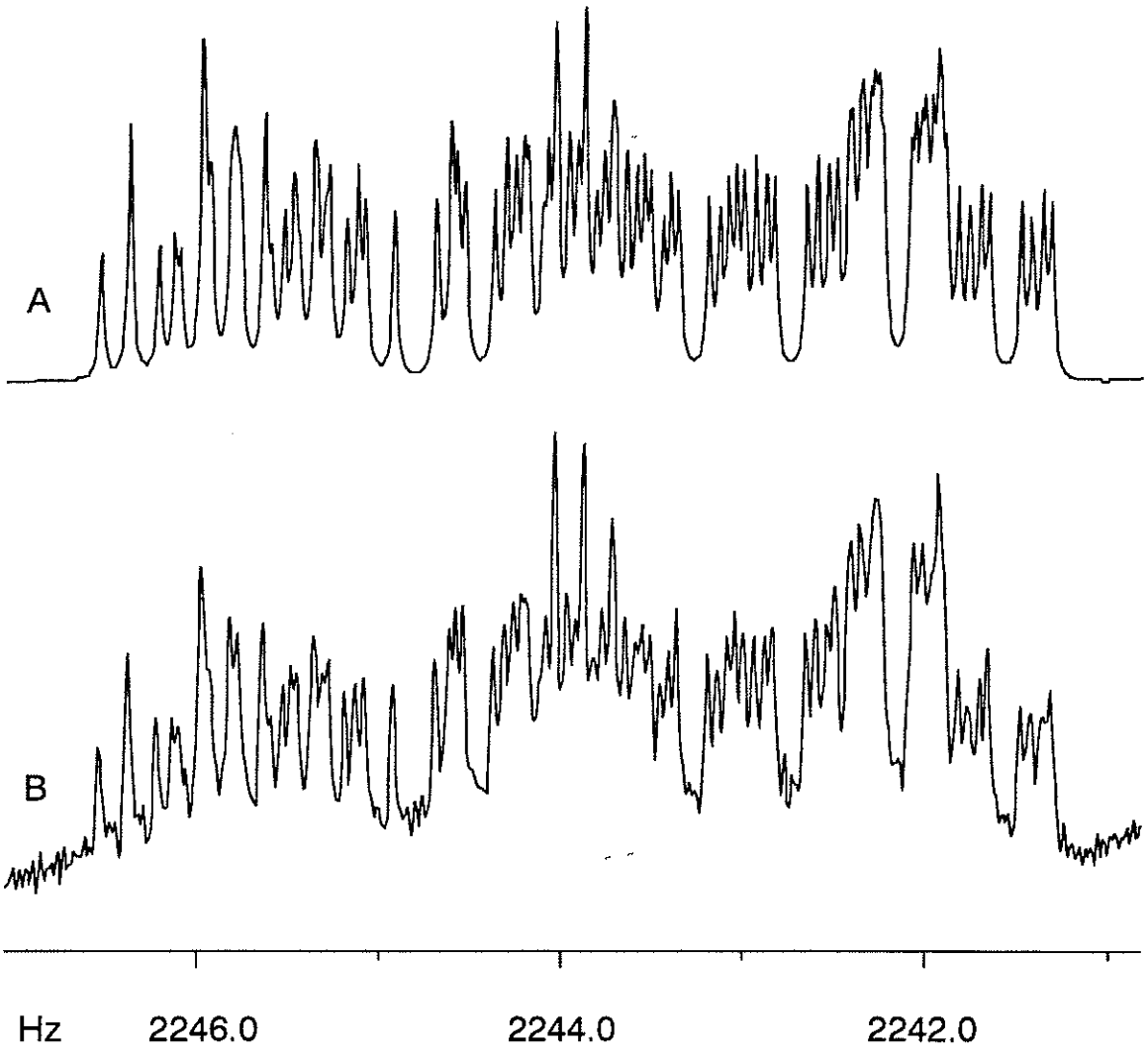

Figure 58: ^{1}H NMR spectrum of overlapping H_6 and H_7 portions of 2-formylstyrene in CS_2/C_6D_{12}. A) Theoretical spectrum with a linewidth of 30 mHz; B) Experimental spectrum.

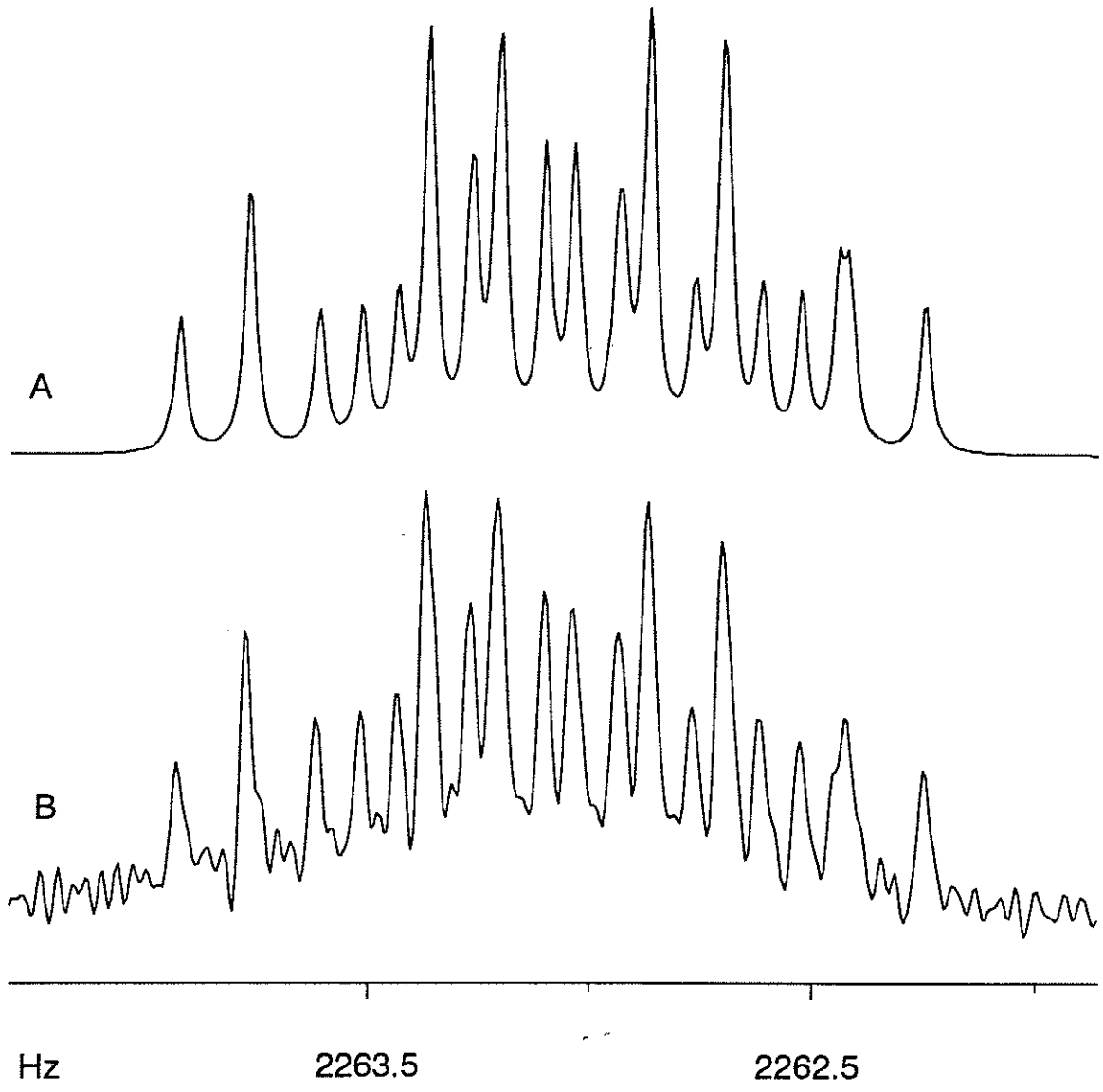

Figure 59: ^{1}H NMR spectrum of 2-formylstyrene of the second highest frequency portion of H_7 in CS_2/C_6D_{12}. A) Theoretical spectrum with a linewidth of 30 mHz; B) Experimental spectrum.

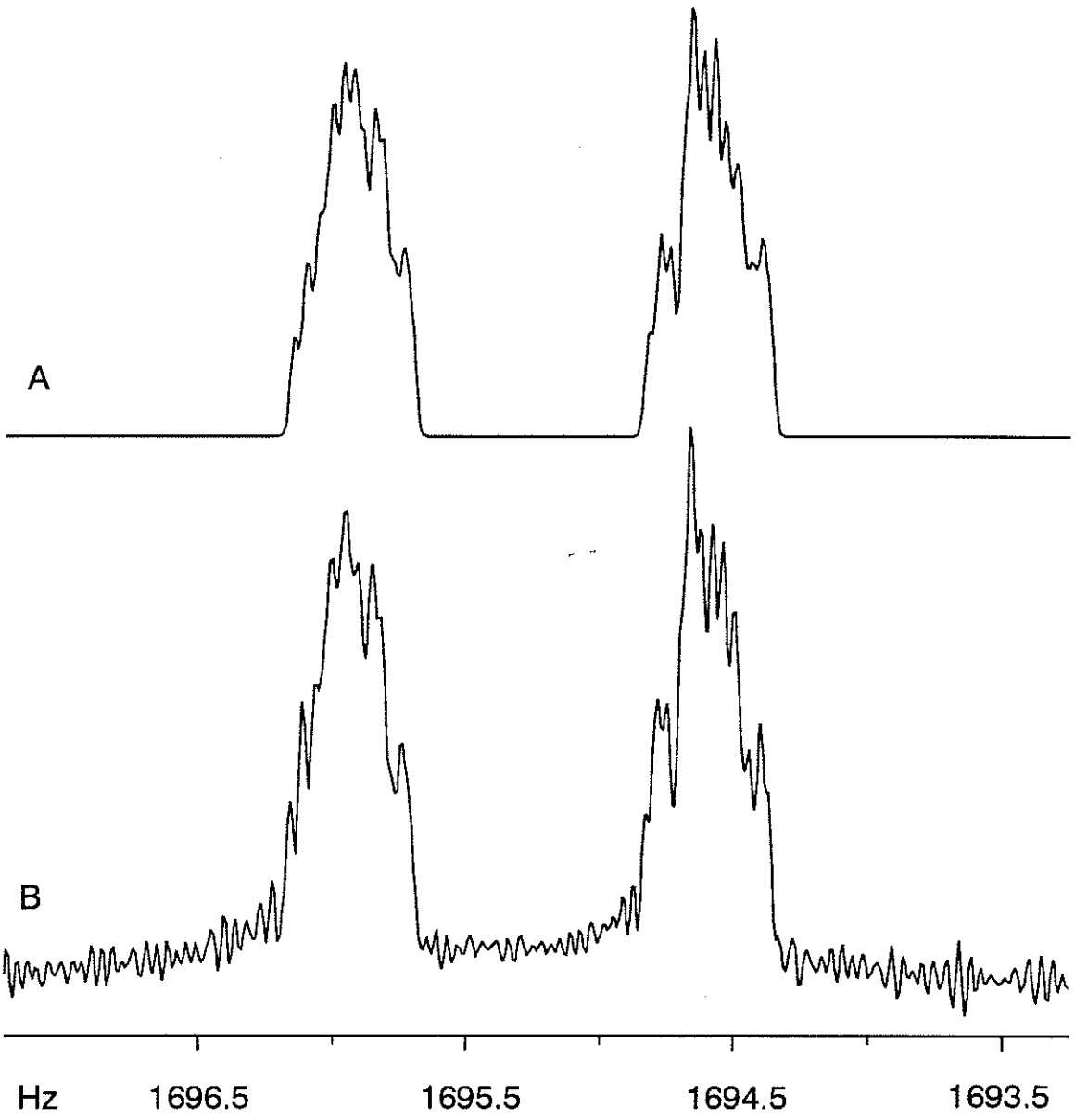

Figure 60: ^{1}H NMR spectrum of 2-formylstyrene H_8 (high frequency portion) in CS_2/C_6D_{12}. A) Theoretical spectrum with 40 mHz linewidth; B) Experimental spectrum.

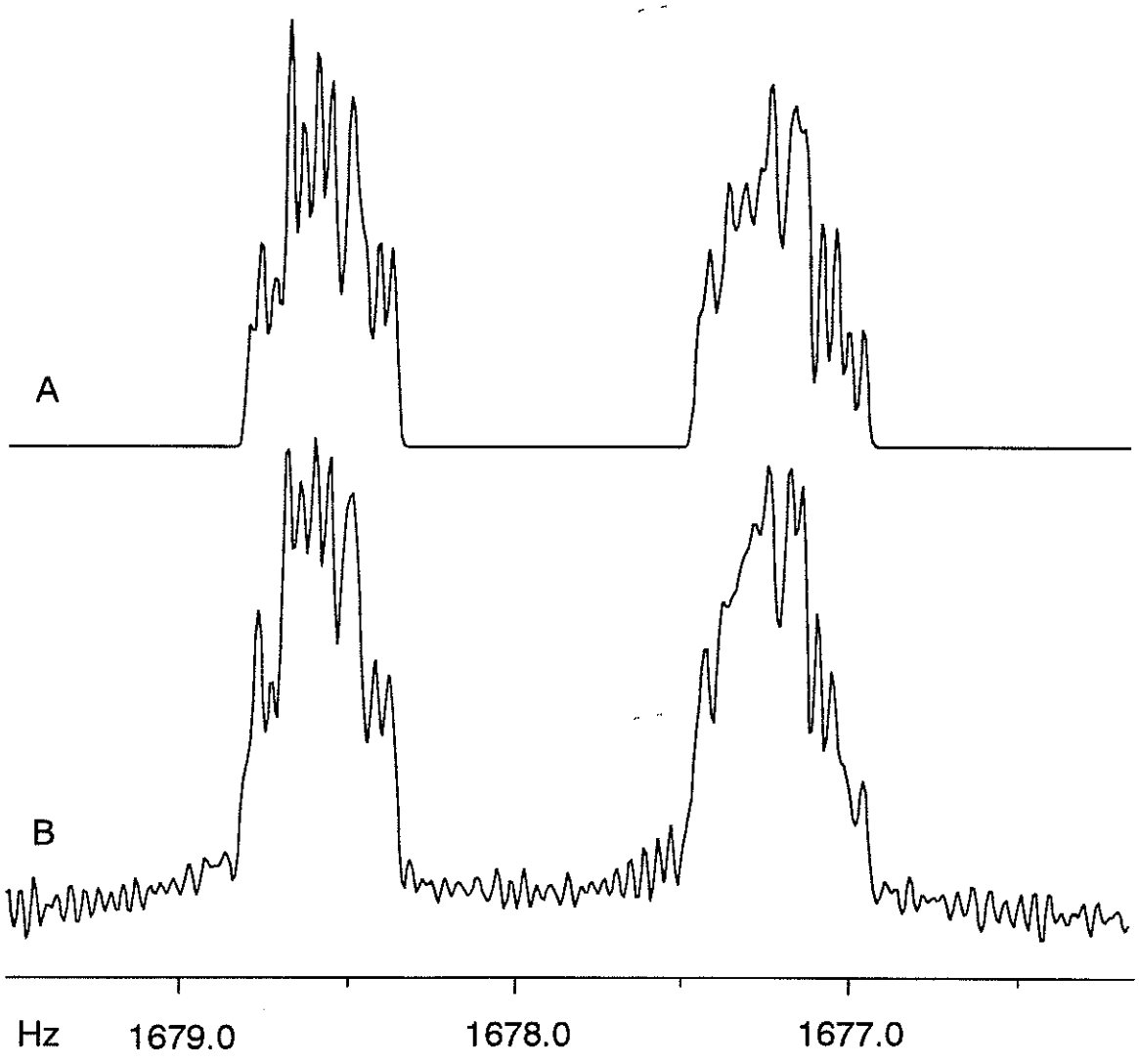

Figure 61: ^{1}H NMR spectrum of 2-formylstyrene H_8 (low frequency portion) in CS_2/C_6D_{12}. A) Theoretical spectrum with 30 mHz linewidth; B) Experimental spectrum.

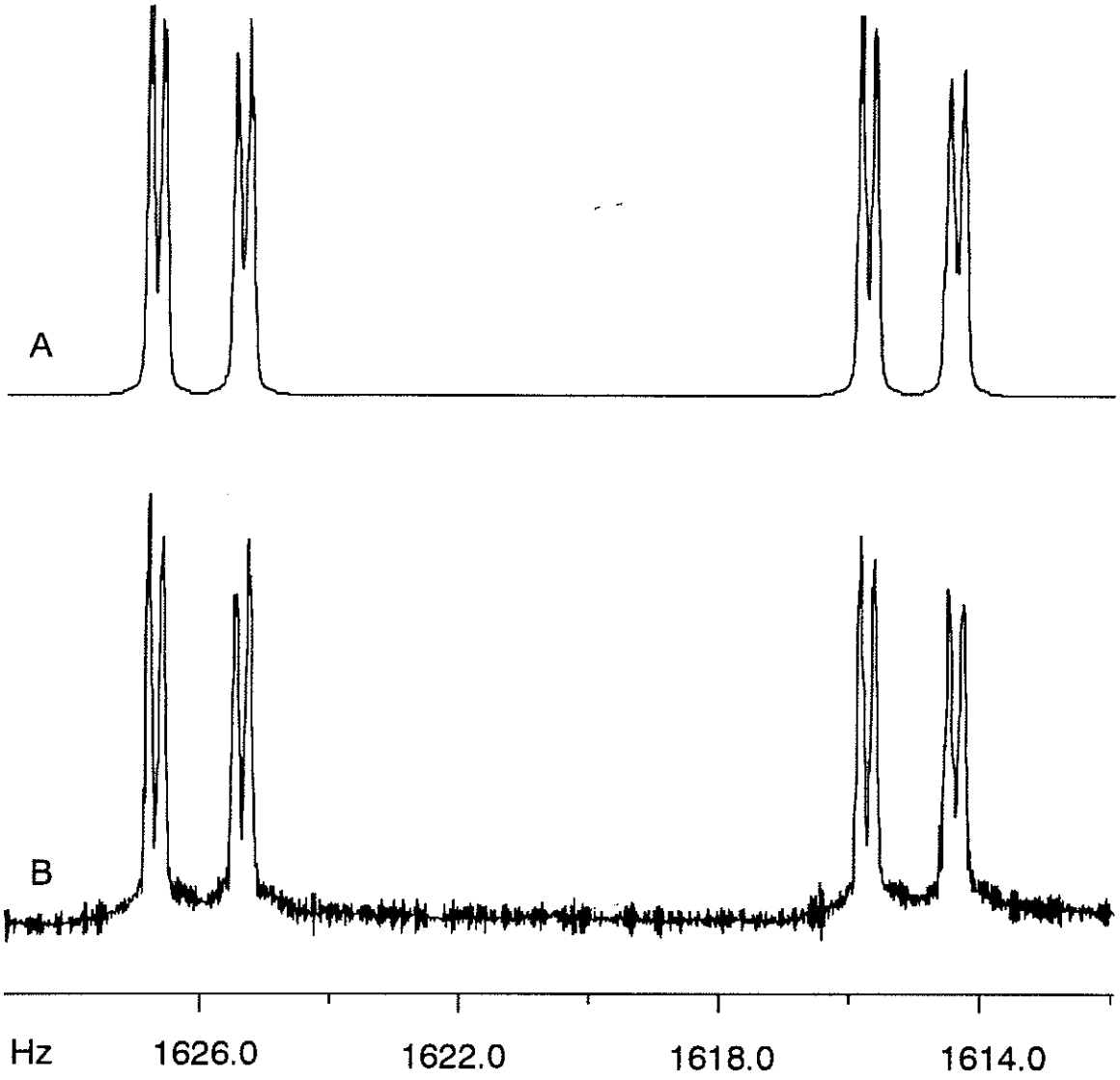

Figure 62: ^{1}H NMR spectrum of 2-formylstyrene H_9 in CS_2/C_6D_{12}. A) Theoretical spectrum; B) Experimental spectrum.

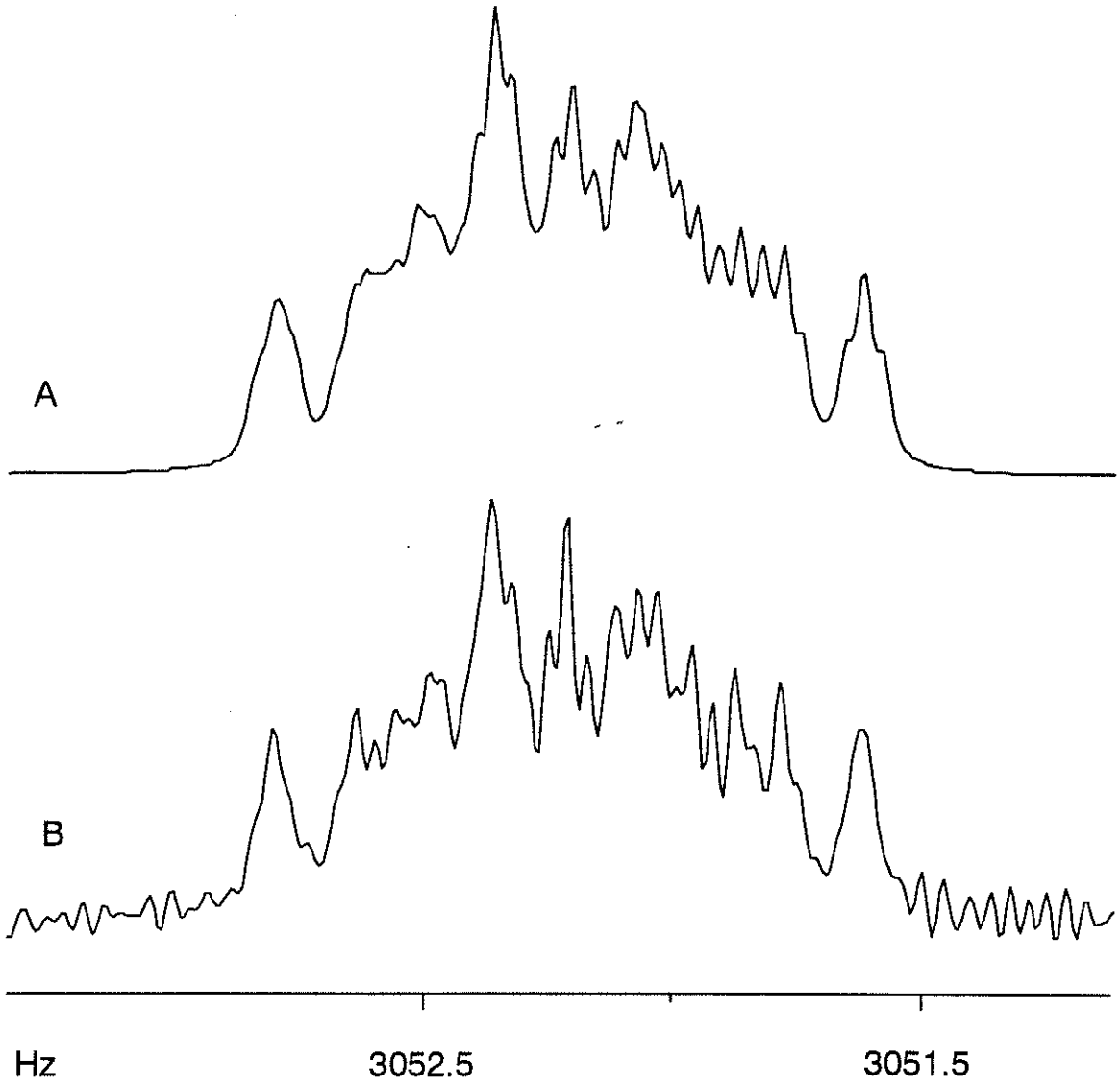

Figure 63: ^{1}H NMR spectrum of the 2-formylstyrene aldehydic proton in acetone-d_6. See text for a discussion of the imperfect agreement with experiment. A) Theoretical spectrum with linewidth of 35 mHz; B) Experimental spectrum.

3.2.2 MO Computations

Molecular orbital computations for 2-formylstyrene were carried out with the 6-31G* and 6-31G** bases. One set of computations characterized the O-*cis* conformer (**A**) as depicted in Figure 41. The ring carbons and the nuclei of the formyl group were held coplanar, while the dihedral angle describing vinyl torsion, θ, was varied in increments of 15° or less. The alpha hydrogen and the two carbon nuclei were constrained to a plane, leaving the positions of the beta hydrogens to optimize. With the large rotational potential for ethylene, such deviations from planarity were not observed to exceed 2°. The second set of calculations, characterizing the O-*trans* conformer (**B**), proceeded like the first, except that for $\theta > 60°$, the planar formyl group was permitted to twist. Values of this twist angle, ϕ, are tabulated in Table 14. The 6-31G* energies for these two sets of computations are given in Table 13 and plotted as a function of θ in Figure 64. At each of the three minima in this figure, the vinyl and formyl twist angles were allowed to relax, better describing the stable conformers.

The barrier to internal rotation in benzaldehyde is calculated as 37.5 $kJ\,mol^{-1}$ with the 6-31G* basis [78], rather higher than, for example, the free energy of activation in solution of 32.2(6) $kJ\,mol^{-1}$ [79, 80, 81]. While there exists some controversy concerning the internal barrier of the free molecule [82], it is agreed that the barrier is not smaller than 27 $kJ\,mol^{-1}$, so that large out-of-plane deviations of the carbonyl group are not expected at 300 K. In contrast, the 6-31G* barrier for styrene is only 12.0 $kJ\,mol^{-1}$ [11], while experimentally, the internal barrier height is 12.8(6) or 13.8(7) $kJ\,mol^{-1}$ (twofold component) with a fourfold component of $-3.3\ kJ\,mol^{-1}$, yielding a very flat potential well near $\theta = 0°$ [4, 5]. Judging from these barriers, one may anticipate that steric strain will force the vinyl group out of the ring plane. The relative energies in Table 13 confirm these expectations, implying that the conformational properties of 2-formylstyrene can be discussed meaningfully in terms of two conformers, depicted in Figure 41, each with a potential for the out-of-plane excursion of the vinyl group.

Both planar conformers are stablized by the π,π conjugational energies and destablized by the energies due to repulsion between the ortho C-H_6 and C_β-H_8 bonds. To a first approximation, therefore, the energy difference of 3.3 $kJ\,mol^{-1}$ between the planar conformers represents the difference in repulsion energy between the H_7,H_{10} and H_7,O interactions. That the latter interaction is repulsive follows from the *non-planar* minimum observed for **A** rather than the planar minimum encountered in styrene.

The stable form of **A** is, indeed, found at $\theta = 38°$, representing a compromise between the loss of some π,π conjugation and a decrease in the two repulsions amounting to 4.0 $kJ\,mol^{-1}$, as in Table 13. If the conjugational energy in 2-formylstyrene is similar to the 12.0 $kJ\,mol^{-1}$ twofold component found for styrene at the 6-31G* level, then about 4.5 $kJ\,mol^{-1}$ of it would be sacrificed at this geometry. Further decomposition of the energies for **A** is not feasible, so it cannot be said whether an *attractive* H_7,O interaction exists at the twist angle of 38°. However, the distance between these nuclei is less than 2.4 Å, similar to the computed H,O distances in H-bonded complexes between water and some fluooromethanes [83]. Furthermore, in 2-hydroxybenzaldehyde, a molecule known to have a strong intramolecular hydrogen bond of about 29 $kJ\,mol^{-1}$ [72, 84], the microwave spectrum of the vapour indicates a H,O distance of 1.76(1) Å [85].

The high energy of **A** at a θ of 90° is about 4.7 $kJ\,mol^{-1}$ larger than that expected for a complete loss of π,π conjugation, very likely due to repulsion between the $2p$ orbital on C_α and the C=O bond. This scenario has at least one documented precedent in 2-alkylthiobenzaldehydes, where only the O-*trans* conformer occurs when the $3p$ orbital on sulfur is twisted into the molecular plane [86].

For conformer **B**, the lowest energy occurs at a θ of 45°, implying that repulsion between the C_α-H_7 bond and the formyl C-H_{10} bond in the planar form is substantial. A local maximum at $\theta = 90°$ is 11.0 $kJ\,mol^{-1}$ lower in energy than for **A**, therefore about 6.3 $kJ\,mol^{-1}$ lower than expected for a complete loss of π conjugational energy.

Table 13: The relative 6-31G* energies ($kJ\,mol^{-1}$) of 2-formylstyrene conformers **A** and **B** for various torsion angles of the vinyl fragment.

Conformer **A**		Conformer **B**	
θ (deg)[a]	*Energy*	θ (deg)[a]	*Energy*
0	3.98	0	7.25
5	3.81	15	5.30
10	3.35	30	1.74
15	2.66	45	0.10
20	1.86	45.1	0.00[c,d]
25	1.07	60	1.36
30	0.44	75	3.88
38.0	0.00[b]	90	5.62
45	0.50	105	5.48
60	4.22	120	4.12
75	10.43	129.6	3.64
90	16.67	135	3.84
		150	7.12
		165	14.16
		180	21.93

a) $\theta = 0$ corresponds to a conformation in which the vinyl group lies in the aromatic plane and the C_α-H_7 bond is directed toward the formyl group (Figure 41). b) The total energy is –420.310 715 *au* and the formyl group twists out-of-plane by 0.1°. c) The total energy is –420.310 883 *au* and the twist angle of the formyl group is 3°. d) This low energy minimum for the O-*trans* conformer lies 0.31 $kJ\,mol^{-1}$ below the corresponding O-*cis* minimum.

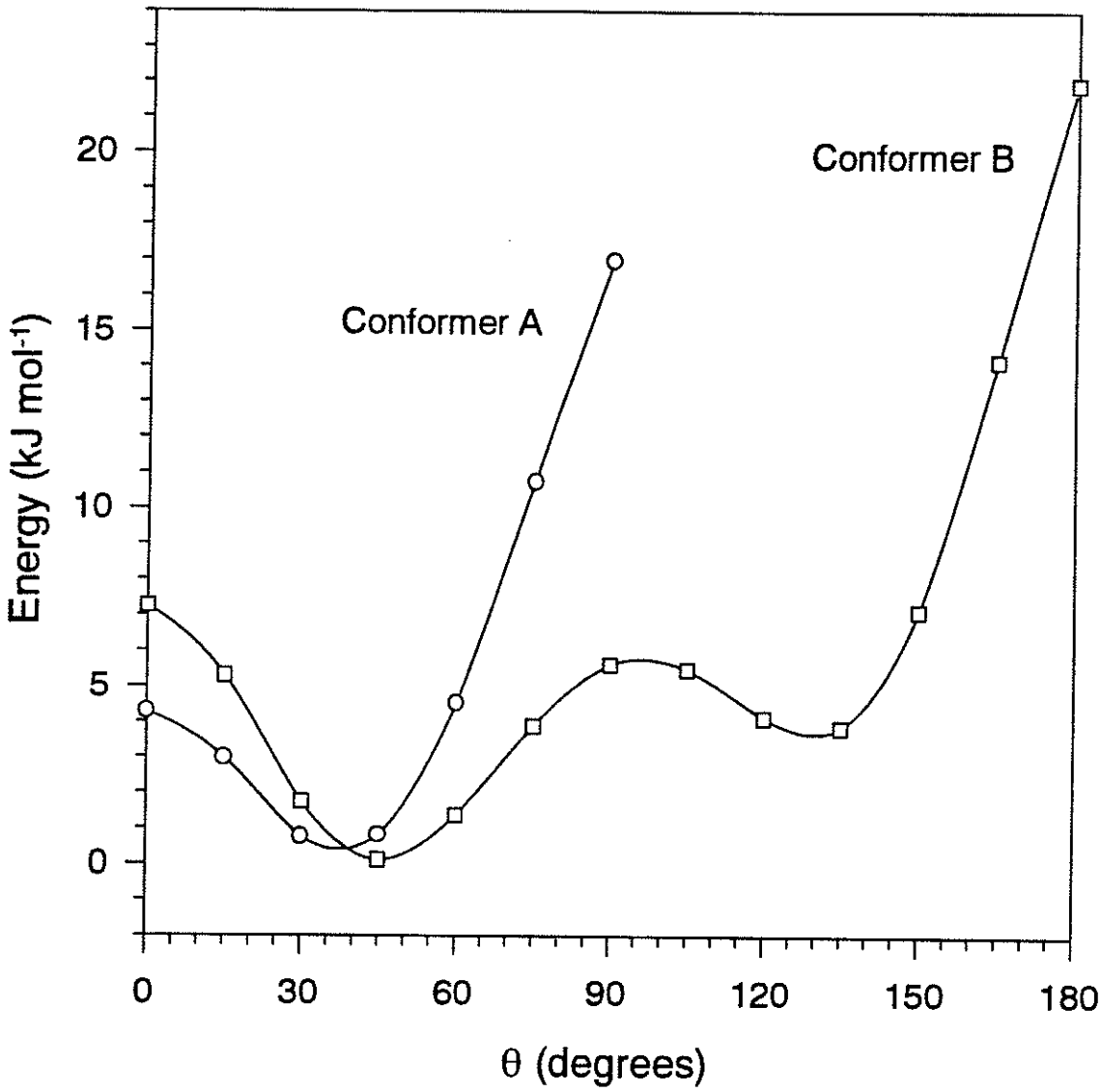

Figure 64: Potential energy diagram for 2-formylstyrene from 6-31G* level MO computations. The planar conformation with $\theta = 0°$ is depicted in Figure 41. In the region of steric congestion ($\theta > 105°$), the formyl group twists substantially away from the aromatic plane (see Table 14).

Table 14: Twist angle, ϕ, of the planar formyl group in 2-formylstyrene conformer **B** for various angles of the vinyl torsion, θ, as computed with the 6-31G* basis.

θ (deg)	ϕ (deg)	θ (deg)	ϕ (deg)
75	-1.4[a]	135	16.5[b]
90	0.9	150	22.8
105	4.5	165	27.5
120	10.0	180	27.4
129.6	14.2		

a) A postive value for the angle indicates that the alpha and formyl C-H bonds both lie below the aromatic plane. b) For $\theta > 135°$, the vinyl proton *cis* to the ring begins to twist out of the vinyl plane to a maximum value of almost 4°.

This may be taken as suggestive of an incipient C-H$\cdots\pi$ hydrogen bond involving the formyl hydrogen and the π system of the vinyl group. As θ increases beyond this point, the π conjugational energy resumes, contributing to a decrease in the total energy, and descending into a second stable conformer for **B**. With further increase in θ, repulsion between the C_β-H_8 and formyl C-H_{10} bonds becomes dominant, producing a local minimum around 129.6° which may be favourable for the fast 1,5-hydrogen shift from the formyl to vinyl fragments, as postulated for the electronically excited state of this compound [30]. At this minimum, the internuclear separation C_β,H_{10} is 2.68 Å and that of H_8,H_{10} is less than 2.6 Å. Alternatively, the formyl C-H_{10} bond is reasonably well-positioned to interact with the $2p$ orbitals of the vinyl double bond — the hydrogen atom lies about 2.7 Å above the midpoint of the C=C bond and about 0.5 Å from the normal to the vinyl plane.

Given the potential energies in Table 13, it is of interest whether they are consistent with the long range coupling constants in Table 12. Those involving the vinyl protons would sample the two energy profiles in Figure 64 as given by a Boltzmann

weighting. The long range coupling constants over five bonds to the formyl protons are excellent measures of the proportions of **A** and **B** [72, 87, 88].

3.2.3 Long range coupling constants

The proportions of A and B

A good measure of the conformational bias of the formyl group in benzaldehyde derivatives comes from the ratio of the five-bond coupling constant to the aldehydic proton, ${}^5J(H_{meta}, CHO)$, to the sum of the two such coupling constants. In 2-formylstyrene, the fractional population of **A** is given by

$$P_A = \frac{{}^5J_{6,10}}{{}^5J_{4,10} + {}^5J_{6,10}} = \frac{0.363}{0.363 + 0.444} = 0.45.$$

Since the values of the coupling constants in Table 12 differ only slightly in polar and nonpolar media, their mean has been used, implying that the proportions of **A** and **B** are independent of solvent.

In this connection, it is interesting that the 6-31G* energies in Table 13 have **A** as 0.31 $kJ\ mol^{-1}$ less stable than **B**. If this is also true at 300 K, then the theoretical fractional population of **A** is 0.47. Of course, this conclusion is valid only if corrections for the zero-point energies, solvent effects and thermal energies and entropies combine in such a way that the free energy difference is essentially unchanged. The long range coupling constants to the formyl proton indicate that such is indeed the case, and this assumption shall be trusted in the ensuing discussion.

Furthermore, the potential energy curves in Figure 64 imply various probabilities for the angles, θ, at a given temperature. The C-H bonds of the vinyl group sample various values of θ and, in so doing, cause the θ-dependent long range coupling constants of their protons to vary.

Computation of $^6J_{4,7}$

Theoretically and experimentally, $^6J_{4,7}$ in styrene is a function of $\sin^2\theta$ [18, 23, 24, 27]. The expectation value of $\sin^2\theta$ can be evaluated by classical averaging as

$$\langle \sin^2\theta \rangle = \sum_i p_i \sin^2\theta$$

where the probability, p_i, at a given angle, is obtained from the energies, E_i, in Table 13 according to

$$p_i = \frac{\exp\left(\frac{E_i}{RT}\right)}{\sum_i \exp\left(\frac{E_i}{RT}\right)}.$$

This procedure yields a value for $\langle \sin^2\theta \rangle$ of 0.450 at 300 K using the experimentally determined populations of **A** and **B**. If the theoretical populations are used, this quantity is 0.454. Moreover, using only the three minima in Figure 64 with the experimental conformer populations, the expectation value of $\sin^2\theta$ comes out to 0.456.

As described above, for phenylallene, two independent developments of $^6J_{4,7}$ in styrene have been suggested. The first, designed to reproduce spectral data for styrene itself, has

$$^6J_{4,\alpha} = -0.149\cos^2\theta - 0.597\sin^2\theta \;\; [24],$$

resulting in a value of -0.351 Hz for 2-formylstyrene. The mean of the two coupling constants in Table 12 is $-0.349(6)$ Hz. In accord with the discussion in the previous section, the average of the data from these two solvents is used because the present model is hardly precise enough to corroborate the existence of different potentials. The second relationship, constructed using data from β,β-dibromo-2,6-dichlorostyrene and 3,5-dichlorostyrene [27], meets with poor success, predicting $^6J_{4,7}$ in 2-formylstyrene as -0.440 Hz.

Computation of $^5J_{3,7}$ and $^5J_{5,7}$

In styrene and some of its derivatives, $^5J_{3,7}$ is reproduced by a single term in $\langle \sin^2 \theta/2 \rangle$. For an evenfold potential, $\langle \sin^2(\theta/2) \rangle$ is 0.5, thus, acetone-d_6 solutions of styrene [25] and 2,6-dichlorostyrene (measured in this laboratory) yield $^5J_{3,7} = {}^5J_{5,7}$ to be 0.368(3) Hz and 0.391(1) Hz, respectively. As one might expect, $\langle \sin^2 \theta \rangle$ in these two compounds is quite different, as reflected in the corresponding values for $^6J_{4,7}$ of $-0.227(2)$ and $-0.540(2)$ Hz. In 2-fluorostyrene, $^5J_{3,7} + {}^5J_{5,7}$ is 0.758(4) Hz, independent of the solvent polarity [23]. From Table 12, this sum for 2-formylstyrene is 0.750(2) Hz for a solution of CS_2/C_6D_{12} and 0.761(2) Hz in acetone-d_6. Finally, $^5J_{3,7}$ in the substantially out-of-plane β,β-dibromo-2,6-dichlorostyrene, is 0.372(1) Hz for both acetone-d_6 and CD_2Cl_2/CCl_4 solutions at 296 K [27]. From these data for planar and nonplanar styrene derivatives, it appears that any term in $\sin^2 \theta$ representing a σ-π contribution, is very small indeed.

In this spirit, $^5J_{3,7}$ can be written as $0.755 \sin^2(\theta/2)$. The energies in Table 12 yield $\langle \sin^2(\theta/2) \rangle$ as 0.214, hence predicting $^5J_{3,7}$ to be 0.162 Hz. By subtraction, $^5J_{5,7}$ must be 0.593 Hz. In comparison with the experimental values of 0.166(5) and 0.590(1), good agreement is apparent. Of course, these ^5J numbers would also be consistent with two planar conformers, but the present models, $^6J_{4,7}$ and theoretical computations do not support that possibility.

Computation of $^4J_{6,7}$

Empirically, $^4J_{6,7}$ has been assessed in styrene and some of its methyl derivatives as

$$^4J_{6,7} = -0.476\cos^2\theta - 0.759\sin^2\theta \ \ [24].$$

Application of this expression to the present compound yields this coupling constant as -0.603 Hz, only 5% lower in magnitude than the $-0.637(2)$ Hz determined experimentally. The term in $\cos^2\theta$ represents the usual π electron spin correlation across the double bond.

Coupling constants between the ring and beta protons

Seven bond coupling constants to H_8 and H_9 have been postulated to follow the expression

$$^7J_{4,8/9} = 0.300\cos^2\theta + 0.065\sin^2\theta,$$

with a small, additional term possibly contributing as much as 0.04 Hz to $^7J_{4,9}$ [23, 24]. A $\langle\sin^2\theta\rangle$ of 0.450 for 2-formylstyrene yields 0.194 Hz for these coupling constants, midway between the measurements of 0.182(2) Hz for $^7J_{4,8}$ and 0.211(7) Hz for $^7J_{4,9}$. In styrene, $^7J_{4,8}$ and $^7J_{4,9}$ are 0.237(3) and 0.281(3) Hz, respectively [25], reflecting the larger value of $\langle\cos^2\theta\rangle$ in the parent compound.

Interestingly, $^6J_{3,8}$ and $^6J_{3,9}$ in styrene are not detected [25]. According to INDO computations [18], $^6J_{3,9}$ is $+0.12$ Hz for the planar conformer corresponding to the all-*trans* arrangement ($\theta = 0°$), and $+0.07$ for the perpendicular conformer. At $\theta = 180°$ however, corresponding to $^6J_{5,9}$ as depicted in Figure 41, a *negative* coupling of -0.18 Hz is calculated. Clearly, in styrene, one measures the mean of $^6J_{3,9}$ and $^6J_{5,9}$, thus accounting for their apparent absence.

An expression for $^6J_{5,9}$ can be developed by including a negative term in $\cos^2\theta$ which decreases in magnitude as spin correlation is lost on increasing θ from 0 to 90°. Inclusion of a second term in $\sin^2\theta/2$, representing a rare positive σ electron contribution [18, 23], can account for the maximum coupling observed for an all-*trans*

arrangement of the intervening bonds. With judiciously chosen coefficients,

$$^6J_{5,9} = -0.10\cos^2\theta + 0.14\sin^2(\theta/2).$$

For styrene in solution, the internal potential indicates a $\langle\cos^2\theta\rangle$ of 0.825, with the usual 0.5 $\langle\sin^2(\theta/2)\rangle$ for an evenfold potential [24]. The resulting coupling constant, $^6J_{5,9} = {}^6J_{3,9}$, is -0.012 Hz, in satisfactory agreement with experiment. For 2-formylstyrene, $\langle\sin^2(\theta/2)\rangle$ is computed as 0.786 for $^6J_{3,9}$ and 0.214 for $^6J_{5,9}$, with the computed potential implying a $\langle\cos^2\theta\rangle$ of 0.550. Hence, $^6J_{3,9}$ becomes $+0.055$ Hz and $^6J_{5,9}$, -0.025 Hz. Again, these values appear to agree well with the observed values of $+0.052(1)$ and $-0.022(6)$ Hz in Table 12.

When this function is applied to 3-fluorostyrene, however, problems arise. All methods agree that the *cis* conformer, which favours a positive $^6J_{5,9}$ according to the above model, is most abundant [23, 29, 89, 90, 91]. The value of $^6J_{5,9}$ in this compound is $+0.06$ Hz [23]. For this to be consistent would require a much smaller $\cos^2\theta$, yet, 3-fluorostyrene is known to be nearly planar, like styrene [23]. This expression, therefore, appears to be useful for some compounds, but clearly requires more study.

For $^6J_{3,8}$ and $^6J_{5,8}$, INDO computations predict values of -0.19 and -0.14 Hz for the planar and perpendicular conformers, respectively [18]. These numbers imply a π electron component, proportional to $\cos^2\theta$, and a σ-π contribution in $\sin^2\theta$, increasing as the π component diminishes. The presence of a finite σ-π component is supported by the -0.1 Hz found for the nonplanar 2,6-dichlorostyrene [18]. In styrene, however, $^6J_{3,8}$ is not detected. One hypothesis is that there exists an additional *positive* contribution, neglected by the INDO parameterization, which is active most prominently at small torsion angles. A speculative mechanism invokes the *through-space*, or *proximate*, interaction between the β-CH and the ortho CH bonds of styrene [18]. In all known cases, such an interaction leads to a negative coupling constant between the protons [18, 77, 92], as indicated in Figure 65, by the parallel crossed arrows for H_6 and H_8.

Schematically, the repulsive overlap of the $1s$ orbitals centered on these protons is

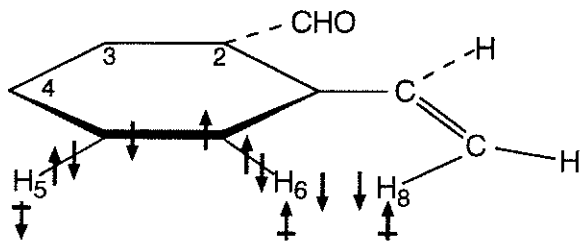

Figure 65: Spin transmission mechanism for 2-formylstyrene, $^6J_{5,8}$

consistent with a parallel-spin preference of the electrons in these orbitals. Given this situation, the spin correlation in the σ bonds of the aromatic ring, determined by the Pauli principle and Hund's rule, leads to the indicated spin state of H_5, and hence the positive contribution to $^6J_{5,8}$ (Figure 65). The angle at which this proximate interaction is maximized remains uncertain, it being very sensitive to interatomic distances and the mutual arrangement of the C-H bonds. In styrene, $^5J_{2,8} = {}^5J_{6,8}$ is not observed, presumably because the negative proximate component cancels the expected positive coupling components, σ and π, over five bonds. In 2-formylstyrene, $^5J_{6,8}$ does not have the large σ component characteristic of the mainly *trans* bond arrangement, and its measured value is $-0.132(5)\ Hz$. This suggests that the through-space mechanism also operates at substantial θ values corresponding to H_6,H_8 distances of 2.4 to 2.5 Å. The proposed spin correlation in Figure 65 is consistent with the small magnitude of $^6J_{5,8}$ in 2-formylstyrene, acting to cancel the negative π and σ-π interactions. These are, of course, as large for $^6J_{3,8}$ as for $^6J_{5,8}$ and are observed to dominate the $-0.084(3)\ Hz$ measured for $^6J_{3,8}$. Notably, this rationalization is also consonant with the magnitudes (signs unknown) of $^6J_{5,8}$ and/or $^6J_{3,8}$ in 2-fluorostyrene and 3-fluorostyrene [23].

The proximate nature of $^5J_{6,8}$ is discussed above. For $^5J_{6,9}$, the coupling constant measured in styrene is $(^5J_{6,9} + {}^5J_{6,9})/2 = 0.158\ Hz$ [25], similar to the numbers for some meta and para substituted derivatives [18, 23, 24]. The negative, proximate contribution to $^5J_{6,8}$=$^5J_{2,8}$ is not present in $^5J_{6,9}$=$^5J_{2,9}$. Valence-bond theory

[18] suggests a π electron term of $0.59\cos^2\theta$ for ${}^5J_{6,9}$, whereas the INDO MO FPT procedure predicts couplings of 0.20 and 0.50 Hz at $\theta = 0$ and 180°, respectively. These numbers imply a σ electron component of appreciable magnitude. However, INDO also calculates ${}^5J_{6,9}$ as 0.33 Hz for the perpendicular conformer. The observed ${}^5J_{6,9}$ in 2-formylstyrene is 0.047(3) Hz. Since $\langle\cos^2\theta\rangle$ is apparently equal to 0.550 and θ values nearing 180° are inappreciable, it appears that both methods strongly overestimate the π and σ electron components. In 2-fluorostyrene, the larger value of $\langle\cos^2\theta\rangle$ produces a ${}^5J_{6,9}$ of 0.084(2) Hz [23]. An improved parameterization of the angle dependence of ${}^5J_{2,9}$ must await further experimental data.

Coupling constants between the vinyl and formyl groups

The five bond coupling between the alpha protons, $^5J_{7,10}$, is $-0.163(1)$ Hz, most likely a proximate coupling constant, similar in nature to the $-0.38(1)$ Hz measured for the analogous parameter in 2-formylisopropylbenzene [77]. Reviews of through-space couplings agree that they are exceedingly sensitive to interatomic distance [56, 57]. In the isopropylbenzene derivative, the experimental and theoretical evidence indicates that the methine C-H bond is closely confined to the aromatic plane. In consequence, its hydrogen atom approaches that of the formyl C-H bond more closely, on average, than in the analogous interaction in 2-formylstyrene. Moreover, the O-*trans* populations in these two related compounds are nearly equal.

The theoretical approach for $^{5/6}J_{n,10}$ $(n = 7, 8, 9)$ in 2-formylstyrene employed the 6-31G* geometries in the CNDO/2 approximation. These were used instead of the INDO formulation because, while both methods give very similar values for the proximate contributions, INDO tends to strongly overestimate the σ electron component of five bond couplings in benzene derivatives. As anticipated, the planar form of **B**, in which H_7 and H_{10} are computed as approaching to within 1.95 Å, has a large, negative $^5J_{7,10}$ of -0.31 Hz. Consonant with the distance sensitivity for proximate coupling constants, $|^5J_{7,10}|$ decreases rapidly with increasing θ. For **A**, $^5J_{7,10}$ is small and positive, less than 0.1 Hz for the planar conformation and becoming negligible by $\theta = 60°$. The potential energy curve in Figure 64, applied as a weighting function to the computed values, yields $^5J_{7,10}$ as -0.07 Hz. The two site analysis, using experimentally determined populations of **A** and **B**, gives -0.11 Hz. In view of the high sensitivity of the proximate component to internuclear distance, this result may be considered satisfactory in comparison with the experimental value.

The six bond coupling constant, $^6J_{8,10}$, is computed by CNDO/2 as small and positive for small vinyl torsion angles in **B**, gently decreasing until $\theta = 105°$, where it exhibits a dramatic plunge into large negative values on close approach of H_8 to H_{10}. CNDO/2 values for **A** are negligible for $^6J_{8/9,10}$. The weighting scheme in Figure 64

predicts a small, positive coupling of 0.01 Hz, to be compared with the measured value of 0.03 Hz. For ${}^{6}J_{9,10}$, the same trend is observed for $\theta = 0$ to 90°, whereupon a sharp increase to large positive numbers is predicted. The angle-averaged coupling is 0.047 Hz, in reasonable accord with the experimental value of 0.032(7) Hz.

3.2.4 Proton chemical shifts

Table 15 contains δ values for the protons of benzaldehyde, styrene and 2-formylstyrene in solutions of acetone-d_6. To within the uncertainties caused by differing concentrations, the ring proton shifts in 2-formylstyrene are reproduced by an additive scheme. This result is not unreasonable in that the formyl group in 2-formylstyrene has almost equal O-*cis* and O-*trans* proportions as in benzaldehyde itself. Further, the computed potential suggests only small average deviations of the carbonyl group from coplanarity, consistent with very similar conjugative shifts caused by this substituent in the parent compound and its derivatives. Also supportive of this conclusion are the uniformly small values observed for the six bond coupling constant to the formyl proton in these two compounds.

Perturbations of the proton chemical shifts of benzene by the vinyl group are rather small. At the para position, the vinyl substituent's π donating character increases the screening by 0.12 *ppm*. Because greatest screening will be observed for the maximally conjugated, planar conformation, larger average twist angles will tend to decrease the screening. If the shift of the para proton varies with $\cos^2\theta$, then the accepted values of $\langle\cos^2\theta\rangle$ of 0.825 and 0.537 for styrene [24] and 2-formylstyrene, respectively, predict an actual additivity of only 0.08 *ppm* for H_4 — a deviation of 0.04 *ppm* from pure additivity. The measured deviation is 0.03(1) *ppm*. At H_5, the shift of which is dominated by the electron-withdrawing formyl group, the deviation is *negative* by 0.02(1) *ppm*. It does appear, therefore, that the ring proton chemical shifts in 2-formylstyrene are consistent with the conformational distribution assumed in the foregoing discussion of long range coupling constants.

The most striking chemical shift in Table 15 is that of H_7. In 2-formylstyrene, this proton is deshielded by 0.95 *ppm* relative to the parent compound. Because H_7 is also characterized by larger values of θ than in styrene, one might expect a *decrease* in its δ value, based on the diamagnetic anisotropy of the benzene ring. This is not observed, however, implying that the measured deshielding originates with the

proximity of the carbonyl moiety. One may postulate that since repulsion between the alpha olefinic C-H_7 bond and the C-H_{10} bond in **B** or the C=O bond in **A** appears to be the main cause of the vinyl group's out-of-plane twist, it is also responsible for the descreening of H_7. Significant deshielding of protons in steric proximity to other groups is well-known [93, 94, 95, 96, 97], some recent examples being found in reference [98]. Notably, in this connection, in 2-fluorostyrene, for which there is no indication of greater vinyl nonplanarity than in styrene [23], H_7 is deshielded by only 0.16 *ppm*. Decomposition of the 0.95 *ppm* into contributions such as those arising from the anisotropy of the carbonyl group or from the mean square electric fields due to fluctuating lone-pair oxygen electrons would not be fruitful at the small interatomic distances applicable to the conformations of Figure 64. Here again, the large shift exhibited by H_7 in 2-formylstyrene is consistent with the conformational distribution of the vinyl group illustrated in Figure 64.

While the chemical shift of H_7 is reasonably attributed to the proximity of the formyl group, the much smaller shifts observed for H_8 and H_9 likely include electric field and mesomeric shifts similar to those characterized for a series of 4-X-styrenes [99], as well as small changes in shielding due to the diamagnetic anisotropy of the benzene ring. Interestingly, in spite of contrasting mesomeric properties for fluorine and the formyl group, chemical shifts for H_8 and H_9 in 2-fluorostyrene are 5.88 and 5.39 *ppm*, remarkably similar to those in 2-formylstyrene. Dissection of the various shift contributions would require data from a series of 2-X-styrenes.

Finally, the formyl proton is deshielded by 0.25 *ppm* by the vinyl group. This must represent a minimum value for a proximity shift, because in **B** the two local minima are situated such that, in sum, a *shielding* should occur by the magnetic anisotropy of the C=C olefinic bond [96].

Table 15: Chemical shifts (*ppm*) of benzaldehyde[a], styrene[b] and 2-formylstyrene[c] in acetone-d_6 solution.

Proton	*Benzaldehyde*	*Styrene*	*2-Formylstyrene*	
			Additivity[d]	*Observed*
ν_3^e	7.601	7.293	7.88	7.87
ν_4	7.698	7.220	7.48	7.51
ν_5	7.601	7.293	7.65	7.63
ν_6	7.928	7.417	7.68	7.69
ν_7	—	6.717	—	7.671
ν_8	—	5.764	—	5.784
ν_9	—	5.194	—	5.480
ν_{10}	10.054	—	—	10.310

a) For a 4.0 *mol*% solution in acetone-d_6, containing also 0.5 *mol*% TMS [73]. b) For a 16 *mol*% solution in acetone-d_6 [25]. c) For a 4.4 *mol*% solution in acetone-d_6 (Table 1). d) The δ values for benzene are 7.324 *ppm* for a 16 *mol*% solution in acetone-d_6 and 7.349 *ppm* for a 2.5 *mol*% solution [23]. This column assumes the mean of these two numbers. e) δ values relative to internal TMS at 300 K (298 K for styrene). Numbering for benzaldehyde follows the parent molecule numbering, and must be adjusted for the formyl group in the '2' position.

4 Suggestions for Further Research

Some potentially enlightening experiments have already been mentioned in connection with phenylallene. Foremost, the angle-dependent J-coupling relationships developed herein must be tested using derivatives characterized by a large torsion angle. Based on similar studies of styrene [18], 2,6-dichlorophenylallene appears to be an obvious candidate, although its lack of protons in the β position might not produce as large a $\langle \sin^2 \theta \rangle$ as in 2,6-dichlorostyrene. Another approach to obtaining a phenylallene derivative with a large out-of-plane twist is to methylate the alpha carbon. The larger barrier notwithstanding, this can be seen in direct analogy to α-methylstyrene in terms of its conformational bias [24]. A third possibility is to follow the lead of 2-formylstyrene, assuming that the steric strain acting on the alpha proton in this compound would produce a similar conformational effect in 2-allenylbenzaldehyde.

Other ring-halogenated derivatives of phenylallene would provide a further testing ground for the proposed mechanisms. 2-Chloro- and 2,5-dichlorophenylallene, for instance, may prove useful in verifying five and seven bond interproton couplings to the *meta* position by introducing a strong, predictable conformational bias. By analogy with styrene, 3- and 4- chlorinated derivatives may be expected to adopt exclusively the planar conformation with nearly equal *cis* and *trans* populations for 3-chlorophenylallene. This expectation rests on the assumption that the allene and vinyl moieties have similar electron withdrawing/releasing properties.

Fluorination at the para position would provide an opportunity to evaluate the long range $^{n}J(^{13}C,^{19}F)$ expressions for this molecule. An early investigation of $^{6}J_{p}^{F,C}$ in 4-fluorophenyl derivatives of methane, ethane and cyclohexane [100] concluded that this coupling constant is predominantly mediated *via* the σ-π system, except in 4-fluorostyrene, where the π electron component dominates. Examination of $^{7/8}J(^{13}C,^{19}F)$ in 4-fluorophenylallene would contribute to an understanding of this coupling mechanism.

Having asserted that $^{8}J_{4\gamma}$ and $^{7}J_{3\gamma}$ in phenylallene are transmitted through the π

electron system (*vide supra*), one may wish to analyze 3- and 4-methyl phenylallene derivatives for verification. Since the hyperfine couplings, Q^H_{CCH} and Q^H_{CH} are of similar magnitude but opposite sign, the measured eight and nine bond coupling constants to the methyl protons should simply change sign with respect to the corresponding lrJs in the parent compound [101].

A completely different approach to the barrier in phenylallene, by observing quadrupolar splittings in the partially aligned molecule, would follow the procedures described by Bastiaan *et al.* [39, 40]. A strategy for assessing alignment factors and the diamagnetic anisotropy uncomplicated by internal rotation would require deuteration at a ring proton. On the other hand, an estimate of the internal rotational potential would involve deuteration at the alpha or gamma protons of phenylallene as carried out for styrene [16].

In view of the interesting conformational properties of 2-formylstyrene and the utility of lrJs in their characterization, other ortho-substituted styrenes may be fruitfully explored. By loose analogy with 2-isopropylbenzaldehyde [77], an MO and NMR analysis of 2-isopropylstyrene would likely elucidate the interplay of the two rather similar rotational barriers and the repulsive interaction between their respective methine protons. Presumably, some out-of-plane vinyl action would be observed in $^6J_{4,\alpha}$, and $^5J_{3/5,\alpha}$ would give insight into the preferred conformation. Additionally, the likelihood of a substantial through-space coupling constant between the vinyl and isopropyl methine protons encourages this investigation.

A similar set of predictions can be made regarding 2-*tert*-butylstyrene. This bulkier group may adopt a staggered conformation with respect to the vinyl alpha proton, thus stablizing the planar form, or it may simply force the vinyl group to twist out of the ring plane. The interactions of these two alkyl groups could be understood using the present methodology. The steric congestion between the *t*-butyl and vinyl groups may well give rise to an interproton through-space coupling component, but when averaged over the nine protons of the *t*-butyl group, it may not be discernable.

Two other potentially intriguing molecules involve the convergence of the styrene and phenylallene systems. With its somewhat higher barrier, the allene group may force an ortho-situated vinyl group out of plane, providing an opportunity to measure the five bond proximate coupling constant between their respective methine protons,along with seven and eight bond couplings between the vinyl group and the methylene protons of the allenyl moiety. With the extensive delocalization of this system, these latter couplings may indeed have competing contributions from two possible pathways: one through the phenyl group, and one *via* proximity effects. Somewhat more exotic would be the analogous *ten-bond* coupling constant which could conceivably be measured in 4-allenylstyrene. Such a coupling would likely be transmitted through the extended π electron system in the predominantly planar molecule.

A recurrent theme in the preceding discussion concerns the measurement of inter-proton through-space coupling constants. From the few such couplings that have been reported, they range in magnitude up to 0.4 Hz and are negative in sign [56, 57]. In this connection, the high resolution ^{1}H NMR spectrum of 2-hydroxynaphthaldehyde (Figure 66) was acquired. In spite of some difficulties encountered in the spectral analysis, the through-space coupling constant between H_8 and the formyl proton was measured as 0.550(1) Hz and its sign determined unambiguously from partial decoupling experiments to be negative. MO computations at the 6-31G* and 6-31G** levels list the internuclear distance as less than 2.0 Å, smaller than the sum of their van der Waals radii. This proximate coupling constant appears to be the largest of its kind ever measured.

Another interesting proton-proton coupling is the $^5J(CHO, OH)$ of +0.266(1) Hz. This coupling constant is observed only in derivatives of salicylaldehyde, where the presence of substituents causes steric compression, increases the electron density in the carbonyl group, or decreases the electron density near the hydroxyl proton [102]. For salicylaldehyde itself, $^5J(CHO, OH)$ is very small, but as the en-

ergy of the intramolecular hydrogen bond increases, a positive coupling between the formyl and hydroxyl protons emerges, apparently transmitted *via* the hydrogen bond. A clear correlation of this coupling with the chemical shift of the hydroxyl proton has been demonstrated for sterically crowded derivatives of salicylaldehydes [102]. In 2-hydroxynaphthaldehyde, $^5J(CHO,OH)$ is comparable in magnitude to the largest of such couplings: $+0.266(2)\ Hz$ as measured in 4,6-dimethoxysalicylaldehyde [102]. Not surprisingly, the chemical shift of the hydroxyl proton in 2-hydroxynaphthaldehyde is 1304 Hz[8], somewhat less shielded than the salicylaldehyde derivatives studied in reference [102]. Moreover, after correcting for the ring current from the second ring in the naphthalenic system, the expression relating $^5J(CHO,OH)$ to ν_{OH} predicts a coupling of 0.27 Hz for this compound.

Having obtained remarkably close agreement with most of the experimental spectrum, one spectral region remains grossly imperfect, requiring more study before the complete analysis can be fully trusted.

From the viewpoint of through-space interactions, an unusual situation has emerged in the analysis of 2,6-difluorostyrene. INDO computations predict a large, negative coupling on close approach of a proton to a fluorine nucleus. Experimentally, $^4J(H_\alpha,F_2)$ is found to be small and positive in 2,6-difluorostyrene ($0.047(2)\ Hz$), while $^5J(H_8,F_2)$ is *large* and positive ($0.856(1)\ Hz$). It appears that INDO is unable to address this situation, and the task, at present, is to sort out the π component, which should change sign based on Q^F_{CF}, and the through-space contribution.

More vexing, perhaps, is the larger barrier computed for 2,6-difluorostyrene than styrene, at all levels of theory from STO-3G to MP2/6-31G*. A simple-minded explanation originates from the hypothesis that the near-planarity of styrene can be attributed to steric repulsion and/or electrostatic repulsion between H_8 and the ortho proton. On substitution of the ortho protons by fluorine nuclei, the steric interaction

[8] A value of 3913.3 Hz was measured at a proton resonance frequency of 300 MHz. The value quoted in the text has been scaled by one-third to account for the original measurements at 100 MHz.

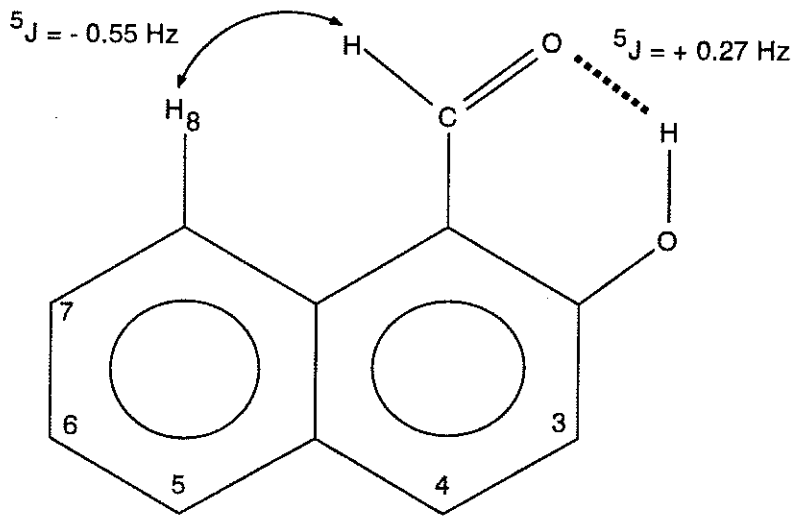

Figure 66: Molecular structure of 2-hydroxynaphthaldehyde and atomic numbering scheme.

should be little changed based on the similar van der Waals radii. Conversely, the positively polarized CH bond is replaced by the *negatively* polarized CF bond. To a first approximation, therefore, the only modification with respect to the rotational barrier is the replacement of a repulsive CH$\cdots$HC interaction by an *attractive* CH$\cdots$FC one, stablizing the planar form and raising the barrier. Experimentally, however, the trustworthy $^6J_{4\alpha}$ *increases* in magnitude, suggesting a *lower* barrier for 2,6-difluorostyrene. This observation may be due to an intrinsic substituent perturbation from the fluorine nuclei, and, in fact, the seven-bond coupling to the spatially remote *trans*-β proton does not change from styrene to the 2,6-difluoro derivative. Clearly, the resolution of this conundrum would benefit the ongoing discussion regarding styrene's planarity.

The verdict is not in on 2,6-difluorostyrene, however, and further study may indeed resolve this question. In particular, solvent calculations may indicate that the conformation of this relatively polar molecule depends on the polarity of the medium. Moreover, high-level calculations of this molecule could well be of interest to molecular spectroscopists, who require accurate geometries and rotational constants for their spectral analyses.

References

[1] K.S. Pitzer, L. Guttman and F.E. Westrum Jr. *J. Amer. Chem. Soc.* **68** 2209 (1946).

[2] L.A. Carriera and T.G. Towns. *J. Chem. Phys.* **63** 5283 (1975).

[3] J.M. Hollas and T. Ridley. *Chem. Phys. Lett.* **75** 94 (1980).

[4] J.M. Hollas, H. Musa, T.Ridley, P.H. Turner, K.H. Weisenberger and V. Fawcett. *J. Mol. Spectrosc.* **94** 437 (1982).

[5] W. Caminati, B. Vogelsanger and A. Bauder. *J. Mol. Spectrosc.* **128** 384 (1988).

[6] J. Janssen and W. Lüttke. *J. Mol. Struct.* **55** 265 (1979).

[7] F. Momicchioli, I. Baraldi and M.C. Bruni. *Chem. Phys.* **70** 161 (1982).

[8] J.E. Almlöf, P.U. Isacsson, P.J. Mjöberg and W.M. Ralowski. *Chem. Phys. Lett.* **26** 215 (1974).

[9] T. Schaefer and G.H. Penner. *Chem. Phys. Lett.* **114** 526 (1985).

[10] C.W. Bock, M. Trachtman and P. George. *Chem. Phys.* **93** 431 (1985).

[11] S. Tsuzuki, K. Tanabe and E. Osawa. *J. Phys. Chem.* **94** 6175 (1990).

[12] R.J. Meier. *J. Phys. Chem.* **97** 10248 (1993).

[13] M. Head-Gordon and J.A. Pople. *J. Phys. Chem.* **97** 10250 (1993).

[14] M. Head-Gordon and J.A. Pople. *J. Phys. Chem.* **97** 1147 (1993).

[15] R. Hargitai, P.G. Szalay, G. Pongor and G. Fogarasi. *J. Mol. Struct. (Theochem).* **306** 293 (1994).

[16] K.L Facchine, S.W. Staley, P.C.M. van Zilj, P.K. Mishra and A.A. Bothner-By. *J. Amer. Chem. Soc.* **110** 4900 (1988).

[17] J.E. Anderson. *Tetrahedron.* **43** 3041 (1987).

[18] M. Barfield, C.J. MacDonald, I.R. Peat and W.F. Reynolds. *J. Amer. Chem. Soc.* **93** 4195 (1971).

[19] M. Barfield and B. Chakrabarti. *J. Amer. Chem. Soc.* **91** 4346 (1969).

[20] J.A. Pople, J.W. McIver, Jr. and N.S. Ostlund. *J. Chem. Phys.* **49** 2960, 2965 (1968).

[21] J.A. Pople, D.L. Beveridge and P.A. Dobosh. *J. Chem. Phys.* **47** 2026 (1967).

[22] W.F. Reynolds, I.R. Peat and G.K. Hamer. *Can. J. Chem.* **52** 3415 (1974) and references therein.

[23] T. Schaefer and R. Sebastian. *Can. J. Chem.* **68** 1383 (1990).

[24] T. Schaefer, R. Sebastian and G.H. Penner. *Can. J. Chem.* **66** 584 (1988).

[25] H. Nies, H. Bauer, K. Roth and D. Rewicki. *J. Magn. Reson.* **39** 521 (1980).

[26] R. Laatikainen and E. Kolehmainen. *J. Magn. Reson.* **65** 89 (1985).

[27] R. Laatikainen, E. Kolehmainen, T. Kuokkanen and K. Tuppurainen. *J. Magn. Reson.* **78** 9 (1988).

[28] C.M. Harper and J.M. Hollas. *Chem. Phys. Lett.* **226** 577 (1994).

[29] J.M. Hollas and M.Z. bin Hussein. *Chem. Phys. Lett.* **154** 228 (1989).

[30] S.V. Kessar and A.K.S. Mankotia. *J. Chem. Soc. Chem. Commun.* 1828 (1993).

[31] T.-y.R. Chen, M.R. Anderson, S. Crossman and D.G. Peters. *J. Org. Chem.* **52** 1231 (1987).

[32] W.J. Dale, L. Starr and C.W. Strobel. *J. Org. Chem.* **26** 2225 (1961).

[33] D.F. Evans and J.P. Maher. *Proc. Chem. Soc. (London),* 208 (1961).

[34] J.S. Martin, A.R. Quirt and K.E. Worvill. The NMR program library. Daresbury Laboratory, Daresbury, UK. (extensively modified by Rudy Sebastian, University of Manitoba.)

[35] Kirk Marat. University of Manitoba. (© 1994).

[36] G. Govil, A. Kemp and D.H. Whiffen. The NMR program library. Daresbury Laboratory, Daresbury, UK. (extensively modified by Rudy Sebastian, University of Manitoba.)

[37] M.J. Frisch, G.W. Trucks, M. Head-Gordon, P.M.W. Gill, M.W. Wong, J.B. Foresman, B.G. Johnson, H.B. Schlegel, M.A. Robb, E.S. Replogle, R. Gomperts, J.L. Andres, K. Raghavachari, J.S. Binkley, C. Gonzales, R.L. Martin, D.J. Fox, D.J. Defrees, J. Baker, J.J.P. Stewart and J.A. Pople. *Gaussian 92*, Revision C. Gaussian, Inc. Pittsburgh, PA (1992).

[38] M.J. Dewar, E.G. Zoebisch, E.F. Healy and J.J.P. Stewart. *J. Amer. Chem. Soc.* **107** 3902 (1985).

[39] E.W. Bastiaan, J. Bulthuis and C. MacLean. *Magn. Reson. Chem.* **24** 723 (1986).

[40] E.W. Bastiaan, C. MacLean, P.C.M. van Zijl and A.A. Bothner-By. *Ann. Repts. NMR Spectrosc.* **19** 35 (1987).

[41] T. Schaefer, R. Sebastian and R.W. Schurko. *Can. J. Chem.* **70** 2365 (1992).

[42] T. Schaefer, R.W. Schurko and G.M. Bernard. *Can. J. Chem.* **72** 1780 (1994).

[43] E.I. Snyder and J.D. Roberts. *J. Amer. Chem. Soc.* **84** 1582 (1962).

[44] S.L. Manatt and D.D. Elleman. *J. Amer. Chem. Soc.* **84** 1579 (1962).

[45] M. Karplus. *J. Chem. Phys.* **33** 1842 (1960).

[46] N.J. Koole, M.J.A. de Bie and P.E. Hansen. *Org. Magn. Reson.* **22** 827 (1984).

[47] M. Barfield and M.D. Johnston, Jr. *Chem. Rev.* **73** 53 (1973).

[48] I. Ando and G.A. Webb. *Org. Magn. Reson.* **15** 111 (1981).

[49] T. Schaefer, K. Chum, D. MacKinnon and M.S. Chauhan. *Can. J. Chem.* **53** 2734 (1975).

[50] W. Runge and J. Firl. *Ber. Bunsen-Gesellschaft,* **79** 913 (1975).

[51] J. Gauss. *J. Chem. Phys.* **99** 3629 (1993).

[52] B. Coussens, K. Pierloot and R.J. Meier. *J. Mol. Struct. (THEOCHEM).* **259** 331 (1992).

[53] D.E. Ewing. *Org. Magn. Reson.* **12** 499 (1993).

[54] E. Breitmaier and W. Voelter. Carbon-13 NMR Spectroscopy. VCH Publishers, New York, NY. Third ed. 1987.

[55] D.W. Rogers and F. McLafferty. *J. Phys. Chem.* **99** 1375 (1995).

[56] J. Hilton and L.H. Sutcliffe. *Prog. NMR Spectrosc.* **10** 27 (1975).

[57] R.H. Contreras and J.C. Facelli. *Ann. Repts. NMR Spectrosc.* **27** 255 (1993).

[58] T. Schaefer, G.H. Penner and R. Sebastian. *Can. J. Chem.* **65** 873 (1987).

[59] T. Schaefer, C. Beaulieu, R. Sebastian and G.H. Penner. *Can. J. Chem.* **68** 581 (1990).

[60] M.T. Rogers. *J. Amer. Chem. Soc.* **69** 457 (1947).

[61] H.M. McConnell. *J. Chem. Phys.* **30** 126 (1959).

[62] T. Schaefer, R. Sebastian and G.H. Penner. *Can. J. Chem.* **63** 2597 (1985).

[63] T. Schaefer, R. Sebastian and G.H. Penner. *Can. J. Chem.* **66** 1495 (1988).

[64] R. Wasylishen and T. Schaefer. *Can. J. Chem.* **50** 1852 (1972).

[65] M. Barfield, C.J. Fallick, K. Hata, S. Sternhell and P.W. Westerman. *J. Amer. Chem. Soc.* **105** 2178 (1983).

[66] M. Barfield, M.J. Collins, J.E. Gready, S. Sternhell and C.W. Tansey. *J. Amer. Chem. Soc.* **111** 4385 (1989).

[67] J.E. Gready, K. Hata, S. Sternhell and C.W. Tansey. *Aust. J. Chem.* **43** 593 (1990).

[68] H.M. McConnell. *J. Mol. Spectrosc.* **1** 11 (1957).

[69] M. Randić and X. Guo. *Int. J. Quant. Chem.* **49** 215 (1994).

[70] I.R. Peat and W.F. Reynolds. *Can. J. Chem.* **48** 2403 (1974).

[71] T. Schaefer and C.S. Takeuchi. *Can. J. Chem.* **67** 1022 (1989).

[72] T. Schaefer, R. Sebastian, D.M. MacKinnon, P.W. Spevack, K.J. Cox and C.S. Takeuchi. *Can. J. Chem.* **71** 960 (1993).

[73] T. Schaefer and C.S. Takeuchi. *Can. J. Chem.* **67** 827 (1989).

[74] M. Hansen and H.J. Jakobsen. *J. Magn. Reson.* **20** 520 (1975).

[75] J.L. Marshall and R. Seiwell. *Org. Magn. Reson.* **8** 419 (1976).

[76] M. Karplus and G.K. Fraenkel. *J. Chem. Phys.* **35** 1312 (1961).

[77] T. Schaefer and K.J. Cox. *Can. J. Chem.* **69** 919 (1991).

[78] T. Schaefer, R. Sebastian and F.E. Hruska. *J. Mol. Struct. (Theochem.)* **281** 269 (1993).

[79] F.A.L. Anet and M. Ahmad. *J. Am. Chem. Soc.* **86** 119 (1964).

[80] T. Drakenberg, R. Jost and J.M. Sommer. *J. Chem. Soc. Chem. Commun.* 1011 (1974).

[81] L. Lunazzi, D. Maccientelli and A. Boicelli. *Tetrahedron Lett.* 1205 (1975).

[82] T. Schaefer, C.S. Takeuchi, G.M. Bernard and F.E. Hruska. *Can. J. Chem.* **73** 106 (1995) and references therein.

[83] I. Alkorta and S. Maluendes. *J. Phys. Chem.* **99** 6457 (1995).

[84] T. Schaefer. *J. Phys. Chem* **79** 1888 (1975).

[85] H. Jones and R.F. Curl, Jr. *J. Mol. Spectrosc.* **42** 65 (1972).

[86] T. Schaefer, G.H. Penner, K.J. Davie and R. Sebastian. *Can. J. Chem.* **63** 777 (1985).

[87] T. Schaefer and C.S. Takeuchi. *Can. J. Chem.* **68** 339 (1990).

[88] R. Laatikainen, K. Tuppurainen, Y. Hiltunen and S. Lötgönen. *Magn. Reson. Chem.* **28** 939 (1990).

[89] T. Schaefer and R. Sebastian. *Chem. Phys. Lett.* **163** 212 (1989).

[90] R.M. Villamañán and J.L. Alonso. *Chem. Phys. Lett.* **159** 97 (1989).

[91] J.J.C. Teixeira-Dias and P.J.A. Ribeiro-Claro. *Struct. Chem* **3** 95 (1992).

[92] H.A. Gaur, J. Vriend and W.G.B. Huysmans. *Tetrahedron Lett.* 1999 (1969).

[93] W.T. Raynes, A.D. Buckingham and H.J. Bernstein. *J. Chem. Phys.* **36** 348 (1962).

[94] R.F. Zürcher. *Prog. NMR Spectrosc.* **2** 205 (1967).

[95] L.M. Jackman and S. Sternhell. Applications of NMR Spectroscopy in Organic Chemistry. Pergamon Press, Oxford. Third edition, 1969. pp. 71,72.

[96] H. Günther. NMR Spectroscopy. Wiley, New York. 1980. pp. 73-77.

[97] R.K. Harris. NMR Spectroscopy. Longman Scientific and Technical, Harlow Essex. 1986. pp. 191-204.

[98] R.J. Abraham, M. Edgar. L. Griffiths and R.L. Powell. *J. Chem. Soc. Perkin 2.* 561 (1995).

[99] G.K. Hamer, I.R. Peat and W.F. Reynolds. *Can. J. Chem.* **51** 897 (1973).

[100] T. Schaefer, J. Peeling, G.H. Penner, A. Lemire and R. Sebastian. *Can. J. Chem.* **63** 24 (1985).

[101] R.A. Hoffman. *Mol. Phys.* **1** 326 (1958).

[102] T. Schaefer, R. Sebastian, R. Laatikainen and S.R. Salman. *Can. J. Chem.* **62** 326 (1984).